

A Comprehensive Heat Transfer Analysis for Thermoplastic Composites Made by
Automated Fiber Placement Using Hot Gas Torch

Mehrshad Moghadamzad

A Thesis

In the Department of
Mechanical, Industrial and Aerospace Engineering

Presented in Partial Fulfillment of the Requirements
For the Degree of Master of Applied Science (Mechanical Engineering) at
Concordia University
Montreal, Quebec, Canada

March 2022

© Mehrshad Moghadamzad, 2022

CONCORDIA UNIVERSITY
School of Graduate Studies

This is to certify that the thesis prepared

By: Mehrshad Moghadamzad

Entitled: A Comprehensive Heat Transfer Analysis for Thermoplastic Composites Made by Automated Fiber Placement Using Hot Gas Torch

and submitted in partial fulfillment of the requirements for the degree of

Master of Applied Science (Mechanical Engineering)

complies with the regulations of the University and meets the accepted standards with respect to originality and quality.

Signed by the final examining committee:

Dr. Mehdi Hojjati _____ Chair

Dr. Mehdi Hojjati _____ Examiner

Dr. Emre Erkmen _____ Examiner

Dr. Suong Van Hoa _____ Thesis Supervisor

Approved by _____

Dr. Martin Pugh

Chair, Department of Mechanical, Industrial, and Aerospace Engineering

Dr. Mourad Debbabi

Dean, Gina Cody School of Engineering and Computer Science

ABSTRACT

A Comprehensive Heat Transfer Analysis for Thermoplastic Composites Made by Automated Fiber Placement Using Hot Gas Torch

Mehrshad Moghadamzad

Thermoplastic composites bring many benefits in terms of mechanical properties and manufacturing. Possibility of healing and recycling and proper strength are some of these desirable characteristics. Automated fiber placement (AFP) process can be used to manufacture both thermoplastic and thermoset composite structures. However, manufacturing of thermoplastic composite structures with free edges using AFP process faces a big challenge. These structures such as flat laminates deform, and these undesirable deformations occur even during the manufacturing process of unidirectional laminates. The distortion of thermoplastic structures with free edges is mainly caused by development of temperature gradients and residual stresses. To investigate the temperature gradients and residual stresses, accurate heat transfer models need to be developed. In this study a two-dimensional transient heat transfer model was developed for thermoplastic structures manufactured by AFP process with a hot gas torch. The accuracy of heat transfer model for AFP process using hot gas torch is highly dependent upon the accuracy of hot gas/air and convection coefficient distributions in the vicinity of the substrate (thermal inputs). Therefore, mathematical models for both thermal inputs were developed in this study. Inter-layer thermal contact resistance and temperature dependencies of the material properties were considered, and the heat transfer model was validated by experimental results. Furthermore, a heat transfer model was developed to include the effects of time between each pass. Then, using the validated heat transfer models and considering temperature histories and the time between each pass, the development of temperature gradients was investigated for various types of mandrels.

ACKNOWLEDGMENTS

I received a great deal of support, assistance, and advice through this study and writing the thesis.

I would like to express my deepest appreciation to my supervisor, Professor Suong Van Hoa, for his valuable guidance, unconditional support, and patience. His insightful advice brought the research to higher levels.

I would like to thank Dr. Mehdi Hojjati and Dr. Emre Erkmen for serving on my examination committee, reading my thesis, and giving their feedback.

I would also like to extend my deepest gratitude to my family, Hamideh, Mishka, Shokouhazam, Jafar, and Mehrnoush for their unconditional love, encouragement, and support.

Contributions

Some of the main and general research contributions are listed in below:

- Developed mathematical models for both hot gas/air temperature and convection coefficient distributions in the vicinity of the substrate (thermal inputs).
- Developed general procedures including a decision table and an algorithm to determine the thermal inputs using experimental results.
- Investigated the inter-layer thermal contact resistance and its effects on the results.
- Validated the heat transfer model using experimental results.
- Developed a heat transfer model to consider the effects of time between each pass and temperature history.
- Investigated the development of temperature and temperature gradients during the manufacturing process for various types of tools with different temperatures.

List of publications:

- **M. Moghadamzad** and S. V. Hoa, “Models for heat transfer in thermoplastic composites made by automated fiber placement using Hot Gas Torch,” *Composites Part C: Open Access*, vol. 7, p. 100214, 2022.
- **M. Moghadamzad** and S. V. Hoa, “Effect of thermal input on the temperature distribution of thermoplastic composites made by automated fiber placement (AFP),” Proceedings of the 36th virtual technical conference of the *American Society for Composites*, organized by Texas A & M University, 2021.
- **M. Moghadamzad** and S. V. Hoa, “Temperature gradients in thermoplastic composites made by automated fiber placement,” Proceedings of the 5th International Symposium on Automated Composites Manufacturing, Bristol, UK, 2022.

Table of Contents

Contributions.....	v
List of Figures.....	viii
List of Tables.....	xii
Chapter 1: Introduction.....	1
Chapter 2: Literature Review and Research Objective.....	4
2.1. Definition of the problem.....	4
2.2. Heat transfer models.....	6
2.3. Objective.....	8
Chapter 3: Experimental Setup and Results.....	10
3.1. Apparatus, material, and test specimen.....	10
3.2. Experimental setup.....	11
3.3. Experimental results and sources of error in results obtained by Tafreshi et al. [11]....	13
Chapter 4: Theoretical Heat Transfer Model [15].....	16
4.1. Transient heat transfer analysis using finite difference method.....	16
4.2. Conduction coefficients (K_x and K_y), density ρ , and specific heat (C_p) of the composite	17
4.3. Conduction coefficient (K_m), density ρ_m , and specific heat (C_{pm}) of the tool.....	19
4.4. Inter-layer thermal contact resistance.....	20
4.5. Global and local coordinate systems.....	21
4.6. Hot gas/air temperature and convection coefficient distributions in the vicinity of laminar (T_k and h_k , $k = 1,2$).....	21
4.7. Formulations.....	23
4.7.1. Interior nodes.....	23
4.7.2. Boundary nodes.....	23
4.8. Stability criterion.....	26
4.9. Determination of the thermal inputs (T_k and h_k).....	27
4.9.1. Non-linear models.....	27
4.9.2. Procedure to determine the unknown parameters(h_{max} , x'_1 , and x'_2).....	30
4.9.3. Stage one of the determinations of unknown parameters (h_{max} , x'_1 , and x'_2).....	34
4.9.4. Stage two of the determinations of the unknown parameters (h_{max} , x'_1 , and x'_2).....	38
4.9.5. Validation of the model through the thickness using experimental results.....	39

4.9.6. Discussion and conclusion.....	41
Chapter 5: Temperature gradients.....	42
5.1. Temperature history and effects of time between each pass	42
5.2. Heat transfer model for the time between each pass.....	42
5.3. Procedure to determine the substrate temperature considering temperature history and effects of time between each pass	44
5.4. Effects of temperature history and time between each pass for aluminum mandrels	45
5.5. Effects of mandrels and their initial temperature on the temperature distributions of the substrate.....	48
5.6. Temperatures of laminates at $t = 10s$ for different mandrels	54
5.6.1. Aluminum mandrel with an initial temperature of 25°C.....	54
5.6.2. Ceramic mandrel.....	56
5.6.3. Hot aluminum mandrel	58
5.7. Temperature gradients through the thickness for different mandrels	60
5.7.1. Aluminum mandrel	60
5.7.2. Ceramic mandrel.....	69
5.7.3. Hot aluminum mandrel	71
5.8. Comparison of temperature gradients through the thickness for different tools.....	74
Chapter 6: Conclusions and Future Work.....	90
6.1. Conclusions	90
6.2. Future Work	91
References.....	92

List of Figures

Figure 1.1: A curved leaf spring made using 4D printing	1
Figure 1.2: AFP machine available at Concordia University	2
Figure 1.3: A deformed unidirectional thermoplastic laminate made by AFP process	3
Figure 2.1: Distortion of composite laminates during and after manufacturing process	4
Figure 2.2: Manufacturing of thermoplastic laminates using AFP process and development of temperature gradients and residual stresses	5
Figure 3.1: Thermoplastic fiber placement heat of the AFP robot available at Concordia University	10
Figure 3.2: Schematic of the test specimen and thermocouple positions	11
Figure 3.3: Experimental setup and location of thermocouples	12
Figure 3.4: Fast-response K-type thermocouple used in the experiment	12
Figure 3.5: Comparison of experimental and theoretical results obtained by Tafreshi et al. [11]	13
Figure 3.6: Hot gas temperature (temperature input) used by Tafreshi et al. [11]	14
Figure 3.7: Convection coefficient used by Tafreshi et al. [11]	14
Figure 4.1: Longitudinal thermal conductivity(K_x) of AS4/APC-2, experimental and fitted curve	18
Figure 4.2: Transverse thermal conductivity(K_y) of AS4/APC-2, experimental and fitted curve	18
Figure 4.3: Density(ρ) of AS4/APC-2, experimental and fitted curve	19
Figure 4.4: Specific heat(C_p) of AS4/APC-2, experimental and fitted curve.....	19
Figure 4.5: Model of inter-layer thermal contact resistance	20
Figure 4.6: Two different zones with respect to the local coordinate system ($x' = 0$).....	22
Figure 4.7: Schematic illustration of boundary nodes (composite laminate + aluminum mandrel)	23
Figure 4.8: General features of input distribution.....	28
Figure 4.9: Illustration of the defined error quantities in the results obtained by Tafreshi et al. [11] in one layer below the top surface (TC3).....	31
Figure 4.10: Illustration of the defined error quantities in the results obtained by Tafreshi et al. [11] in nine layers below the top surface (TC2)	32
Figure 4.11: Illustration of the defined error quantities in the results obtained by Tafreshi et al. [11] in twelve layers below the top surface (TC1)	32
Figure 4.12: Procedure to determine the unknown parameters	33
Figure 4.13: Initial input temperature distribution.....	34
Figure 4.14: Initial convection coefficient distribution	35
Figure 4.15: Laminate temperature distribution using the initial values of unknown parameters (TC3).....	35
Figure 4.16: Updated input temperature distribution.....	36

Figure 4.17: Updated convection coefficient.....	37
Figure 4.18: Laminate temperature distribution in one layer below the top surface (TC3) using the updated values of unknown parameters	37
Figure 4.19: Laminate temperature distribution in one layer below the top surface (TC3) with and without inter-layer thermal contact resistance	38
Figure 4.20: Laminate temperature distribution in one layer below the top surface (TC3) considering inter-layer thermal contact resistance.....	39
Figure 4.21: Laminate temperature distribution in nine layers below the top surface (TC2) considering inter-layer thermal contact resistance.....	40
Figure 4.22: Laminate temperature distribution in twelve layers below the top surface (TC1) considering inter-layer thermal contact resistance.....	40
Figure 5.1: Composite laminate and mandrel heat transfer mechanism during the time between each pass	43
Figure 5.2: Schematic illustration of boundary nodes for the time between each pass	43
Figure 5.3: Temperature at the mid-section of the substrate while layer 5 is being deposited, the time between each pass is equal to zero.....	46
Figure 5.4: Temperature at the mid-section of the substrate while layer 10 is being deposited, the time between each pass is equal to zero.....	46
Figure 5.5: Temperature at the mid-section of the substrate while layer 5 is being deposited, the time between each pass is equal to eight seconds.....	47
Figure 5.6: Temperature at the mid-section of the substrate while layer 10 is being deposited, the time between each pass is equal to eight seconds.....	47
Figure 5.7: Temperature at the mid-section of layer 1 while layer 5 is being deposited for different mandrels	49
Figure 5.8: Temperature at the mid-section of layer 2 while layer 5 is being deposited for different mandrels	49
Figure 5.9: Temperature at the mid-section of layer 3 while layer 5 is being deposited for different mandrels	50
Figure 5.10: Temperature at the mid-section of layer 4 while layer 5 is being deposited for different mandrels	50
Figure 5.11: Temperature at the mid-section of layer 9 while layer 10 is being deposited for different mandrels	51
Figure 5.12: Temperature at the mid-section of layer 8 while layer 10 is being deposited for different mandrels	52
Figure 5.13: Temperature at the mid-section of layer 7 while layer 10 is being deposited for different mandrels	52
Figure 5.14: Temperature at the mid-section of layer 6 while layer 10 is being deposited for different mandrels	53
Figure 5.15: Temperatures of layers 1 to 4, layer 5 is being deposited	54
Figure 5.16: Temperatures of layers 5 to 9, layer 10 is being deposited	55

Figure 5.17: Temperatures of layers 1 to 4, layer 10 is being deposited	55
Figure 5.18: Temperatures of layers 1 to 4, layer 5 is being deposited	56
Figure 5.19: Temperatures of layers 5 to 9, layer 10 is being deposited	57
Figure 5.20: Temperatures of layers 1 to 4, layer 10 is being deposited	57
Figure 5.21: Temperatures of layers 1 to 4, layer 5 is being deposited	58
Figure 5.22: Temperatures of layers 5 to 9, layer 10 is being deposited	59
Figure 5.23: Temperatures of layers 1 to 4, layer 10 is being deposited	59
Figure 5.24: Temperatures through the thickness (tool to layer 4) at $x = 6in$	61
Figure 5.25: Temperature gradients through the thickness at $x = 6in$	61
Figure 5.26: Temperatures through the thickness (layers 5 to 9) at $x = 6in$	62
Figure 5.27: Temperature gradients through the thickness at $x = 6in$	62
Figure 5.28: Temperatures through the thickness (tool to layer 4) at $x = 8in$	63
Figure 5.29: Temperature gradients through the thickness at $x = 8in$	63
Figure 5.30: Temperatures through the thickness (layers 5 to 9) at $x = 8in$	64
Figure 5.31: Temperature gradients through the thickness at $x = 8in$	64
Figure 5.32: Temperatures through the thickness (tool to layer 4) at $x = 10in$	65
Figure 5.33: Temperature gradients through the thickness at $x = 10in$	65
Figure 5.34: Temperatures through the thickness (layers 5 to 9) at $x = 10in$	66
Figure 5.35: Temperature gradients through the thickness at $x = 10in$	66
Figure 5.36: Temperatures through the thickness (tool to layer 4) at $x = 12in$	67
Figure 5.37: Temperature gradients through the thickness at $x = 12in$	67
Figure 5.38: Temperatures through the thickness (layers 5 to 9) at $x = 12in$	68
Figure 5.39: Temperature gradients through the thickness at $x = 12in$	68
Figure 5.40: Temperatures through the thickness (tool to layer 4) at $x = 6in$	69
Figure 5.41: Temperature gradients through the thickness at $x = 6in$	69
Figure 5.42: Temperatures through the thickness (layers 5 to 9) at $x = 6in$	70
Figure 5.43: Temperature gradients through the thickness at $x = 6in$	70
Figure 5.44: Temperatures through the thickness (tool to layer 4) at $x = 6in$	71
Figure 5.45: Temperature gradients through the thickness at $x = 6in$	72
Figure 5.46: Temperatures through the thickness (tool to layer 4) at $x = 6in$	72
Figure 5.47: Temperature gradients through the thickness at $x = 6in$	73
Figure 5.48: Temperature-time graph for different tools, layer 9 at top and layer 8 at bottom....	74
Figure 5.49: Temperature gradients between layers 9 and 8 ($G_{9,8}$) for different tools	75
Figure 5.50: Temperature-time graph for different tools, layer 8 at top and layer 7 at bottom....	76
Figure 5.51: Temperature gradients between layers 8 and 7 ($G_{8,7}$) for different tools	77
Figure 5.52: Temperature-time graph for different tools, layer 7 at top and layer 6 at bottom....	78
Figure 5.53: Temperature gradients between layers 7 and 6 ($G_{7,6}$) for different tools	79
Figure 5.54: Temperature-time graph for different tools, layer 6 at top and layer 5 at bottom....	80
Figure 5.55: Temperature gradients between layers 6 and 5 ($G_{6,5}$) for different tools	81
Figure 5.56: Temperature-time graph for different tools, layer 5 at top and layer 4 at bottom....	81

Figure 5.57: Temperature gradients between layers 5 and 4 ($G_{5,4}$) for different tools	82
Figure 5.58: Temperature-time graph for different tools, layer 4 at top and layer 3 at bottom....	83
Figure 5.59: Temperature gradients between layers 4 and 3, $G_{4,3}$ for different mandrels	84
Figure 5.60: Temperature-time graph for different tools, layer 3 at top and layer 2 at bottom....	84
Figure 5.61: Temperature gradients between layers 3 and 2 ($G_{3,2}$) for different tools	85
Figure 5.62: Temperature-time graph for different tools, layer 2 at top and layer 1 at bottom....	86
Figure 5.63: Temperature gradients between layers 2 and 1 ($G_{2,1}$) for different tools	87
Figure 5.64: Temperature-time graph for different tools, layer 1 at top and tool at bottom.....	88
Figure 5.65: Temperature gradients between layer 1 and tool ($G_{1, tool}$) for different tools.....	89

List of Tables

Table 4.1: Conduction heat transfer coefficients, specific heat, and density of AS4/APC-2 [7].	17
Table 4.2: Primary coefficients and stability criterion.....	27
Table 4.3: Decision mechanism based on the signs of ei	33
Table 5.1: Characteristics of the system and materials properties.....	45
Table 5.2: Characteristics of the system and materials properties.....	48

Chapter 1: Introduction

Composite materials provide interesting characteristics such as light weight, high strength, high stiffness, fatigue resistance, and corrosion resistance. In addition, complex geometries can be manufactured using composite materials with less numbers of components in comparison to metallic materials [1]. Manufacturing of complex composite structures using 4D printing method, which does not need complex molds, creates more advantages for composite materials [2,3]. Figure 1.1 shows a composite spring made using the method of 4D printing of composites.



Figure 1.1: A curved leaf spring made using 4D printing

Source: [2]

Composite structures can be manufactured using different methods such as hand-lay-up, filament winding, pultrusion, automated tape placement, and automated fiber placement (AFP). Automated composites manufacturing methods (automated tape and fiber placement) are mainly used to manufacture aircraft structures due to higher speed of manufacturing and quality of the manufactured parts. The highest rate of hand-lay-up is almost equal to 2.2 lb/hr (1 kg/hr), whereas 15 to 25 lb/hr (6.82 to 11.36 kg/hr) of composite tapes can be deposited using automated tape placement. Automated manufacturing methods can be used to manufacture both thermoset and thermoplastic composite structures [1].

Thermoplastic composites provide desirable characteristics in terms of mechanical properties and manufacturing such as possibility of healing and recycling, proper strength and stiffness, higher elongation than thermosets, and no shelf-life effect on manufacturing [1]. Automated fiber placement (AFP) process facilitates manufacturing of new components using thermoplastic composites such as cylindrical shaped structures, curved panels, and flat laminates. Thermoplastic composite structures made by AFP process may not need subsequent treatments such as autoclave processing, which is required for thermoset composites. This creates a significant advantage for

processing of thermoplastic composites using AFP process. Increasing interests in thermoplastic structures made by AFP process has been indicated in [4-8]. In the AFP process of thermoplastic composites, a moving heat source such as hot gas torch, heat lamp, laser, or infrared heats up the thermoplastic tapes. Next, the heated tapes are consolidated onto the substrate in a cyclic process with a constant velocity to manufacture the composite structure. The AFP process has been explained in several sources [1,9,10,11,12,19]. The AFP machine available at Concordia University uses a hot gas torch, and it is shown in figure 1.2.

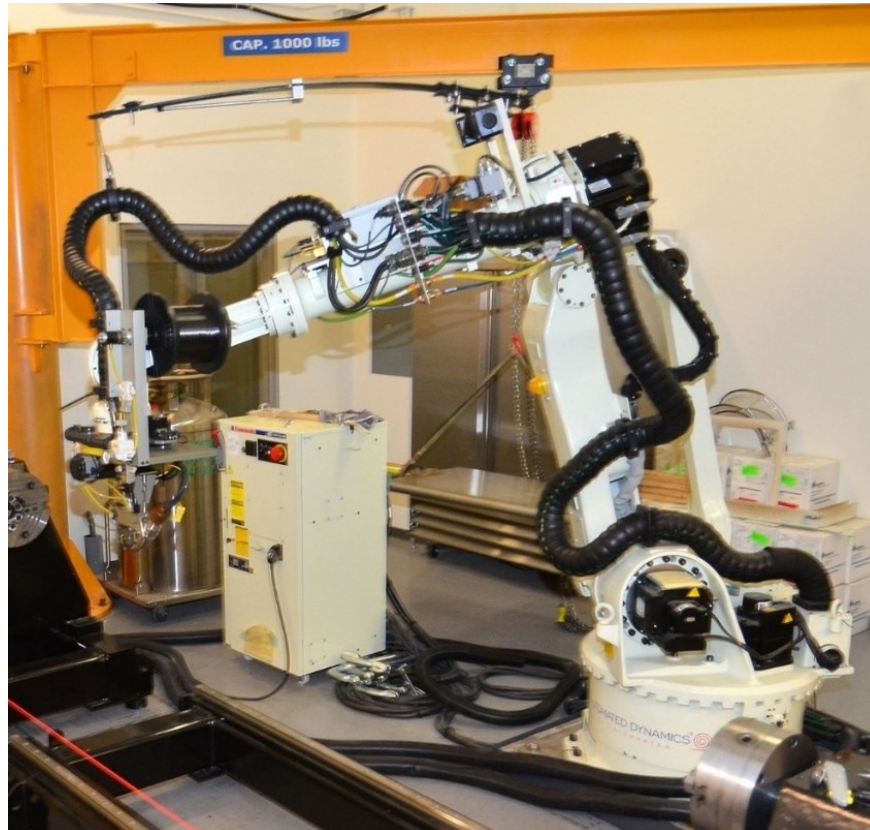


Figure 1.2: AFP machine available at Concordia University

Source: [13]

Although thermoplastic composites provide suitable characteristics, thermoplastic structures with free edges such as flat laminates suffer from deformations due to residual stresses. Deformations of thermoplastic structures with free edges, which occurs even during the AFP process, are caused by temperature gradients. The main source of these temperature gradients is the variation of temperature and cooling rates at different locations of the thermoplastic structures (moving heat source). Figure 1.3 shows the undesirable distortion of a unidirectional thermoplastic laminate made by AFP process.



Figure 1.3: A deformed unidirectional thermoplastic laminate made by AFP process

Source: [14]

To address this issue (deformation of thermoplastic structures with free edges), it is necessary to investigate the development of temperature and temperature gradients in these structures during the AFP process. As a result, it is essential to develop an accurate heat transfer model for the AFP process. To develop accurate heat transfer models for the AFP process, the followings are to be done:

1. It is of high importance to have proper estimations of thermal inputs. It has been shown that hot gas/air temperature and convection coefficient distributions in the vicinity of the substrate (thermal inputs) play major roles in the accuracy of the heat transfer models for the AFP process using hot gas torch [15,16]. Therefore, a big portion of this study was dedicated to the determination of the thermal inputs.
2. Levy et al. [17,18] showed that neglecting inter-layer thermal contact resistance might cause 50% or more errors in the accuracy of thermal conductivities of composite structures through the thickness. This highly depends upon the quality of bonding between layers in the composite structures. Thus, inter-layer thermal contact resistance needs to be considered in the heat transfer model and investigated.
3. Transient nature of the problem needs to be taken into account due to variation of temperature with respect to time.
4. Temperature dependencies of thermal conductivities, density, and specific heat is to be considered.
5. Validation of the theoretical results obtained from the heat transfer model using experimental results is necessary.

By having an accurate heat transfer model, one is able to investigate temperature variations and development of temperature gradients in the composite structures during the AFP process.

Chapter 2: Literature Review and Research Objective

2.1. Definition of the problem

Automated fiber placement (AFP) provides several advantages for manufacturing of composite structures such as increase in the quality of the composite structures and speed of manufacturing process. Furthermore, manufacturing of complex and various geometries has been made possible by automated fiber placement including structures with and without free edges. Cylinders, conical structures, and rings are examples of structures without free edges. Flat laminates, flat panels, and shells are some examples of structures with free edges. Manufacturing of thermoplastic composite structures with free edges using automated fiber placement faces a major challenge due to distortion of these structures. The undesirable deformation of these structures might occur even during the manufacturing process. Figures 1.3 and 2.1. illustrate distortion of thermoplastic laminates, which were manufactured using automated fiber placement.



Figure 2.1: Distortion of composite laminates during and after manufacturing process

Source: [19]

To address this issue, it is necessary to analyze the manufacturing process of thermoplastic structures made by automated fiber placement in terms of temperature development (heating up and cooling down of the thermoplastic tapes and substrate). The process of temperature development for the hot gas torch AFP process is as follows:

1. Thermoplastic tapes are fed into the nip point. The viscosity of thermoplastics is relatively high, so they need to be heated during the manufacturing process. To do so, high amounts of heat energy is required. Since the AFP robot available at Concordia University is a hot gas torch one, the heat required in the process is provided by the hot nitrogen gas torch (stage A in 2.2)
2. Consolidation or compaction roller applies compaction loads required for the process. Compression of the heated thermoplastic tapes causes the resin to flow through the fibers network. This leads to resin flow in all directions including through the thickness of the deposited layers. As a result, bonds between layers form [1,21,22]. In this stage, heat is transferred from the heated tape to the previously deposited layers and mandrel via

conduction. In addition, some amounts of heat are transferred from the heated composite tape to the ambient air via convection (stage B in figure 2.2).

3. The deposited thermoplastic layers cool down. When the torch passes over a specific location of the substrate, that location begins to cool down. The top layer of the substrate, the bottom section of the mandrel, and both right and left sides of them are exposed to the ambient air. Hence, heat is transferred from the substrate and mandrel to the ambient air via convection. The residual stresses develop in this stage due to several reasons such as development of temperature gradients, mismatch in thermal expansion coefficients, and crystallization in the substrate (stage C in figure 2.2). The details of this process could be found in [21].
4. Deposition of new layers contribute the previously deposited layers to heat up due to heat transfer via conduction within the substrate. The temperature gradients developed in this stage and different shrinkage of layers lead to development of residual stresses (stage D in figure 2.2). More details could be found in [21].

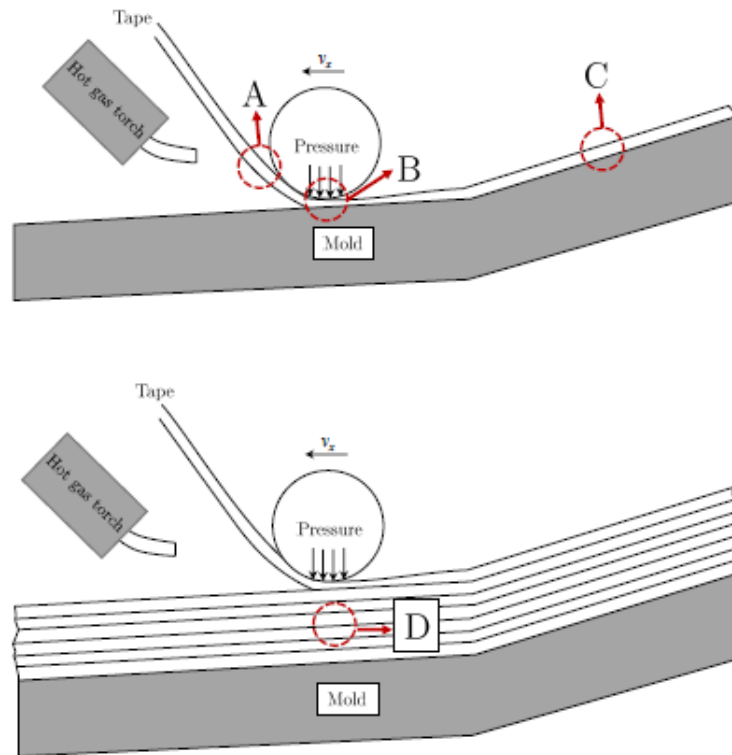


Figure 2.2: Manufacturing of thermoplastic laminates using AFP process and development of temperature gradients and residual stresses

Source: [21]

This can be concluded that the development of residual stresses and distortion of thermoplastic structures with free edges, which have been manufactured by AFP, occurs mainly due to the existence of temperature gradients. The temperature gradients develop in all directions (especially through the thickness) because of rapid heating and cooling and different cooling rates at different

layers of the substrate. This issue has been explained in several sources [19-21,23-25]. To resolve this issue, Hoa et al. [21] replaced the cold mandrel in the AFP process with a hot mandrel with a temperature higher than glass transition temperature. By doing so, they were able to manufacture a flat thermoplastic laminate using automated fiber placement. Nonetheless, this is an expensive solution and creates some limitations in terms of manufacturing. In addition, Lamontia et al. [26,27] could manufacture flat thermoplastic laminates using AFP process. In the manufacturing process, the head of AFP machine with a single roller was replaced with a multiple roller head. This solution is expensive, and it is not affordable for most organizations. Despite these efforts, manufacturing of thermoplastic structures with free edges using AFP process has remained challenging. In order to resolve this issue, accurate heat transfer models are required. By having an accurate heat transfer model, development of temperature and temperature gradients as the main source of residual stresses can be investigated.

2.2. Heat transfer models

Many heat transfer analyses have been performed for various manufacturing processes of thermoplastic structures. Tierney and Gillespie [28] conducted a steady state and one-dimensional heat transfer analysis for ATP process of thermoplastics. This heat transfer model was very simplified, and several important aspects of the heat transfer were neglected. For instance, the transient nature of the problem and temperature dependencies of material properties such as conduction coefficients, density, and specific heat was not considered in the heat transfer model. Dai and Ye [29] developed a transient and one-dimensional heat transfer model for tape winding process. The model was solved using analytical methods, and temperature dependencies of material properties were neglected. Weiler et al. [30] conducted a transient and one-dimensional heat transfer analysis for laser-assisted ATP process. The model was solved analytically, and average values of material properties were considered in the heat transfer model. Li et al. [35] simulated transient temperature field using ANSYS (dynamic mesh) in thermoplastic tape lay-up process and compared the results with analytical solution of one-dimensional heat transfer model. The model was not validated with experimental results. Beyeler et al. [31] performed a steady-state and two-dimensional heat transfer analysis using mapping technique and finite difference method for tape laying process (laser-assisted) with a focused heat source. The theoretical results were not compared to experimental ones. Nejhad et al. [32] developed a two-dimensional and steady-state heat transfer model for tape laying of thermoplastics. Numerical and analytical solutions of the model were provided, but the results were not validated using experimental results. A two-dimensional and steady-state heat transfer model was proposed for ATP and filament winding process by Mantell and Springer [33]. The theoretical results in this study were not compared to experimental ones. Sonmez and Hahn [34] performed a two-dimensional steady-state heat transfer analysis using finite element method for ATP process of thermoplastic composites. Also, they assumed the compaction roller as a heat sink with constant temperature. The theoretical results were not validated using experimental ones. Zhao et al. [37] investigated heat transfer using finite element method in thermoplastic rings made by AFP process. The results obtained from the two-dimensional transient heat transfer model used for thermal stress analysis, but theoretical results were not compared to experimental results. A parametric study using finite element method for heat transfer in tow placement of thermoplastics was done by Han et al. [36]. The two-dimensional transient heat transfer model was not validated using experimental results. Stokes-Griffin and Compston [41] analyzed heat transfer in laser-assisted AFP process for

thermoplastic composites. The transient heat transfer model was validated using experimental results. A three-dimensional steady state heat transfer analysis was conducted by James and Black [38] using finite difference method for filament winding process. The temperature dependencies of material properties were neglected, and the results obtained from the heat transfer analysis were compared to experimental results. Toso et al. [39] simulated three-dimensional transient heat transfer in thermoplastic tape winding process with a hot gas torch using finite element method and ANSYS, and the results were compared to experimental results. Hassan et al. [40] performed a three-dimensional transient heat transfer analysis using finite element method for filament winding of thermoset composites. The theoretical results were validated by the experimental ones obtained from composite rings, which were made by filament winding.

In most of these studies, the effects of inter-layer thermal contact resistance were not considered in the heat transfer model. However, recent studies show that neglecting inter-layer thermal contact resistance in composite structures can highly affect the accuracy of heat transfer models. Levy et al. [42] investigated the relation between the degree of intimate contact and thermal contact resistance and proposed a function for their relationship. Moreover, the study indicated that inter-layer thermal contact resistance in composites might be high and cannot be neglected. Levy et al. [43] modeled the inter-layer thermal contact resistance in a laser-assisted tape placement process. It was shown that the quality of bonding between layers of composites affects inter-layer thermal contact resistance and accuracy of the heat transfer model through the thickness. Jeyakodi [5] performed a three-dimensional transient heat transfer analysis using ABAQUS for laser-assisted AFP process, and the results were used to obtain residual stresses. The temperature dependencies of specific heat, thermal conductivities, density, and inter-layer thermal contact resistance were considered in the model. Jeyakodi [5] tested a wide range of inter-layer thermal contact resistance in their study. Nonetheless, the assumed values for the inter-layer thermal contact resistance and theoretical temperature results were not validated using experimental results. Kollmannsberger et al. [44] developed a two-dimensional and transient heat transfer model for laser-assisted AFP process, and the effects of inter-layer thermal contact resistance (caused by improper bonding) on the results were investigated. The theoretical results were compared to the experimental ones. Tafreshi et al. [11] provided a two-dimensional and transient heat transfer model using finite difference method in the AFP process with hot gas torch. The theoretical results in this study were compared to experimental results. Although the maximum value of theoretical temperature of the composite laminate agrees with the maximum value of experimental temperature, the theoretical curves do not follow the experimental ones due to simplifications made in the model.

Hot gas/air temperature and convection heat transfer coefficient distributions in the vicinity of composite substrate (thermal inputs) play major role in the accuracy of heat transfer analysis of AFP process with hot gas torch [15,16]. Several studies were done to estimate these thermal inputs. Wang et al. [45] assumed a constant convection heat transfer coefficient equal to $100 W/(m^2K)$ in their study. Kim et al. [46] assumed the convection coefficient to be $900 W/(m^2K)$ and $250 W/(m^2K)$ up to 11mm from the nip point for the lower and upper surfaces of heating zone, respectively. Somnez and Hahn [34] assumed that the convection coefficient is equal to $2500 W/(m^2K)$ for the heated length (15mm). The estimated value of the convection coefficient (constant value) by Shih and Loos [47] was equal to $350 W/(m^2K)$. Tafreshi et al. [11] assumed that the convection coefficient is equal to $990 W/(m^2K)$ for a length of 10mm (length of hot gas torch), and it drops to $10 W/(m^2K)$ at both sides of hot gas torch. Toso et al. [39] measured the hot gas temperature in the vicinity of substrate and hot gas torch by an infrared camera. They

assumed that temperature varies linearly in adjacent pixels, and temperature gradients were developed only through the thickness. Next, the convection coefficient was estimated in the vicinity of hot gas torch. To do so, they assumed pure conduction at the surface of substrate and hot gas. In this study, the temperature dependencies of hot gas thermal conductivity in y direction (through the thickness) and inter-layer thermal contact resistance were neglected. Zacheri et al. [48] conducted a heat transfer analysis using ABAQUS to estimate the convection coefficient for a hot gas torch assisted AFP process. Zacheri et al. [48] performed a three-dimensional heat transfer analysis. However, they did not validate the theoretical results with experimental ones through the thickness of the substrate. The hot gas temperature distribution at the top surface and in the vicinity of the laminate, which is an important thermal input for the hot gas torch AFP process, was not provided. Furthermore, the inter-layer thermal contact resistance was not considered in their study. This can affect the accuracy of thermal conductivities of the composites through the thickness and theoretical temperature results. These effects depend mainly upon the quality of bonding between layers of the composite structures. The effects of inter-layer thermal contact resistance can be very high for composite structures with improper bonding. In a study done by Levy et al. [18], it was shown that neglecting the inter-layer thermal contact resistance can lead to 50% or more errors in the accuracy of thermal conductivities through the thickness of composite structures. Hence, the inter-layer thermal contact resistance needs to be considered and investigated in heat transfer models for composite structures.

2.3. Objective

To date, most studies in the field of heat transfer analysis of automated fiber placement process are related to AFP machines with heat sources of laser. Thermal inputs in laser-assisted AFP process are different from hot gas torch-assisted AFP process. On the other hand, structures with no free edges have been studied in the most of hot gas torch AFP processes (filament winding). In addition, simplifications or assumptions made in the studies related to the hot gas torch-assisted AFP process has caused the accuracy of the heat transfer models to reduce. Some of the key factors, which are missing in the studies related to the heat transfer analysis of hot gas torch-assisted AFP process, are as follows (at least one of the key factors is neglected) [15]:

1. The transient nature of the study (steady-state heat transfer analysis) is neglected.
2. The temperature dependencies of density, thermal conductivities, and specific heat are neglected.
3. The inter-layer thermal contact resistance is neglected.
4. The distributions of both thermal inputs are not provided, or uniform distributions for both thermal inputs have been assumed.
5. The theoretical results have not been validated by experimental results.

In this study, a two-dimensional transient heat transfer analysis has been conducted for the hot gas torch-assisted AFP process of thermoplastic laminates using finite difference method (energy balance). To increase the accuracy of the heat transfer model, mathematical models for both thermal inputs (hot gas/air temperature and convection coefficient distributions in the vicinity of substrate) have been developed. Furthermore, inter-layer thermal contact resistance and temperature dependencies of material properties have been considered. Finally, the theoretical results have been validated by using experimental results. Then, the development of temperature and temperature gradients have been investigated using the validated heat transfer model. The

results of this study can be used to investigate residual stresses and deformations of thermoplastic structures with no free edges.

Chapter 3: Experimental Setup and Results

3.1. Apparatus, material, and test specimen

The materials used in this study are carbon fiber/PEEK (AS4/APC-2) tapes with a width of 6.35mm supplied from CYTEC. The apparatus, which is an automated fiber placement machine, was supplied from Trelleborg Corporation. It operates with a Kuka robot, and it has 6 degrees of freedom. The temperature at the tip of the nozzle of the nitrogen gas torch in this study is 875 °C. The torch is inclined at an angle of 6° with respect to horizontal axis, and the vertical distance from the tip of the nozzle to the top surface of the substrate is 10 mm. The composite tape (thermoplastic matrix) is melted by the hot gas torch (nitrogen gas), and a steel roller with a diameter of 12.7 mm consolidates the material. The compaction forces applied by the AFP robot are 178 N for all cases. The hot gas torch moves with a constant speed of 25.4 mm/sec. The test specimen is a flat laminate with a length of 508 mm, which was manufactured by depositing twenty layers of unidirectional thermoplastic tapes on a flat aluminum tool with a thickness of 50.8 mm.

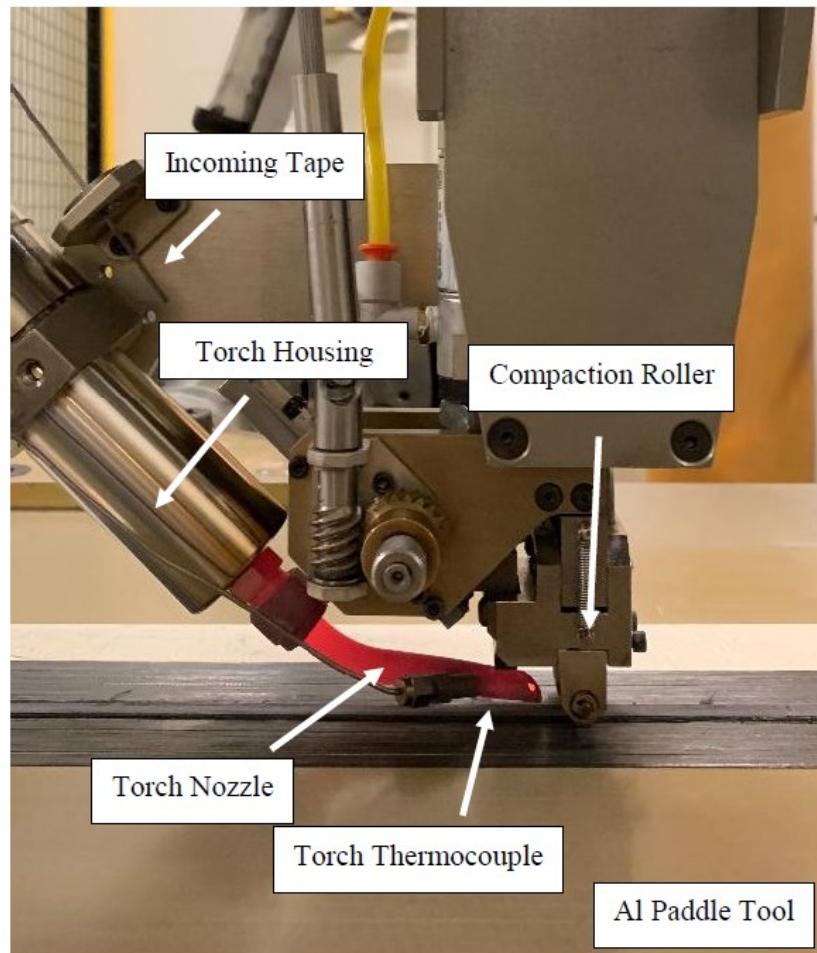


Figure 3.1: Thermoplastic fiber placement heat of the AFP robot available at Concordia University

Source: [19]

A differential scanning calorimetry (DSC) of the prepregs was performed by Hoang [23]. The glass transition temperature of the prepregs was estimated to be almost 143°C, and the degree of crystallinity was found to be approximately 16.5 % [23].

3.2. Experimental setup

To measure the temperature developed during the AFP process in a thermoplastic laminate, Tafreshi et al. [11,19] placed three thermocouples (denoted by TC) through the thickness and at the mid-section of the mentioned test specimen (figures 3.2 and 3.3). These thermocouples were placed at one layer, nine layers, and twelve layers below the top surface of the thermoplastic laminate (TC3, TC2, and TC1). After placing the thermocouples, the thermoplastic laminate was cooled down to room temperature (25 °C). Next, the hot gas torch of the AFP robot with a temperature of 875 °C moved above the top surface of thermoplastic laminate with a constant speed of 25.4 mm/s without material deposition. At this stage, the temperatures through the thickness of the thermoplastic laminate (TC3, TC2, and TC1) were recorded. Tafreshi et al. [11,19] used fast-response k-type thermocouples to measure temperature developed in the thermoplastic laminate during the AFP process (figure 3.4).

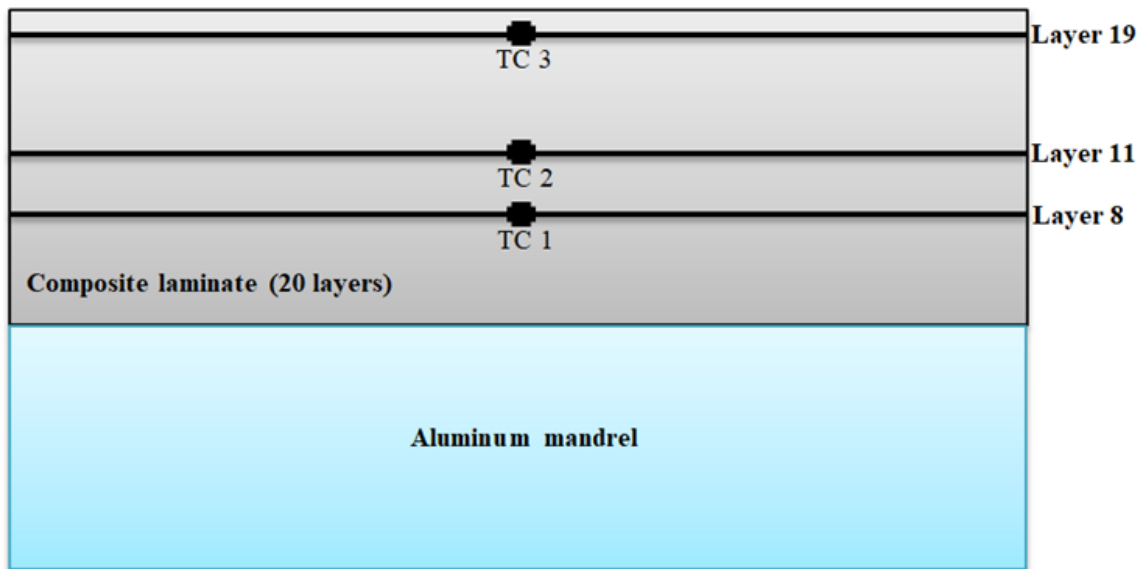


Figure 3.2: Schematic of the test specimen and thermocouple positions

Source: [15]

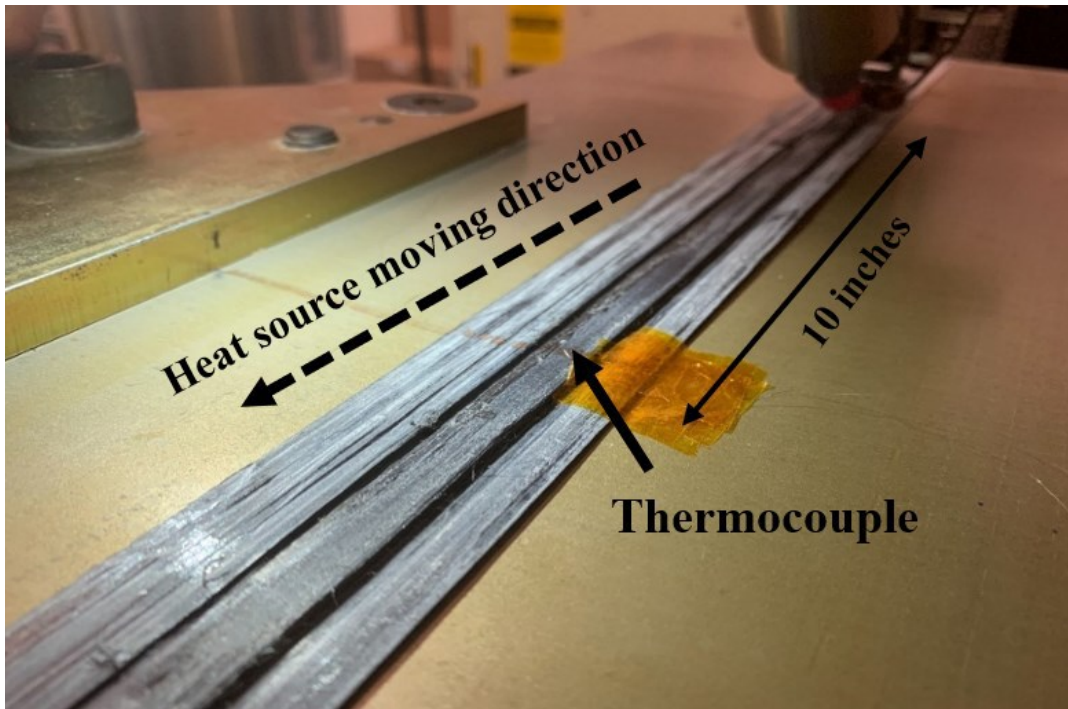


Figure 3.3: Experimental setup and location of thermocouples

Source: [19]

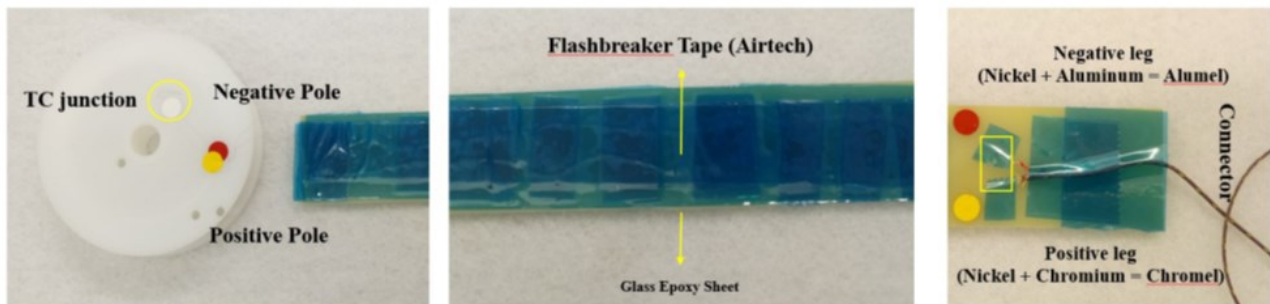


Figure 3.4: Fast-response K-type thermocouple used in the experiment

Source: [19]

Further details about the experimental work can be found in [19].

3.3. Experimental results and sources of error in results obtained by Tafreshi et al. [11]

Tafreshi et al. [11] performed a two-dimensional and transient heat transfer analysis using finite difference method and MATLAB. Then, they compared theoretical and experimental results. The comparison of the results indicates that the theoretical results are not in proper agreements with the experimental ones, and there are discrepancies between them except at the peak of TC3 (one layer below the top surface).

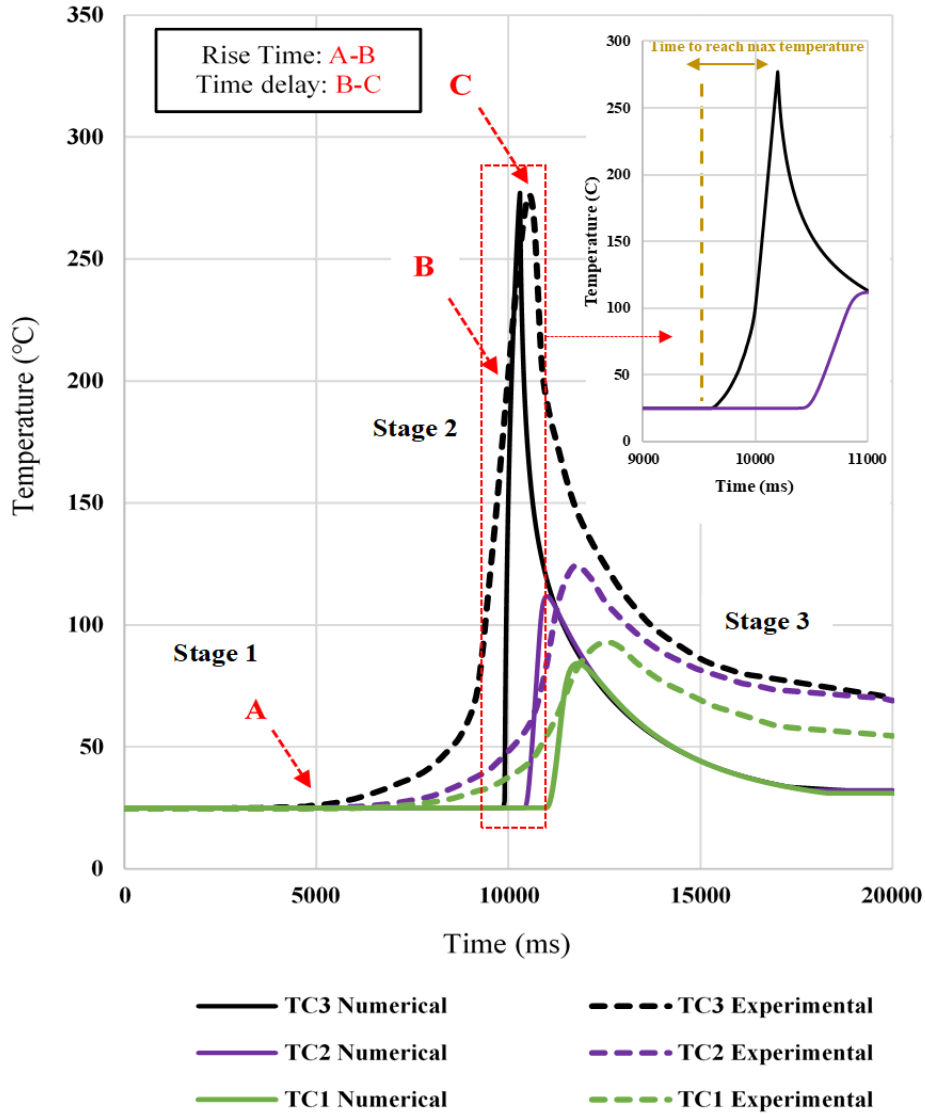


Figure 3.5: Comparison of experimental and theoretical results obtained by Tafreshi et al. [11]

Source: [11]

The main sources of error in the theoretical results obtained by Tafreshi et al. [11] are assumptions and simplifications made in the thermal inputs, which are as follows:

1. The hot gas temperature in the vicinity of the laminate is equal to 875°C for a length of 10 mm (length of hot gas torch), and it drops suddenly to the room temperature (25°C) at both sides of the hot gas torch. The input temperature used by Tafreshi et al. [11] has been illustrated in figure 3.6.
2. The convection coefficient in the vicinity of the laminate is equal to $990\text{ W}/(\text{m}^2\text{K})$ for a length of 10 mm (length of hot gas torch), and it drops suddenly to the ambient air convection coefficient ($10\text{ W}/(\text{m}^2\text{K})$) at both sides of the hot gas torch. The convection coefficient used by Tafreshi et al. [11] has been indicated in figure 3.7.

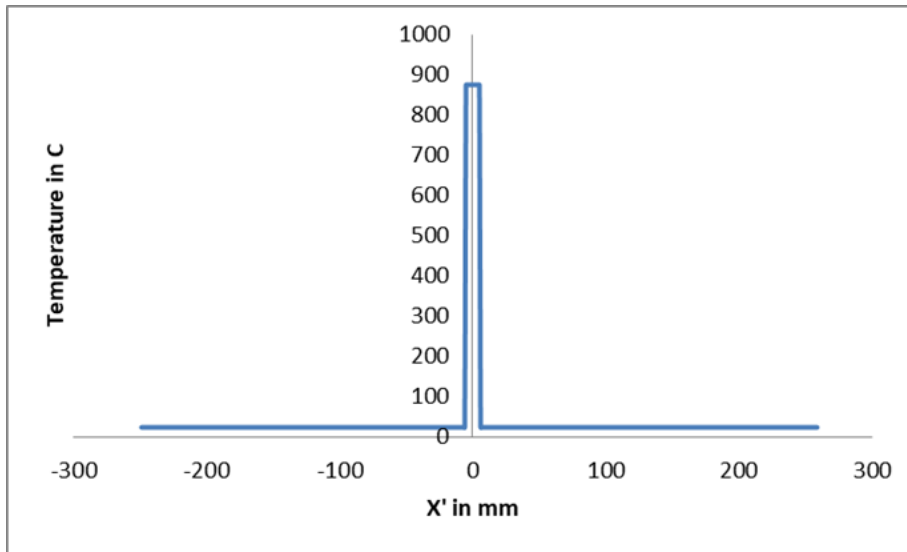


Figure 3.6: Hot gas temperature (temperature input) used by Tafreshi et al. [11]

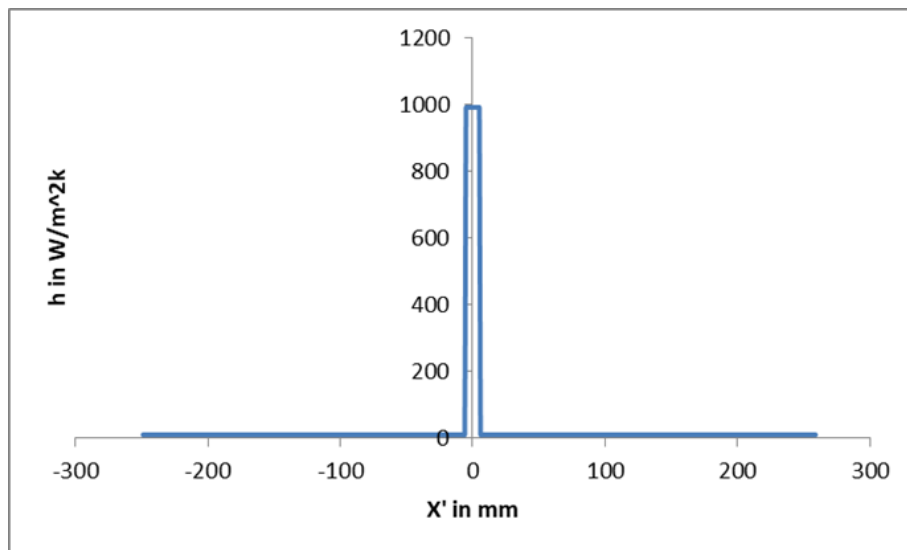


Figure 3.7: Convection coefficient used by Tafreshi et al. [11]

In figures 3.6 and 3.7, x' equal to zero shows the location of the torch at any time (t). In practice, the hot gas temperature does not drop suddenly from its maximum value (875 °C) to room temperature (25°C). Similarly, the convection coefficient cannot drop suddenly from its maximum value $990 W/(m^2K)$ to its minimum value ($10 W/(m^2K)$). Thus, it is of high importance to find proper distributions for both hot gas temperature and convection coefficient in the vicinity of the substrate (thermal inputs) [15,16].

Chapter 4: Theoretical Heat Transfer Model [15]

4.1. Transient heat transfer analysis using finite difference method

Heat is transferred via conduction inside the composite, mandrel, and their interface. All the boundary edges are exposed to heat transfer via convection. Left and right sides of the composite and mandrel and the bottom of the mandrel are in heat exchange with the ambient air via convection. The top side of the composite is mainly affected by the moving hot gas torch, which moves with a speed of 25.4 mm/s . Thus, it is in heat exchange with the hot gas/air via convection. In this study, finite difference method (energy balance) and computer coding (MATLAB) are used to solve the transient heat transfer model. To do so, the laminate is split into M sub-regions in x -direction and N -sub regions in y -direction (totally $(M+1) \times (N+1)$ nodes). The distance between each node of the laminate in x -direction (Δx) is equal to the length of laminate divided by M , and the distance between each node in y -direction (Δy) is equal to the thickness of laminate divided by N . The tool is divided into M sub-regions in x -direction (the laminate and tool have the same length) and N_m sub-regions in y -direction. The distance between each node of the tool in x -direction (Δx) is equal to the length of tool divided by M , and the distance between each node in y -direction (Δy_m) is equal to the thickness of tool divided by N_m . Mesh size analysis was conducted by increasing the number of sub regions (reducing the mesh size) in both laminate and tool and in both x and y directions to make sure that the theoretical temperatures vary no more than 0.25% ($\Delta x = 1 \text{ mm}$, $\Delta y = \Delta y_m = 0.1 \text{ mm}$).

Since the temperatures vary with respect to position and time in this study (transient heat transfer), time needs to be discretized in addition to the space. As a result, a proper time step (Δt) should be determined. Then, the nodal temperatures are calculated using the time step (Δt) until the temperatures for the entire process is computed. If the time step (Δt) is not small enough, the accuracy of the results will be highly affected. The appropriate size of time step (Δt) was found by stability criterion, and it is presented in the section 4.8.

Two different finite difference (energy balance) methods of transient heat transfer analysis could be used, which are called explicit and implicit. The explicit method is selected because it is easier to use, especially, in computer coding [49].

$$\text{Explicit method: } \sum_{\text{All sides}} \dot{Q}^i + \dot{E}_{\text{gen,element}}^i = \rho V_{\text{element}} C_p \frac{T_{m,n}^{i+1} - T_{m,n}^i}{\Delta t} \quad (1) [49]$$

\dot{Q}^i : heat transferred into the volume element from all sides during Δt

$\dot{E}_{\text{gen,element}}^i$: heat generated within the volume element during Δt

$\rho V_{\text{element}} C_p \frac{T_m^{i+1} - T_m^i}{\Delta t}$: change in the energy content of the volume element during Δt

$T_{m,n}^i$: the temperature at node (m, n) at time step i

Using equation (1) the temperature equations of all nodes can be found.

Note: $x = m\Delta x$, $y = n\Delta y$, and $t_i = i\Delta t$

4.2. Conduction coefficients (K_x and K_y), density (ρ), and specific heat (C_p) of the composite

As it has been shown in [7], that conduction heat transfer coefficients, specific heat, and density of composite materials are temperature dependent. Since the composite temperature varies during the process, it is of high importance to include the values of longitudinal thermal conductivity(K_x), transverse thermal conductivity(K_y), density(ρ), and specific heat(C_p) as functions of composite temperature in the model.

Table 4.1: Conduction heat transfer coefficients, specific heat, and density of AS4/APC-2 [7].

T in °C	K_x in W/(m.K)	K_y in W/(m.K)	ρ in Kg / m ³	C_p in J / (Kg.K)
0	3.5	0.42	1601	800
50	4.6	0.52	1598	930
100	5.1	0.6	1593	1040
150	5.9	0.7	1586	1260
200	5.9	0.7	1575	1300
250	6.1	0.7	1563	1400
300	6.7	0.75	1551	1550
350	6.8	0.68	1537	1650

The temperature dependent material properties (table 4.1) have been fitted with the following equations (equations 2 to 5).

$$K_x(T) = -2 \times 10^{-5}T^2 + 0.016 T + 3.667 \quad (2) [15]$$

$$K_y(T) = -5 \times 10^{-6}T^2 + 0.0024 T + 0.417 \quad (3) [15]$$

$$\rho(T) = -0.0004T^2 - 0.055T + 1601.6 \quad (4) [15]$$

$$C_p(T) = -0.0012T^2 + 2.8298T + 797.08 \quad (5) [15]$$

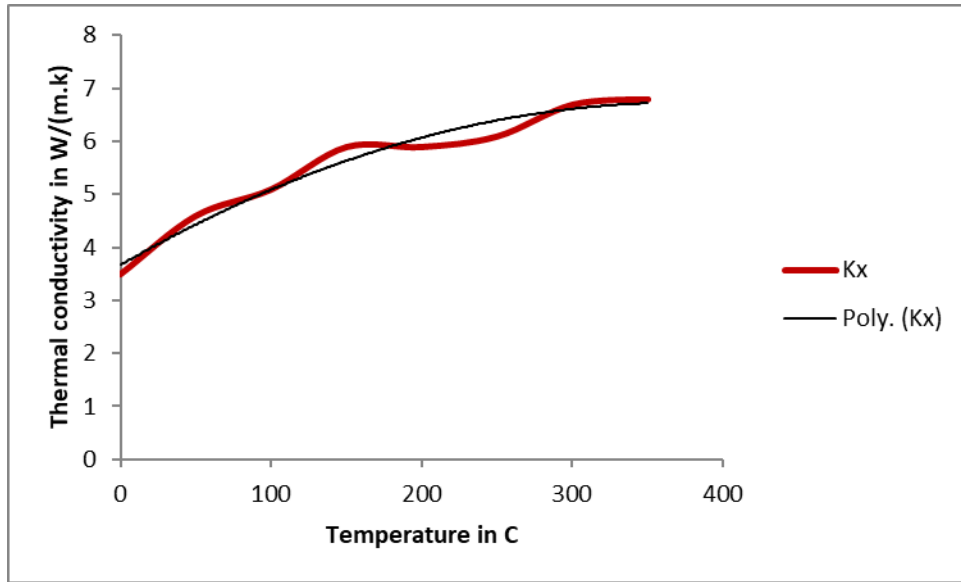


Figure 4.1: Longitudinal thermal conductivity(K_x) of AS4/APC-2, experimental and fitted curve

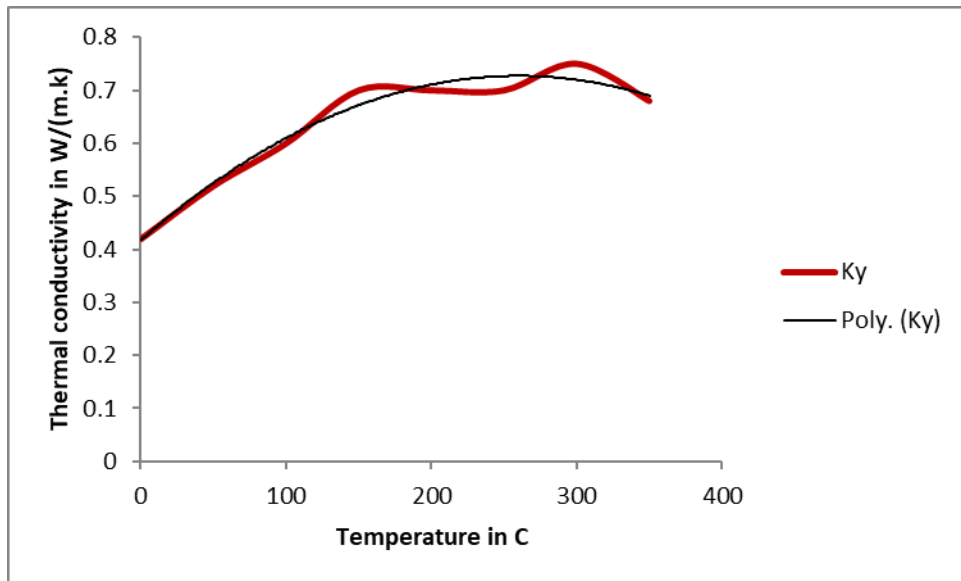


Figure 4.2: Transverse thermal conductivity(K_y) of AS4/APC-2, experimental and fitted curve

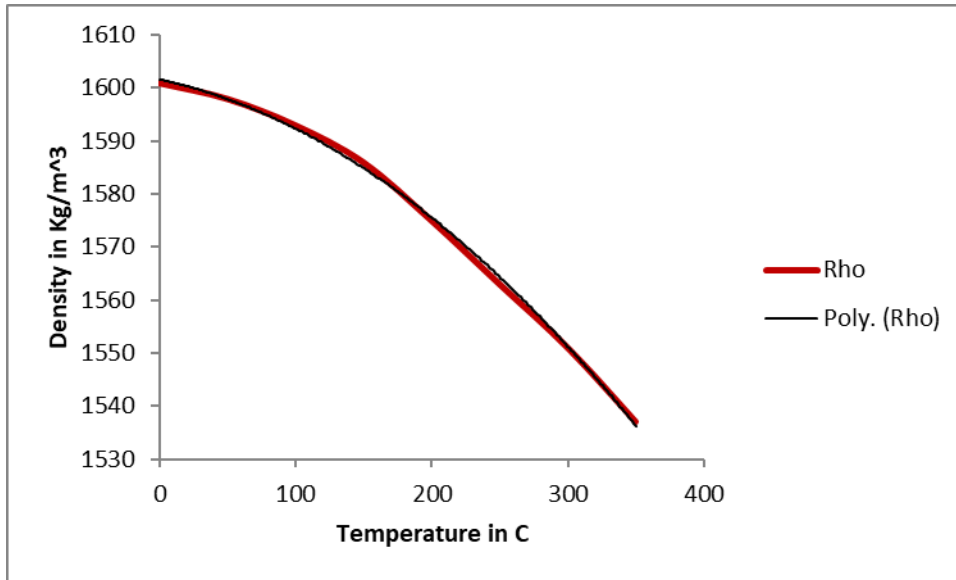


Figure 4.3: Density(ρ) of AS4/APC-2, experimental and fitted curve

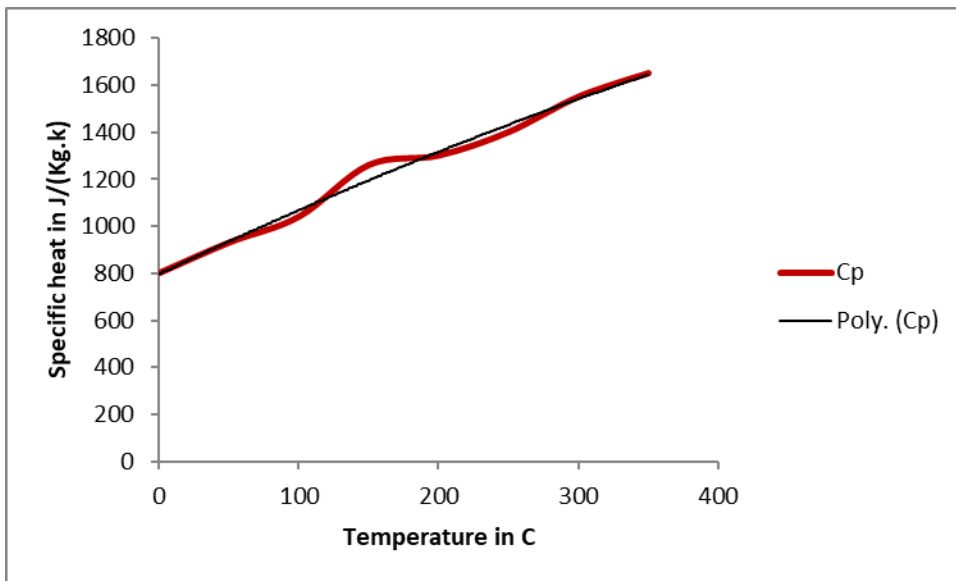


Figure 4.4: Specific heat(C_p) of AS4/APC-2, experimental and fitted curve

4.3. Conduction coefficient (K_m), density (ρ_m), and specific heat (C_{pm}) of the tool

An aluminum flat paddle tool is used in this study. Hence, conduction coefficient, density, and specific heat are equal to $237W/(mK)$, $2700Kg/m^3$, and $905J/(Kg.K)$, respectively [9].

4.4. Inter-layer thermal contact resistance

In practice, there is no perfectly smooth surface. In other words, microscopic peaks and valleys exist in any surfaces such as composites and metals. By pressing two surfaces, peaks create perfect contacts at the interface. Nonetheless, the valleys form gaps filled with a fluid such as air (imperfect contact). This means that there are many air gaps with different sizes at the interface, and these air gaps resist heat transfer (insulator). This phenomenon is called thermal contact resistance, and its value is highly dependent upon the roughness of surfaces at the interface. Type of fluid, temperature, and pressure at the interface are other factors, which could affect thermal contact resistance [49].

Levy et al. [42,43] and Kollmannsberger et al. [44] showed that improper bonding causes inter-layer thermal contact resistance in composites. Inter-layer thermal contact resistance causes the thermal conductivities of composites through the thickness to change [42]. Thus, the inter-layer thermal contact resistance affects the accuracy of heat transfer models, and it could have major effects in results for poor quality composites due to improper bonding.

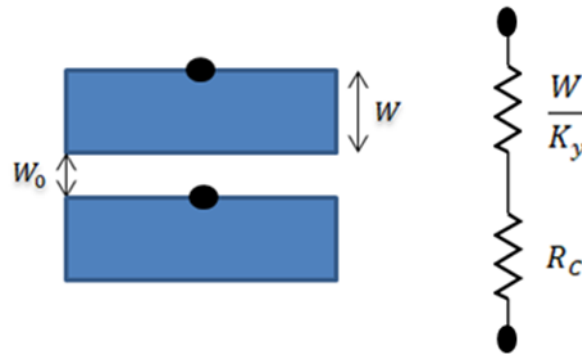


Figure 4.5: Model of inter-layer thermal contact resistance

Source: [15]

In real life, the value of inter-layer thermal contact resistance might differ from one layer to another. This occurs mainly due to different air gap sizes (different surface roughness) at the interfaces. In this study a constant inter-layer thermal contact resistance (R_c) is assumed, and the model used in the finite difference model is shown in figure 4.5. The model indicates how the thermal conductivity of the composite in Y direction (through the thickness) varies from node to node due to the thermal contact resistance. The width of each composite layer and the width of asperity or gap between layers (imperfect bonding) are denoted by W and W_0 , respectively. Although by assuming a constant inter-layer thermal contact resistance some accuracy might be lost, the complexity of the problem and number of unknowns reduce significantly. The validity of this assumption has been indicated by comparing the theoretical results to experimental ones in the section 6. Kollmannsberger et al. [44], also, assumed a constant inter-layer thermal contact resistance in their study. The inter-layer thermal contact resistance (R_c) affects the thermal conductivity through the thickness, so the thermal conductivity of the composite through the

thickness (K_y) needs to be replaced by the effective thermal conductivity through the thickness ($K_{y'}$).

$$\frac{W+W_0}{K_{y'}(T)} = \frac{W}{K_y(T)} + R_c \rightarrow K_{y'}(T) = \left(\frac{K_y(T)}{W+R_c K_y(T)} \right) (W + W_0) \quad (6) [15]$$

The effective composite thermal conductivity in Y direction ($K_{y'}(T)$) is shown in the equation (6). In ideal conditions ($R_c = W_0 = 0$) the effective thermal conductivity through the thickness ($K_{y'}$) would be equal to the thermal conductivity through the thickness (K_y). In this study, the inter-layer thermal contact resistance (R_c) have been found and presented in section 4.9.4.

4.5. Global and local coordinate systems

Global coordinate system (XY): the horizontal axis (X) is along the length of composite and motion of the hot gas torch. The vertical axis (Y) is through the thickness of composite laminate, and its origin (O) is located at the top left corner of the composite (figure 4.6).

Local coordinate system ($X'Y'$): is a moving coordinate system. The horizontal axis (X') is along the length of composite and motion of the hot gas torch. The vertical axis (Y') is through the thickness of composite laminate (figure 4.6). It is assumed that the maximum temperature of the hot gas in the vicinity of the laminate is equal to the hot gas torch temperature (875°C). Since the torch moves along the X-axis with a constant speed (25.4 mm/s) the location of the maximum temperature of hot gas (T_{max}) changes with respect to X-axis. The origin of the horizontal axis of local coordinate system ($x' = 0$) is defined to be at the location of maximum hot gas temperature (T_{max}) at each time (t). At the beginning of the process ($t = 0$) the torch is at $x = 0$. Thus, the horizontal distance between the two origins at time (t) is equal to $d = vt$.

4.6. Hot gas/air temperature and convection coefficient distributions in the vicinity of laminate (T_k and h_k , $k = 1,2$)

The heat source is a hot gas torch in this study, and it moves above the substrate. Hence, the determination of both hot gas/air temperature and convection coefficient distributions in the vicinity of laminate (thermal inputs) is of high importance.

In this study the laminate is split into two different zones with respect to the local coordinate system ($X'Y'$), which are called zone one and zone two.

Zone 1 (upstream): This zone is located at the negative side of horizontal local coordinate system ($x' < 0$) at any time (t). The length of this zone (L_1) changes with respect to time, and it is equal to $L_1(t) = vt$. The hot gas/air temperature and convection coefficient distributions in the vicinity of laminate above this zone are denoted by T_1 and h_1 , respectively (figure 4.6).

Zone 2 (downstream): This zone is located at the positive side of horizontal local coordinate system ($x' > 0$) at any time (t). The length of this zone (L_2) changes with respect to time, and it is equal to $L_2(t) = \text{length of composite} - L_1(t)$. The hot gas/air temperature and convection coefficient distributions in the vicinity of laminate above this zone are denoted by T_2 and h_2 , respectively (figure 4.6).

As it is illustrated in figure 4.6, the maximum values of both hot gas/air temperature and convection coefficient (T_{max} and h_{max}) are located at $X' = 0$ at any time (convection coefficient is a temperature dependent parameter).

Since the hot gas/air temperature cannot drop suddenly from its maximum value (T_{max}) to its minimum value (room temperature) in practice, a decreasing distribution is assumed for the hot gas/air temperature in the vicinity of the laminate. Convection coefficients are temperature dependent parameters. As a result, it is assumed that there is a linear relationship between the hot gas/air temperature and convection coefficient in the vicinity of the laminate.

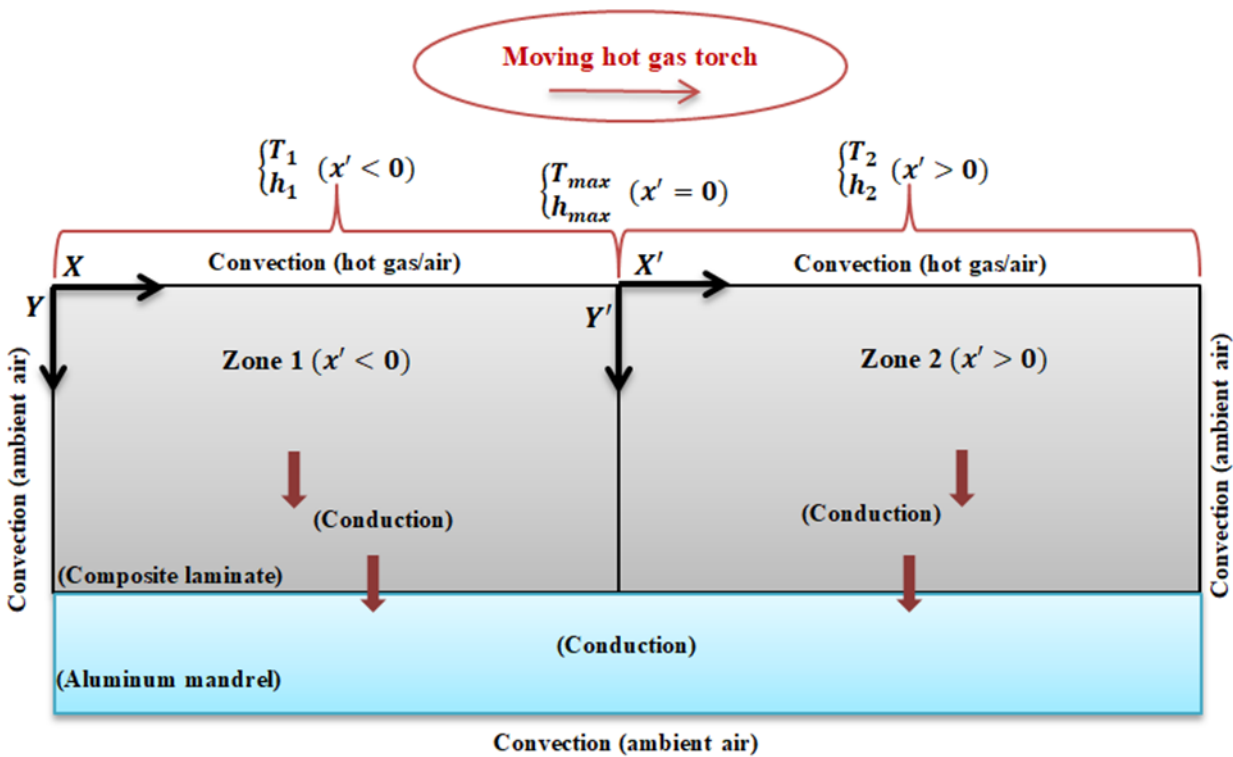


Figure 4.6: Two different zones with respect to the local coordinate system ($x' = 0$)

Source: [15]

Having an accurate estimation of the temperature variation of composite laminate is impossible without finding proper approximations of both hot gas/air temperature and convection coefficient in the vicinity of laminate (thermal inputs). Hence, a big portion of this study was dedicated to the determination of mathematical models of the thermal inputs. The mathematical models of the thermal inputs and determination of its unknown parameters are presented in the section 4.9.

4.7. Formulations

The temperature equation of each node depends on its location in the composite or mandrel, and it is found using the energy balance equation (1). Each node falls into two main categories, which are called interior nodes and boundary nodes.

4.7.1. Interior nodes

1. Composite laminate interior nodes (heat transfer only via conduction)

$$T_{m,n}^{i+1} = K_x \frac{\Delta t}{\rho C_p (\Delta x)^2} [T_{m-1,n}^i + T_{m+1,n}^i] + K_y \frac{\Delta t}{\rho C_p (\Delta y)^2} [T_{m,n-1}^i + T_{m,n+1}^i] + [1 - \frac{2\Delta t}{\rho C_p} (\frac{K_x}{(\Delta x)^2} + \frac{K_y}{(\Delta y)^2})] T_{m,n}^i \quad (7) \quad [15]$$

2. Mandrel(tool) interior nodes (heat transfer only via conduction)

$$T_{m,n}^{i+1} = K_m \frac{\Delta t}{\rho_m C_{pm} (\Delta x)^2} [T_{m-1,n}^i + T_{m+1,n}^i] + K_m \frac{\Delta t}{\rho_m C_{pm} (\Delta y_m)^2} [T_{m,n-1}^i + T_{m,n+1}^i] + [1 - \frac{2\Delta t k_m}{\rho_m C_{pm}} (\frac{1}{(\Delta x)^2} + \frac{1}{(\Delta y_m)^2})] T_{m,n}^i \quad (8) \quad [15]$$

4.7.2. Boundary nodes

A schematic of the boundary nodes is shown in figure 4.7.

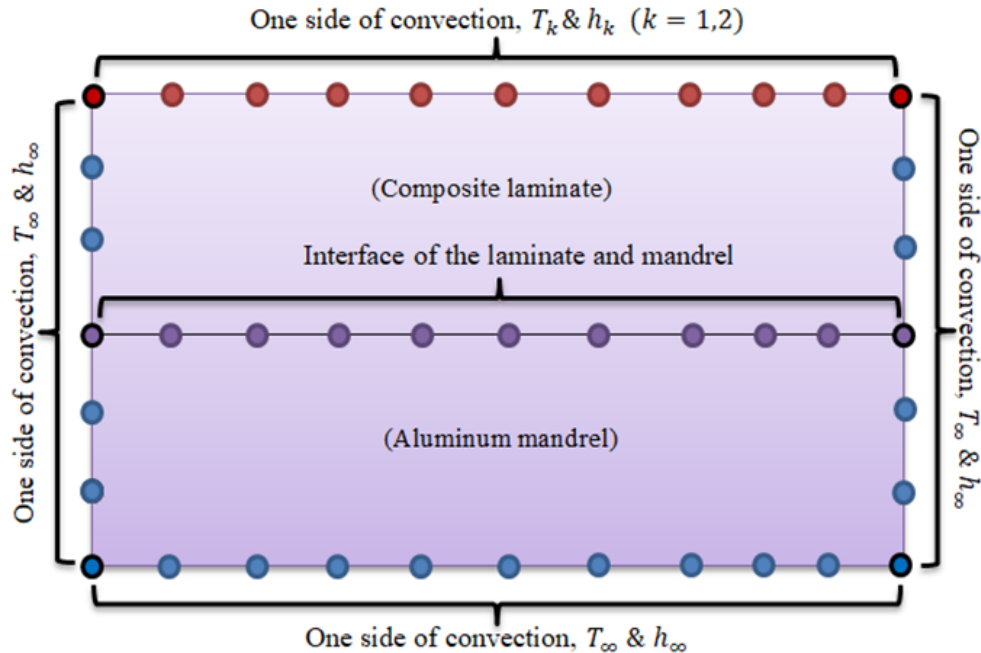


Figure 4.7: Schematic illustration of boundary nodes (composite laminate + aluminum mandrel)

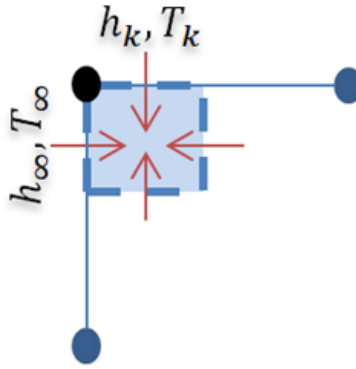
Source: [15]

There are two types of boundary conditions in this study, which are convection and interface boundary conditions.

4.7.2.1. *Boundary nodes which are not located at the interface of the laminate and mandrel (no interface boundary condition).*

1. *Two top corner nodes (two sides of convection)*

The top corner nodes are in heat exchange with the hot gas/air at the top (h_k and T_k) and ambient air (h_∞ and T_∞) at one side (the other two sides are exposed to heat transfer via conduction). Schematics for energy balances on the volume element of boundary nodes, which are not located at the interface, are illustrated above related formulas. The black node indicates the target node, and blue nodes indicate its adjacent nodes.

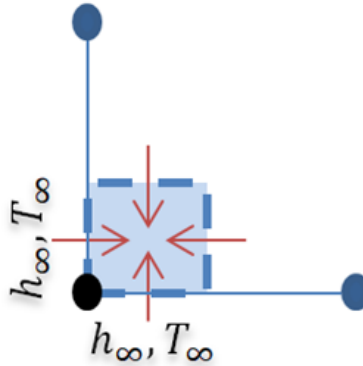


$$T_{1,j}^{i+1} = \frac{2\Delta t}{\rho C_p} \left[\frac{h_\infty T_\infty}{\Delta x} + \frac{h_k T_k}{\Delta y} + \frac{K_x T_{2,j}^i}{(\Delta x)^2} + \frac{K_y T_{1,j-1}^i}{(\Delta y)^2} \right] + \left[1 - \frac{2\Delta t}{\rho C_p} \left(\frac{h_\infty}{\Delta x} + \frac{h_k}{\Delta y} + \frac{k_x}{(\Delta x)^2} + \frac{k_y}{(\Delta y)^2} \right) \right] T_{1,j}^i \quad (9) [15]$$

$j = N + N_m + 1$. The temperature of top right corner node is found similarly.

2. *Two bottom corner nodes (two sides of convection)*

These nodes are in heat exchange with the ambient air at two sides.

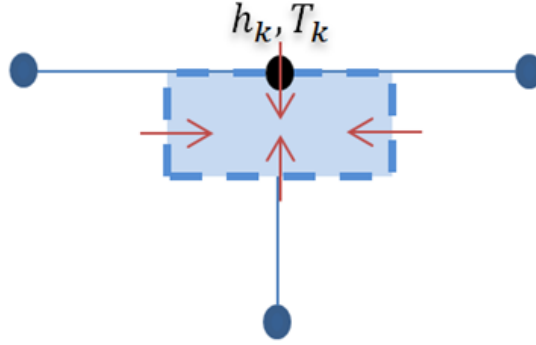


$$T_{1,1}^{i+1} = \frac{2\Delta t K_m}{\rho_m c_{pm}} \left[h_\infty T_\infty \left(\frac{1}{\Delta x} + \frac{1}{\Delta y_m} \right) + \frac{T_{2,1}^i}{(\Delta x)^2} + \frac{T_{1,2}^i}{(\Delta y_m)^2} \right] + \left[1 - \frac{2\Delta t K_m}{\rho_m c_{pm}} \left(h_\infty \left(\frac{1}{\Delta x} + \frac{1}{\Delta y_m} \right) + \frac{1}{(\Delta x)^2} + \frac{1}{(\Delta y_m)^2} \right) \right] T_{1,1}^i \quad (10) [15]$$

The temperature of bottom right corner node is found similarly.

3. Top boundary nodes with only one side of convection

The top boundary nodes except the two corner nodes are exposed to one side of heat transfer with the hot gas/air via convection.

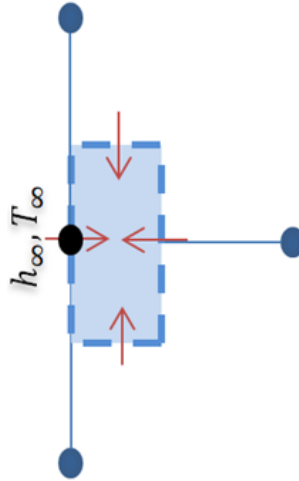


$$T_{m,j}^{i+1} = \frac{2\Delta t}{\rho c_p} \left[\frac{h_k T_k}{\Delta y} + \frac{K_x (T_{m-1,j}^i + T_{m+1,j}^i)}{2(\Delta x)^2} + \frac{K_y T_{m,j-1}^i}{(\Delta y)^2} \right] + \left[1 - \frac{2\Delta t}{\rho c_p} \left(\frac{h_k}{\Delta y} + \frac{K_x}{(\Delta x)^2} + \frac{K_y}{(\Delta y)^2} \right) \right] T_{m,j}^i \quad (11) [15]$$

$j = N + N_m + 1$ and $2 \leq m \leq M$.

4. Left, right, and bottom boundary nodes (only one side of convection)

The left, right, and bottom boundary nodes (except the corner nodes) are exposed to one side of heat transfer with the ambient air via convection.



$$T_{1,j}^{i+1} = \frac{2\Delta t}{\rho C_p} \left[\frac{h_\infty T_\infty}{\Delta x} + \frac{K_x T_{2,j}^i}{(\Delta x)^2} + \frac{K_{y'}(T_{1,j-1}^i + T_{1,j+1}^i)}{2(\Delta y)^2} \right] + \left[1 - \frac{2\Delta t}{\rho C_p} \left(\frac{h_\infty}{\Delta x} + \frac{K_x}{(\Delta x)^2} + \frac{K_{y'}}{(\Delta y)^2} \right) \right] T_{1,j}^i \quad (12) [15]$$

$2 \leq j \leq N + N_m$. Similarly, the temperatures of right and bottom boundary nodes are found.

4.7.2.2. Boundary nodes located at the interface of laminate and mandrel.

1. Boundary nodes at the leftmost or right most of the interface (One side of convection)

These boundary nodes are exposed to one side of heat transfer with the ambient air via convection.

$$T_{1,j}^{i+1} = \frac{2\Delta t}{\rho C_p} \left[\frac{h_\infty T_\infty}{\Delta x} + \frac{K_x T_{2,j}^i}{(\Delta x)^2} + \frac{K_{y'} T_{1,j+1}^i}{2\Delta y \Delta y_{avg}} + \frac{K_m T_{1,j-1}^i}{2\Delta y_m \Delta y_{avg}} \right] + \left[1 - \frac{2\Delta t}{\rho C_p} \left(\frac{h_\infty}{\Delta x} + \frac{K_x}{(\Delta x)^2} + \frac{K_{y'}}{2\Delta y \Delta y_{avg}} + \frac{K_m}{2\Delta y_m \Delta y_{avg}} \right) \right] T_{1,j}^i \quad (13) [15]$$

$j = N_m + 1$. The temperature of the rightmost node is found similarly.

$$\text{Note: } \Delta y_{avg} = \frac{\Delta y + \Delta y_m}{2}$$

2. Interface nodes without convection

$$T_{m,j}^{i+1} = \frac{\Delta t}{\rho C_p} \left[\frac{K_x T_{m-1,j}^i}{(\Delta x)^2} + \frac{K_x T_{m+1,j}^i}{(\Delta x)^2} + \frac{K_{y'} T_{m,j+1}^i}{\Delta y \Delta y_{avg}} + \frac{K_m T_{m,j-1}^i}{\Delta y_m \Delta y_{avg}} \right] + \left[1 - \frac{\Delta t}{\rho C_p} \left(\frac{2K_x}{(\Delta x)^2} + \frac{K_{y'}}{\Delta y \Delta y_{avg}} + \frac{K_m}{\Delta y_m \Delta y_{avg}} \right) \right] T_{m,j}^i \quad (14) [15]$$

$j = N_m + 1$ and $2 \leq i \leq M$.

The ambient air temperature (T_∞) is equal to 25°C, and its convection coefficient (h_∞) is equal to 10 W/(m²K) [50]. The hot gas/air temperature (T_k) and convection coefficient (h_k) distributions in the vicinity of laminate (thermal inputs) were determined in this study using mathematical models, and it would be presented in the section 4.9.

4.8. Stability criterion

Although the explicit method is easier to use rather than implicit method, it is not unconditionally stable due to time stability issue. Thus, the upper limit of time step (Δt) needs to be determined. In order to do so, all the primary coefficients (coefficients of $T_{m,n}^i$) are to be greater than or equal to zero [49].

Table 4.2: Primary coefficients and stability criterion

Source: [15]

Equation number	Primary coefficient	Stability criterion
(7)	$1 - \frac{2\Delta t}{\rho C_p} \left(\frac{K_x}{(\Delta x)^2} + \frac{K_{y'}}{(\Delta y)^2} \right)$	$\Delta t \leq \frac{\rho C_p}{2 \left(\frac{K_x}{(\Delta x)^2} + \frac{K_{y'}}{(\Delta y)^2} \right)}$
(8)	$1 - \frac{2\Delta t k_m}{\rho_m C_{pm}} \left(\frac{1}{(\Delta x)^2} + \frac{1}{(\Delta y_m)^2} \right)$	$\Delta t \leq \frac{\rho_m C_{pm}}{2 k_m \left(\frac{1}{(\Delta x)^2} + \frac{1}{(\Delta y_m)^2} \right)}$
(9)	$1 - \frac{2\Delta t}{\rho C_p} \left(\frac{h_\infty}{\Delta x} + \frac{h_k}{\Delta y} + \frac{k_x}{(\Delta x)^2} + \frac{k_{y'}}{(\Delta y)^2} \right)$	$\Delta t \leq \frac{\rho C_p}{2 \left(\frac{h_\infty}{\Delta x} + \frac{h_k}{\Delta y} + \frac{k_x}{(\Delta x)^2} + \frac{k_{y'}}{(\Delta y)^2} \right)}$
(10)	$1 - \frac{2\Delta t K_m}{\rho_m C_{pm}} \left(h_\infty \left(\frac{1}{\Delta x} + \frac{1}{\Delta y_m} \right) + \frac{1}{(\Delta x)^2} + \frac{1}{(\Delta y_m)^2} \right)$	$\Delta t \leq \frac{\rho_m C_{pm}}{2 K_m \left(h_\infty \left(\frac{1}{\Delta x} + \frac{1}{\Delta y_m} \right) + \frac{1}{(\Delta x)^2} + \frac{1}{(\Delta y_m)^2} \right)}$
(11)	$1 - \frac{2\Delta t}{\rho C_p} \left(\frac{h_k}{\Delta y} + \frac{k_x}{(\Delta x)^2} + \frac{k_{y'}}{(\Delta y)^2} \right)$	$\Delta t \leq \frac{\rho C_p}{2 \left(\frac{h_k}{\Delta y} + \frac{k_x}{(\Delta x)^2} + \frac{k_{y'}}{(\Delta y)^2} \right)}$
(12)	$1 - \frac{2\Delta t}{\rho C_p} \left(\frac{h_\infty}{\Delta x} + \frac{k_x}{(\Delta x)^2} + \frac{k_{y'}}{(\Delta y)^2} \right)$	$\Delta t \leq \frac{\rho C_p}{2 \left(\frac{h_\infty}{\Delta x} + \frac{k_x}{(\Delta x)^2} + \frac{k_{y'}}{(\Delta y)^2} \right)}$
(13)	$1 - \frac{2\Delta t}{\rho C_p} \left(\frac{h_\infty}{\Delta x} + \frac{K_x}{(\Delta x)^2} + \frac{k_{y'}}{2\Delta y \Delta y_{avg}} + \frac{K_m}{2\Delta y_m \Delta y_{avg}} \right)$	$\Delta t \leq \frac{\rho C_p}{2 \left(\frac{h_\infty}{\Delta x} + \frac{K_x}{(\Delta x)^2} + \frac{k_{y'}}{2\Delta y \Delta y_{avg}} + \frac{K_m}{2\Delta y_m \Delta y_{avg}} \right)}$
(14)	$1 - \frac{2\Delta t}{\rho C_p} \left(\frac{K_x}{(\Delta x)^2} + \frac{k_{y'}}{2\Delta y \Delta y_{avg}} + \frac{K_m}{2\Delta y_m \Delta y_{avg}} \right)$	$\Delta t \leq \frac{\rho C_p}{2 \left(\frac{K_x}{(\Delta x)^2} + \frac{k_{y'}}{2\Delta y \Delta y_{avg}} + \frac{K_m}{2\Delta y_m \Delta y_{avg}} \right)}$

All the equations in table 4.2 are solved to find the time steps. Among the obtained time steps, the minimum value is selected ($\Delta t = 0.001s$). Since the density, specific heat, and convection and conduction coefficients of the composite are functions of temperature, their maximum or minimum values are used to determine the lowest upper limit of time step (min density and specific heat, max convection, and conduction coefficients). To make sure that the results are stable, different values of time steps such as 0.002, 0.0013, 0.0016, 0.0006, and 0.0008s were tested in addition to 0.001s. By doing so, the theoretical results varied no more than 0.03%.

4.9. Determination of the thermal inputs (T_k and h_k)

4.9.1. Non-linear models

In order to determine the hot gas/air temperature and convection coefficient distributions in the vicinity of laminate (thermal inputs), non-linear models were developed in this study. Since the hot gas/air temperature does not drop suddenly from the highest temperature ($T_{max} = 875^\circ C$) to room temperature ($T_\infty = 25^\circ C$), a decreasing exponential function was assumed for the input temperature (T_k). Convection coefficients are temperature dependent parameters [49]. As a result, it was assumed that there is a linear relationship between the two thermal inputs (T_k and h_k). In other words, the convection coefficient in the vicinity of laminate (h_k) is a linear function of the hot gas/air temperature in the vicinity of laminate (T_k).

In this study, inter-layer thermal contact resistance is added to the heat transfer model to increase the accuracy of the theoretical results. To reduce the complexity of the problem, the thermal inputs were determined in two stages. In the first stage, the inter-layer thermal contact resistance is neglected. Then in the second stage, the inter-layer thermal contact resistance is added to the model.

The non-linear distribution of the hot gas/air temperature in the vicinity of laminate (input temperature) is illustrated in figure 4.8. The laminate is split into two zones with respect to the local coordinate system (figure 4.6), and the thermal inputs (T_k and h_k) are to be determined for each of these two zones ($k = 1,2$). The maximum of hot gas/air temperature (T_{max}) is at $x' = 0$ at any time (t). Then, it decreases exponentially at both sides ($x' < 0$ and $x' > 0$) to the room temperature (25°C). The characteristics of each zone are as follows:

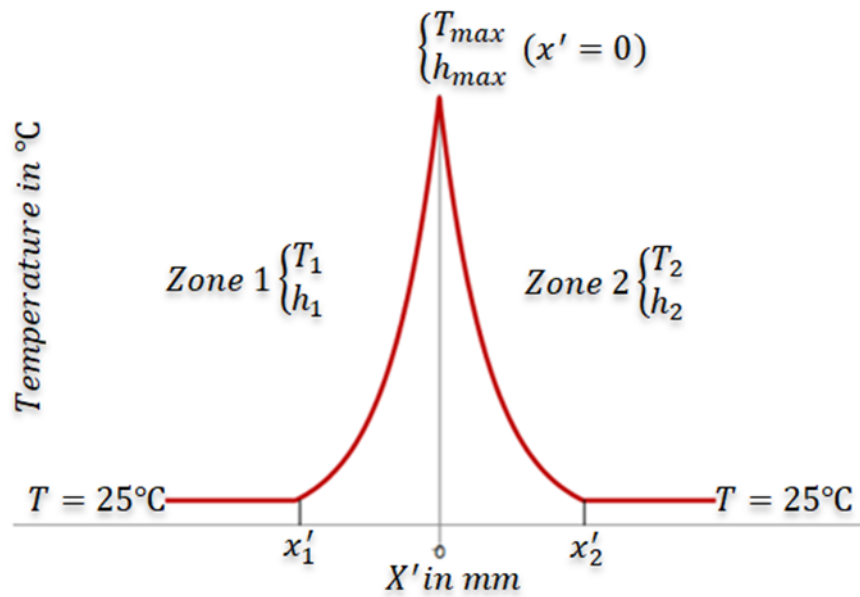


Figure 4.8: General features of input distribution

Source: [15]

Zone 1:

The following are assumed.

$$T_1(x') = \begin{cases} 25 & x' < x'_1 \\ a_1 e^{-b_1 x'} & x'_1 \leq x' \end{cases} \quad (15) [15]$$

It is assumed that the convection coefficient in zone 1 (h_1) varies linearly with respect to the hot gas/air temperature in this zone (T_1). Thus, the following model is considered for the convection coefficient in the vicinity of laminate (h_1). The ambient air temperature (T_∞) is equal to 25°C , and its convection coefficient is equal to $10 \text{ W}/(\text{m}^2\text{K})$ [50].

$$h_1(T_1) = \begin{cases} 10 & x' < x'_1 \\ a_{11} T_1 + b_{11} & x'_1 \leq x' \end{cases} \quad (16) [15]$$

Since T_1 is a function of x' , h_1 could be expressed as a function of x' .

$$h_1(T_1(x')) = \begin{cases} 10 & x' < x'_1 \\ a_{11}a_1e^{-b_1x'} + b_{11} & x'_1 \leq x' \end{cases} \quad (17) [15]$$

Unknown coefficients for zone 1

There are five unknowns in the above equations ($x'_1, a_1, b_1, a_{11},$ and b_{11}), and some of which could be found using the boundary conditions.

$$\begin{cases} T_1(x' = 0) = T_{max} & (\text{hot gas torch temperature}) \\ T_1(x' = x'_1) = T_\infty & (\text{ambient temperature}) \end{cases} \quad (18) [15]$$

$$\begin{cases} h_1(T_1 = T_{max}) = h_{max} \text{ W}/(m^2K) \\ h_1(T_1 = T_\infty) = 10 \text{ W}/(m^2K) \end{cases} [50] \quad (19) [15]$$

By applying these conditions, the number of unknowns reduces to two (x'_1 and h_{max}).

$$T_1(x' = 0) = T_{max} \rightarrow a_1 = T_{max} = 875^\circ\text{C} \quad (20) [15]$$

$$T_1(x' = x'_1) = T_\infty \rightarrow b_1 = -\frac{\ln\left(\frac{T_\infty}{T_{max}}\right)}{x'_1} = -\frac{\ln\left(\frac{25}{875}\right)}{x'_1} \quad (21) [15]$$

$$h_1(T_1 = T_{max}) = h_{max} \rightarrow b_{11} = h_{max} - a_{11}T_{max} = h_{max} - 875a_{11} \quad (22) [15]$$

$$h_1(T_1 = T_\infty) = 10 \rightarrow a_{11} = \frac{h_{max}-10}{T_{max}-T_\infty} = \frac{h_{max}-10}{875-25} \quad (23) [15]$$

In order to determine T_1 and h_1 , both x'_1 and h_{max} need to be calculated.

Zone 2:

Like zone one, the following equations are assumed for T_2 and h_2 .

$$T_2(x') = \begin{cases} a_2e^{b_2x'} & x' \leq x'_2 \\ 25 & x'_2 < x' \end{cases} \quad (24) [15]$$

$$h_2(T_2) = \begin{cases} a_{12}T_2 + b_{12} & x' \leq x'_2 \\ 10 & x'_2 < x' \end{cases} \quad (25) [15]$$

$$h_2(T_2(x')) = \begin{cases} a_{12}a_2e^{b_2x'} + b_{12} & x' \leq x'_2 \\ 10 & x'_2 < x' \end{cases} \quad (26) [15]$$

Unknown coefficients for zone 2

There are five unknowns in the above equations ($x'_2, a_2, b_2, a_{12},$ and b_{12}), and some of which could be found using the boundary conditions.

$$\begin{cases} T_2(x' = 0) = T_{max} & (\text{hot gas torch temperature}) \\ T_2(x' = x'_2) = T_{\infty} & (\text{ambient temperature}) \end{cases} \quad (27) [15]$$

$$\begin{cases} h_2(T_2 = T_{max}) = h_{max} & W/(m^2K) \\ h_2(T_2 = T_{\infty}) = 10 & W/(m^2K) \end{cases} [50] \quad (28) [15]$$

By applying these conditions, the number of unknowns reduces to two (x'_2 and h_{max}).

$$T_2(x' = 0) = T_{max} \rightarrow a_2 = T_{max} = 875^{\circ}\text{C} \quad (29) [15]$$

$$T_2(x' = x'_2) = T_{\infty} \rightarrow b_2 = \frac{\ln\left(\frac{T_{\infty}}{T_{max}}\right)}{x'_2} = \frac{\ln\left(\frac{25}{875}\right)}{x'_2} \quad (30) [15]$$

$$h_2(T_2 = T_{max}) = h_{max} \rightarrow b_{12} = h_{max} - a_{12}T_{max} = h_{max} - 875a_{12} \quad (31) [15]$$

$$h_2(T_2 = T_{\infty}) = 10 \rightarrow a_{12} = \frac{h_{max}-10}{T_{max}-T_{\infty}} = \frac{h_{max}-10}{875-25} \quad (32) [15]$$

To determine T_2 and h_2 , both x'_2 and h_{max} need to be found.

According to the above equations, there are totally three unknowns (h_{max} , x'_1 , and x'_2) in the proposed models.

4.9.2. Procedure to determine the unknown parameters (h_{max} , x'_1 , and x'_2)

In order to determine the above unknown parameters, the main focus needs to be on the node which is highly affected by convection (TC3). The procedure starts by some initial assumed values for h_{max} , x'_1 , and x'_2 . Using the MATLAB tool and initial values the theoretical temperature of the laminate (output temperature) is calculated. The output temperature distribution is then compared against the experimental temperature distribution. In order to do so, three error quantities are defined in the equations (33), (34), and (35). Figures 4.9, 4.10, and 4.11 show the location of application for these errors.

$$e_1 = \frac{(\text{experimental peak temperature} - \text{theoretical peak temperature})}{\text{experimental peak temperature}} \times 100 \quad (33) [15]$$

$$e_2 = \frac{(\text{experimental end temperature} - \text{theoretical end temperature})}{\text{experimental end temperature}} \times 100 \quad (34) [15]$$

$$e_3 = \frac{(\text{experimental rise time of temperature} - \text{theoretical rise time of temperature})}{\text{experimental rise time of temperature}} \times 100 \quad (35) [15]$$

End temperature: is the temperature of the composite at the end of process ($t = 20s$).

Rise time of temperature: is the time (t) at which the temperature of the composite starts to increase from the initial temperature (room temperature).

In this study, the same upper limit for all the three defined errors have been considered to avoid different levels of accuracy at rise time, peak temperature, and end temperature. High values of error contribute to less work and less accuracy in the theoretical results. Too small values of error lead to higher work and take lots of time (if achievable). Therefore, an upper limit equal to

5% is considered for the defined errors (e_1 , e_2 , and e_3). If all the errors are less than 5%, the assumed values of the parameters are accepted. If any of the errors is more than 5%, the assumed values for the unknown parameters are updated in an iterative process (flowchart shown in figure 4.12). The values of unknown parameters are updated based on the sign of defined errors (at each iteration) using the decision mechanism shown in table 4.3.

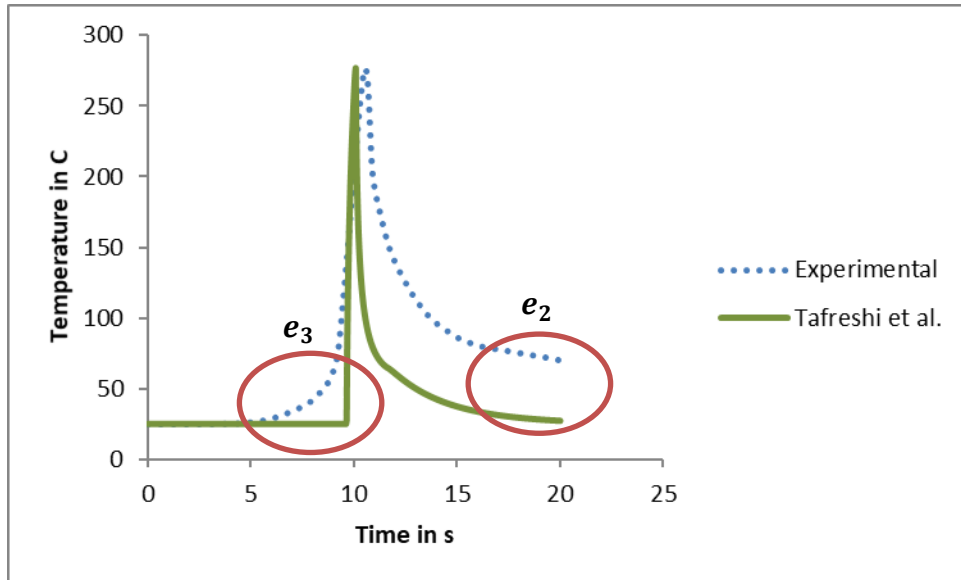


Figure 4.9: Illustration of the defined error quantities in the results obtained by Tafreshi et al. [11] in one layer below the top surface (TC3)

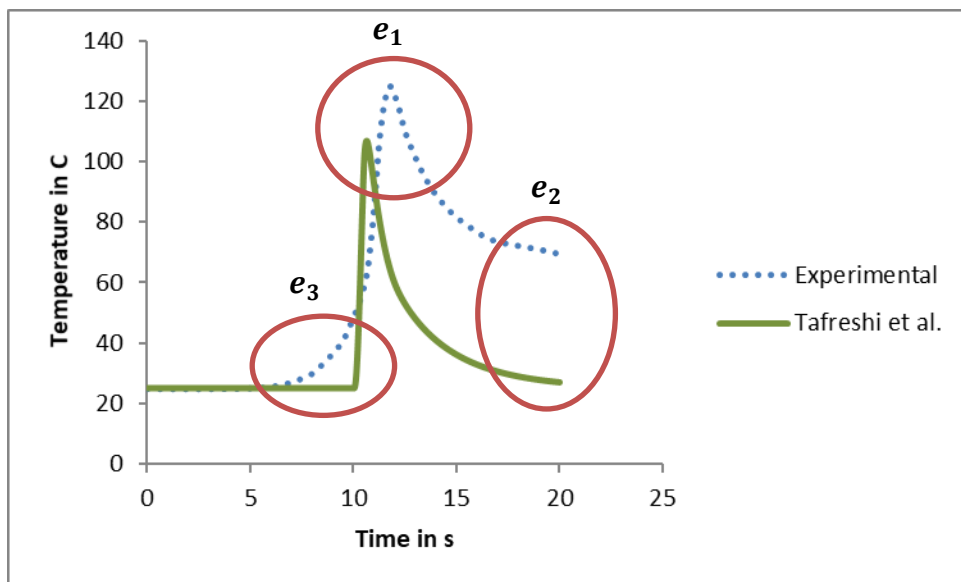


Figure 4.10: Illustration of the defined error quantities in the results obtained by Tafreshi et al. [11] in nine layers below the top surface (TC2)

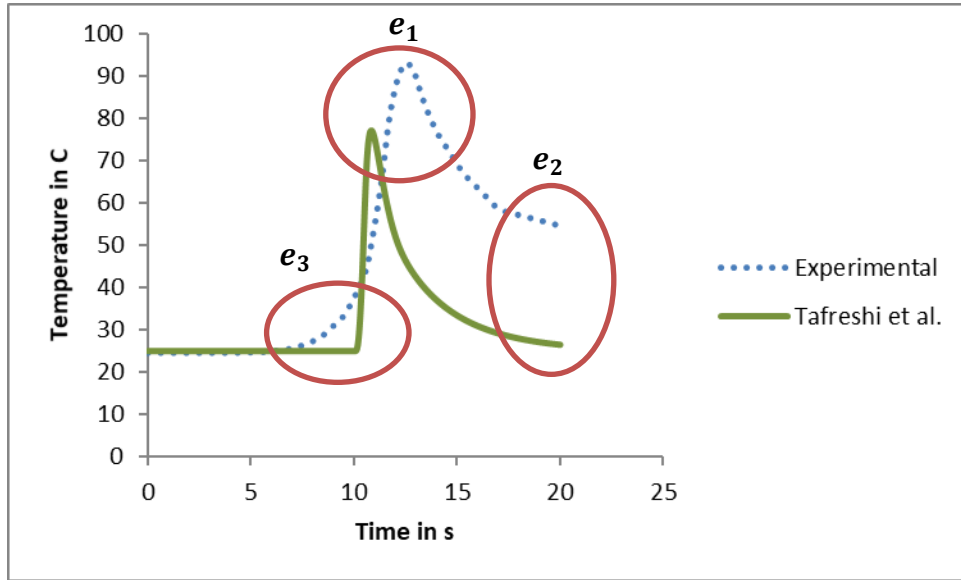


Figure 4.11: Illustration of the defined error quantities in the results obtained by Tafreshi et al. [11] in twelve layers below the top surface (TC1)

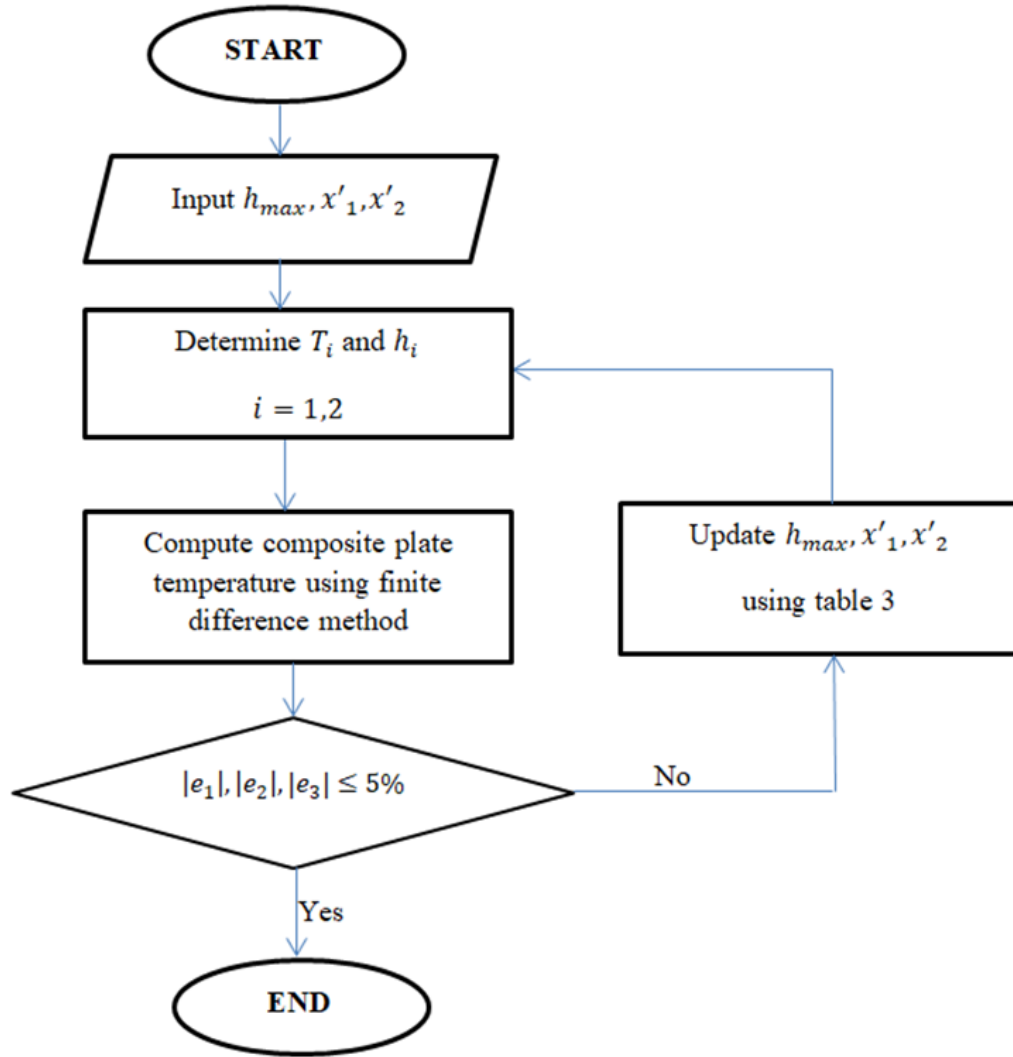


Figure 4.12: Procedure to determine the unknown parameters

Table 4.3: Decision mechanism based on the signs of e_i

		e_2		e_3	
		+	-	+	-
e_1	+	Increase h_{max} and/or decrease x'_1	Increase h_{max} and/or increase x'_1	Increase h_{max} and/or decrease x'_2	Increase h_{max} and/or increase x'_2
	-	Reduce h_{max} and/or decrease x'_1	Reduce h_{max} and/or increase x'_1	Reduce h_{max} and/or decrease x'_2	Reduce h_{max} and/or increase x'_2

4.9.3. Stage one of the determinations of unknown parameters (h_{max} , x'_1 , and x'_2)

At this stage, the inter-layer thermal contact resistance was neglected ($R_c = W_o = 0$). In other words, it was assumed that the effective thermal conductivity through the thickness ($K_{y'}$) is equal to the thermal conductivity through the thickness (K_y). The followings are assumed as the initial values.

$$h_{max} = 990 \text{ W}/(m^2K) \text{ [11]}, x'_1 = -100mm, \text{ and } x'_2 = 100mm$$

Then, the unknown coefficients are calculated using these initial values.

$$a_1 = 875, b_1 = -\frac{\ln\left(\frac{25}{875}\right)}{-100} \cong -0.04, a_{11} = \frac{990-10}{875-25} \cong 1.15, b_{11} = 990 - 875a_{11} \cong -18.82$$

$$a_2 = 875, b_2 = \frac{\ln\left(\frac{25}{875}\right)}{100} \cong -0.04, a_{12} = \frac{990-10}{875-25} \cong 1.15, b_{12} = 990 - 875a_{12} \cong -18.82$$

Using these values, the hot gas/air temperature and convection coefficient distributions in the vicinity of the laminate (thermal inputs) are shown in figures 4.13 and 4.14.

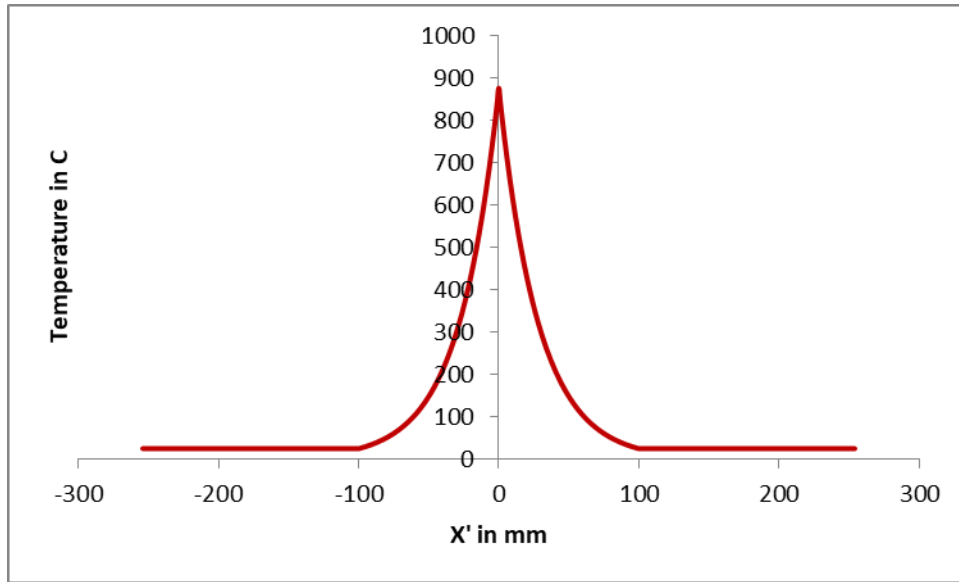


Figure 4.13: Initial input temperature distribution

Source: [15]

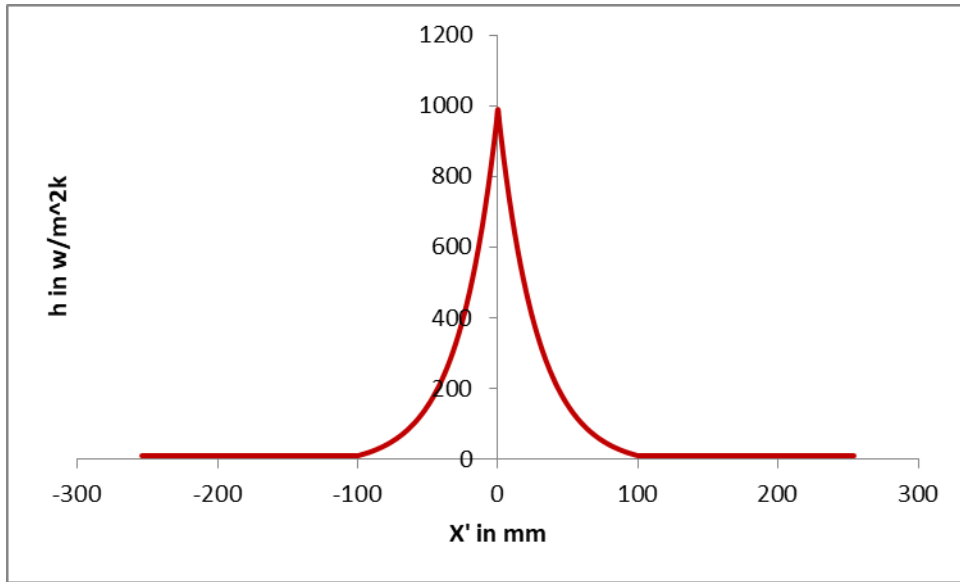


Figure 4.14: Initial convection coefficient distribution

Source: [15]

The theoretical laminate temperature (output temperature) distribution for TC3 (one layer below the top surface) is shown in figure 4.15.

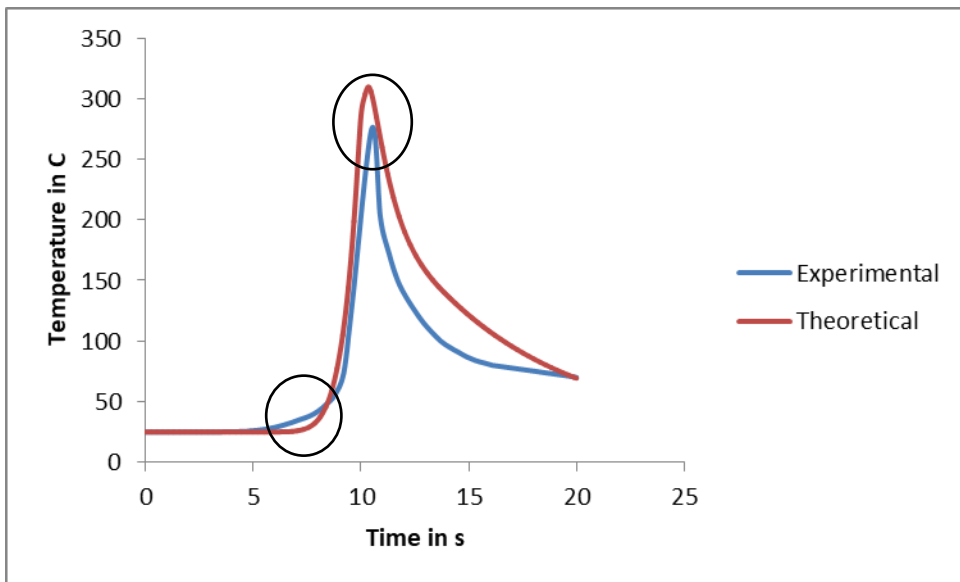


Figure 4.15: Laminate temperature distribution using the initial values of unknown parameters (TC3)

Source: [15]

From figure 4.15, e_1 and e_3 are not within the acceptable range. Therefore, the assumed values for the unknown parameters need to be modified based on table 4.3. These parameters could decrease and increase by five units at each iteration to obtain the desired values of $e_i (i = 1, 2)$.

After several iterations, the following results are obtained:

$$\left\{ \begin{array}{l} h_{max} = 990 \text{ W}/(m^2K) \\ x'_1 = -100 \text{ mm} \\ x'_2 = 100 \text{ mm} \end{array} \right. \xrightarrow{\text{updating } h_{max} \text{ \& } x'_1 \text{ \& } x'_2} \left\{ \begin{array}{l} h_{max} = 570 \text{ W}/(m^2K) \\ x'_1 = -90 \text{ mm} \\ x'_2 = 135 \text{ mm} \end{array} \right.$$

Next, the unknown coefficients are found using the updated values.

$$a_1 = 875, b_1 = -\frac{\ln\left(\frac{25}{875}\right)}{-90} \cong -0.04, a_{11} = \frac{570-10}{875-25} \cong 0.66, b_{11} = 570 - 875a_{11} \cong -7.5$$

$$a_2 = 875, b_2 = \frac{\ln\left(\frac{25}{875}\right)}{135} \cong -0.03, a_{12} = \frac{570-10}{875-25} \cong 0.66, b_{12} = 570 - 875a_{12} \cong -7.5$$

The updated distributions are shown in figures 4.16 and 4.17.

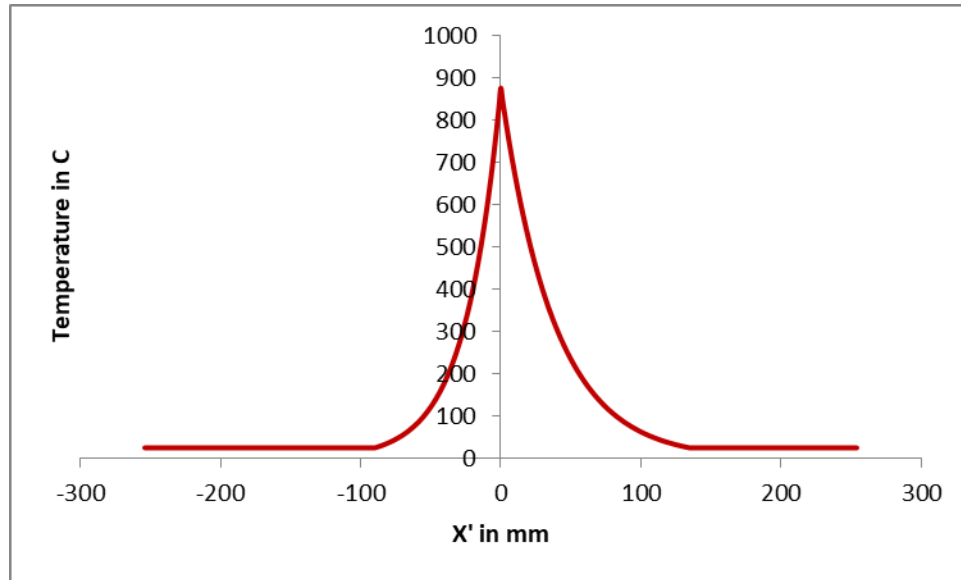


Figure 4.16: Updated input temperature distribution

Source: [15]

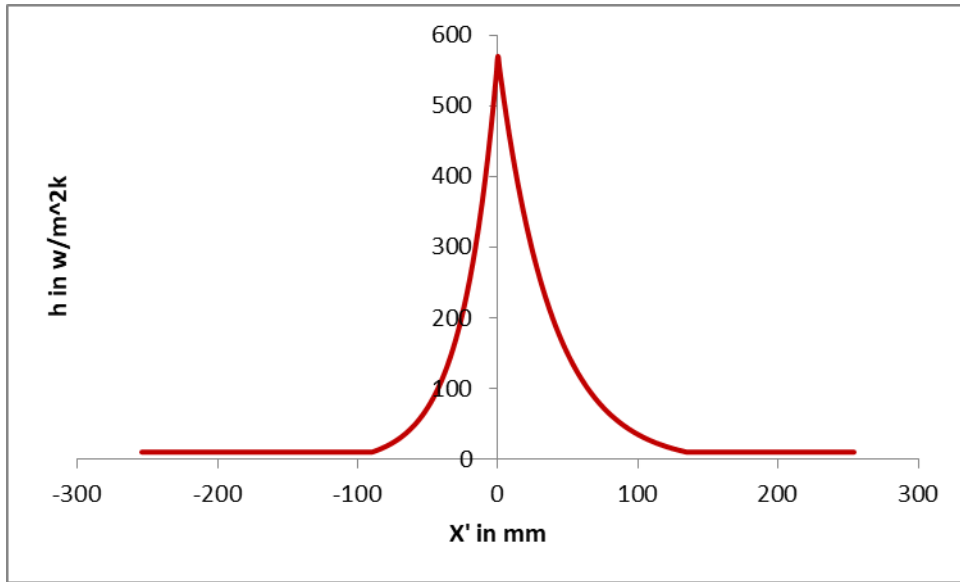


Figure 4.17: Updated convection coefficient

Source: [15]

Using these input distributions, the output temperature distribution for TC3 is shown in figure 4.18.

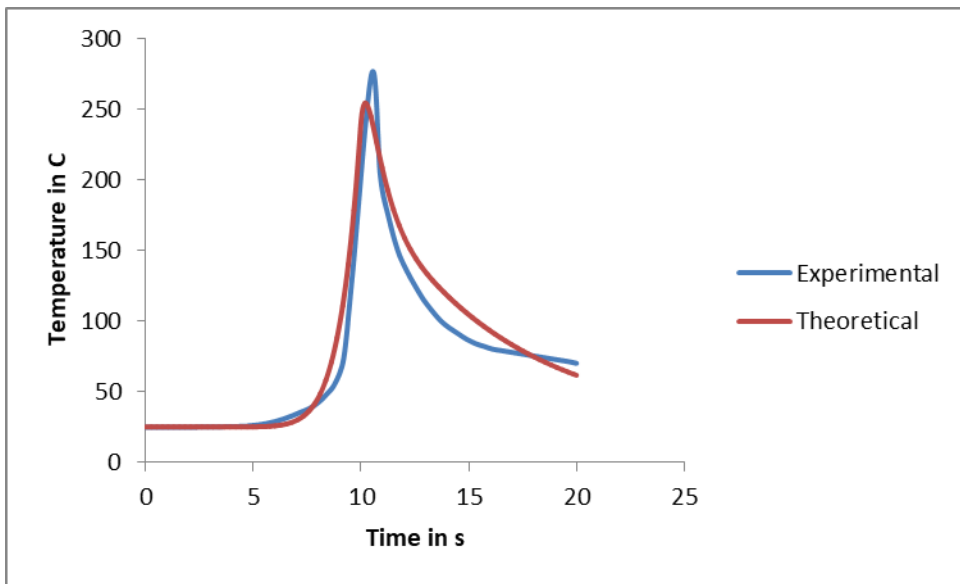


Figure 4.18: Laminate temperature distribution in one layer below the top surface (TC3) using the updated values of unknown parameters

Source: [15]

The updated values of unknown parameters (h_{max} , x'_1 , and x'_2) leads all the errors (e_1 , e_2 , e_3) to be within the acceptable range.

4.9.4. Stage two of the determinations of the unknown parameters (h_{max} , x'_1 , and x'_2)

The width of gap between layers or asperities (W_0) was estimated to be $21.1\mu m$ by Levy et al. [18]. Moreover, Levy et al. [18] showed that the inter-layer thermal contact resistance (R_c) varies from $5 \times 10^{-5} (m^2K)/W$ to $5 \times 10^{-4}(m^2K)/W$ depending on the temperature. In this study, a constant width of asperities ($W_0 = 21.1 \mu m$ [42]) and a constant inter-layer thermal contact resistance (R_c) is assumed. Then, the inter-layer thermal contact resistance (R_c) is estimated using the provided range by Levy et al. [42]. To do so, the output temperature (composite temperature) is computed for the provided range of inter-layer thermal contact resistance (R_c) in [42] (*starting from* $5 \times 10^{-5} (m^2K)/W$ *with* $\Delta R_c = 4.5 \times 10^{-6}$). The three defined errors (equations 33, 34, and 35) were calculated for each value of the inter-layer thermal contact resistance (R_c). The value of inter-layer thermal contact resistance, which leads to the minimum errors ($e_1, e_2, \text{ and } e_3$), is selected for this study. The following results were obtained by following the mentioned procedure in this stage, and the output temperature is indicated in figure 4.19.

$$\begin{cases} h_{max} = 570 \text{ W}/(m^2K) \\ x'_1 = -90 \text{ mm} \\ x'_2 = 135 \text{ mm} \end{cases} \quad \begin{cases} R_c = 6 * 10^{-5} (m^2K)/W \\ W_0 = 21.1 \mu m [42] \end{cases}$$

Using the above values as the unknown parameters, the following results are obtained.

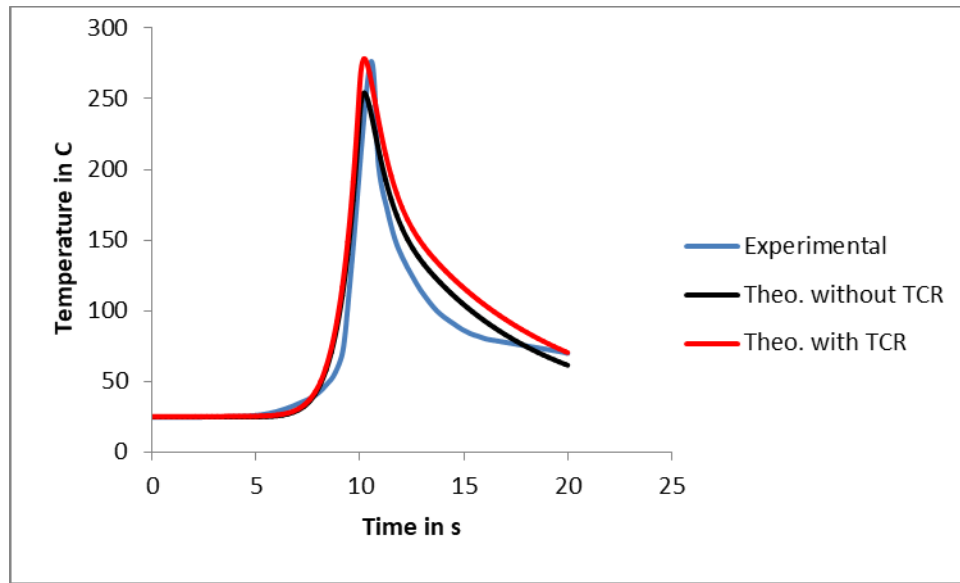


Figure 4.19: Laminate temperature distribution in one layer below the top surface (TC3) with and without inter-layer thermal contact resistance

Source: [15]

In figure 4.19, the graphs “Theo. without TCR” and “Theo. with TCR” show the theoretical results obtained in this study by neglecting and considering the inter-layer thermal contact resistance, respectively. Considering the inter-layer thermal contact resistance in the heat transfer model causes the accuracy of the theoretical results to improve. This improvement occurs mainly at the peak and end temperature of the theoretical results. However, figure 4.19 indicates that the effect of inter-layer thermal contact resistance is not significant in this study. This is an indication of proper bonding between layers and quality of the test specimen manufactured by the AFP machine available at Concordia University.

4.9.5. Validation of the model through the thickness using experimental results

The experiments were performed by Tafreshi et al. [11], and a summary of the experimental work has been provided in chapter 3. According to figure 4.19, the results obtained from the heat transfer model are in good agreements with experimental results for TC3, which is located one layer below the top surface of the laminate. To validate the heat transfer model, it is essential to compare the theoretical temperature of the laminate with the experimental temperature of laminate through the thickness (TC2 and TC1).

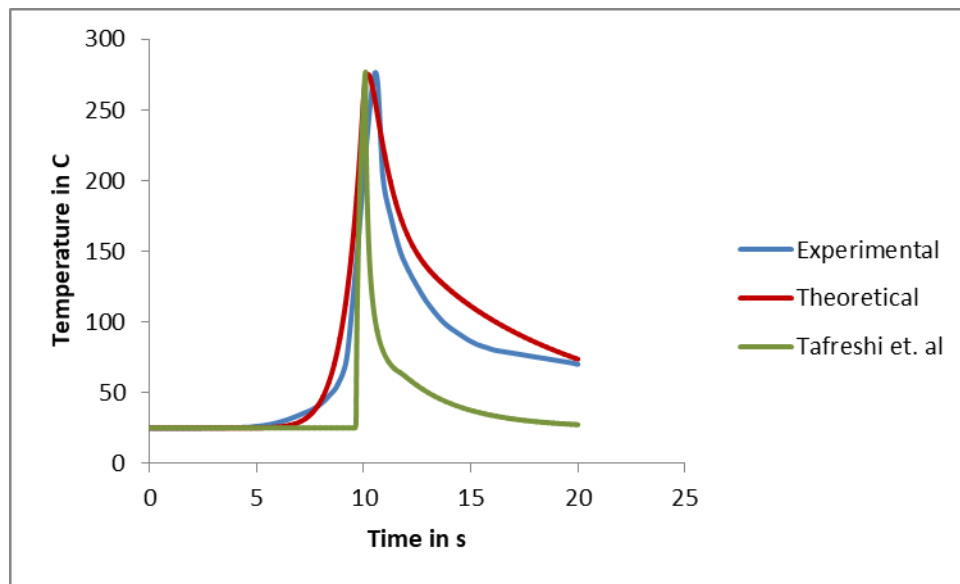


Figure 4.20: Laminate temperature distribution in one layer below the top surface (TC3) considering inter-layer thermal contact resistance

Source: [15]

Note: “Theoretical” graph illustrates the theoretical results obtained in this study.

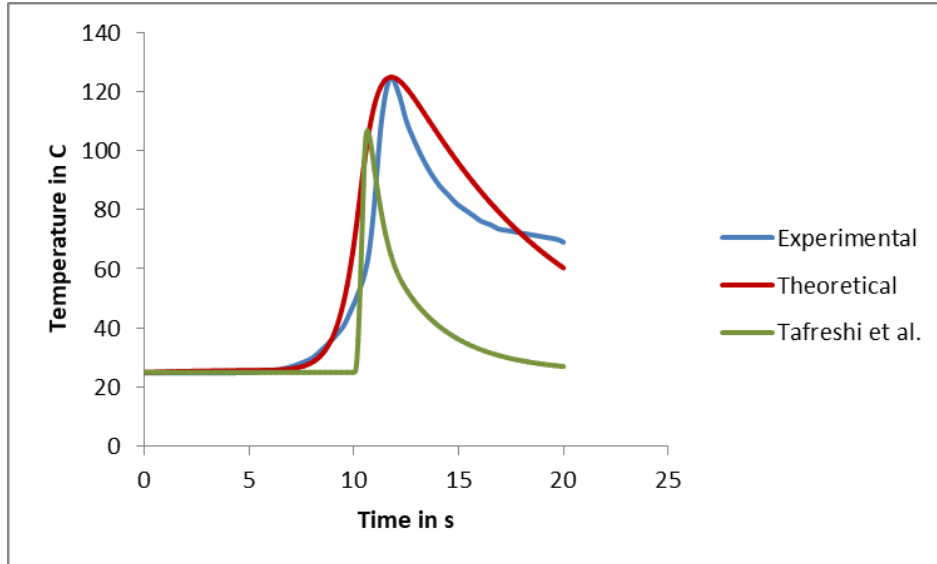


Figure 4.21: Laminate temperature distribution in nine layers below the top surface (TC2) considering inter-layer thermal contact resistance

Source: [15]

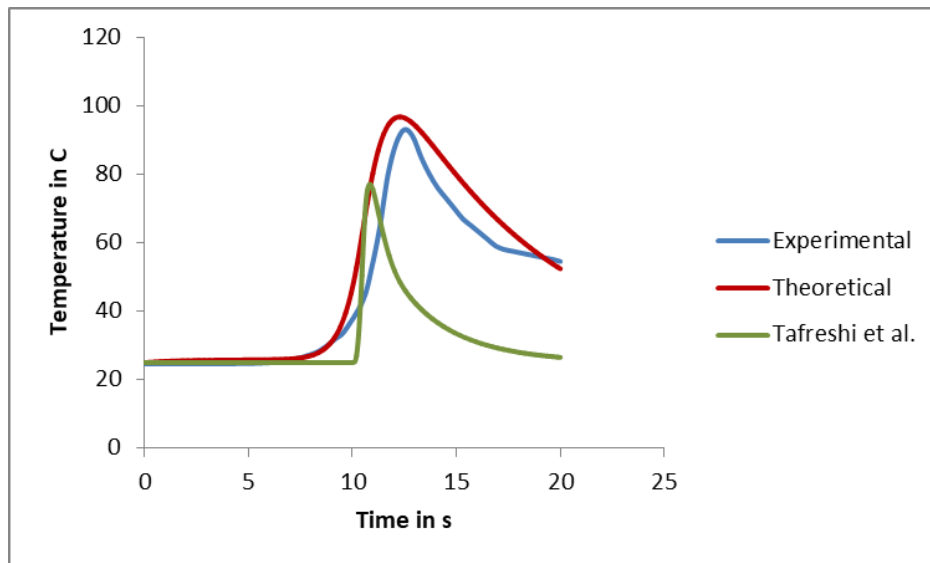


Figure 4.22: Laminate temperature distribution in twelve layers below the top surface (TC1) considering inter-layer thermal contact resistance

Source: [15]

According to the figures 4.20 to 4.22, the followings could be concluded for heat transfer analysis of composites made by AFP using hot gas troch:

1. Hot gas/air temperature and convection coefficient distributions in the vicinity of substrate (thermal inputs) play major role in the accuracy of the theoretical results, and their distributions need to be determined.
2. The effects of inter-layer thermal contact resistance could be high in substrates with improper bonding, so it should be considered and investigated in heat transfer analysis of composites. In this study, considering the inter-layer thermal contact resistance slightly improves the theoretical results (e_1 and e_2 decreased by 5% for TC3).

4.9.6. Discussion and conclusion

The purpose of providing the heat transfer model is to obtain accurate temperature distributions of thermoplastic composite laminates made by AFP. The accurate temperature distributions are essential to determine the residual stresses and deformations of the laminates, which occurs during and after the manufacturing process. The transient natures of the process and temperature dependencies of the composite properties are to be taken into account to increase the accuracy of the theoretical results. However, the hot gas/air temperature and convection coefficient distributions in the vicinity of the laminate (heat inputs of the model) play the main role in the accuracy of the theoretical results. This is due to the fact that the moving hot gas torch is in heat exchange with the top surface of laminate via convection. In this study, the heat inputs were split into two different zones with different distributions. These heat input distributions were determined using the provided non-linear models, decision table and algorithm, and experimental results. Also, it was assumed that the convection coefficient is linearly dependent on the hot gas/air temperature in the vicinity of laminate. The obtained results show that it is an acceptable assumption. Furthermore, the inter-layer thermal contact resistance was investigated and added to the heat transfer model. Considering a constant inter-layer thermal contact resistance caused the accuracy of the theoretical results to improve. In addition, the theoretical results through the thickness of the composite were validated by experimental results.

Chapter 5: Temperature gradients

5.1. Temperature history and effects of time between each pass

In the study presented in the previous chapters, material deposition was neglected. The test specimen was a unidirectional thermoplastic laminate, which was cooled down to the room temperature before a heating course is applied. Thus, the temperature history developed during the material deposition was neglected in the heat transfer model (the initial temperature of all layers and tool are equal to room temperature). This was necessary to reduce the complexity of the problem and determine the thermal inputs. In practice, the material (thermoplastic tape) is deposited layer-by-layer in a cyclic process. Each time that the hot gas torch passes over the previously deposited layers and tool their temperature increases. As a result, the temperatures of the previously deposited layers and tool will no longer be equal to the room temperature (25°C) at the beginning of the next cycle or pass. To include the temperature history of the previously deposited layers and tool in the transient heat transfer model the followings have been done in the study of this chapter:

1. The temperatures of both substrate (all layers) and tool at the end of each pass (a course of material deposition) were recorded using the developed MATLAB code and Microsoft Excel.
2. To include the effects of time between each pass (course) in the heat transfer model, a new transient heat transfer model using finite difference method and MATLAB coding was developed.

By doing so, the effects of temperature history have been included in the heat transfer model. This contributes the accuracy of the temperature and temperature gradients of the substrate obtained from the heat transfer model to increase.

Note: The roller and incoming tape were neglected in the material deposition process to reduce the complexity of the problem.

5.2. Heat transfer model for the time between each pass

In real life, at the end of one course of material deposition it takes times for the hot gas torch to get to the initial position to deposit the next layer. During this time the deposited layers and tool are exposed to the ambient air, and the hot gas torch does not add any more heat. Since the temperature of the deposited layers and tool are higher than the room temperature, the heat is transferred from the substrate and tool to the surrounding air. The boundary conditions for heat transfer process during the time between each pass are different from the model presented in chapter 4. This occurs because the hot gas torch is no longer in heat exchange with the top layer of the deposited substrate during this time (figure 5.1). Therefore, the boundary conditions for the top layer of the substrate needs to be updated.

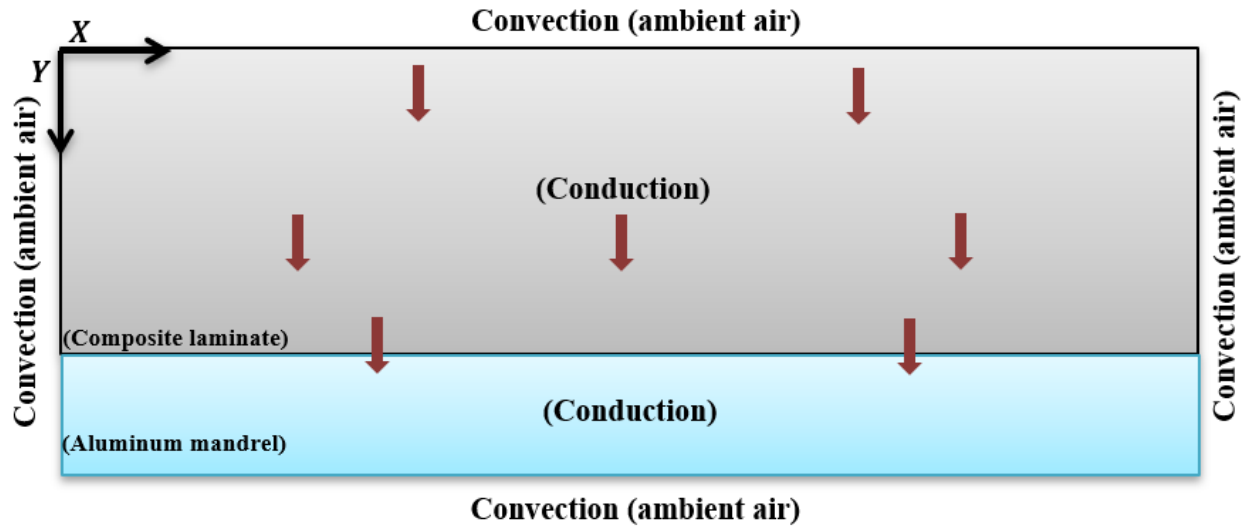


Figure 5.1: Composite laminate and mandrel heat transfer mechanism during the time between each pass

According to figures 5.1 and 5.2, the boundary conditions at the top edge of the substrate for the time between each pass is different from the case where the hot gas torch moves and is effective at the top of the substrate. All the temperature equations are the same as equations presented in chapter 4, but equations (9) and (11) need to be updated. These equations are related to two top corner nodes (two sides of convection) and top boundary nodes with only one side of convection. Using equation (1), these temperature equations are obtained.

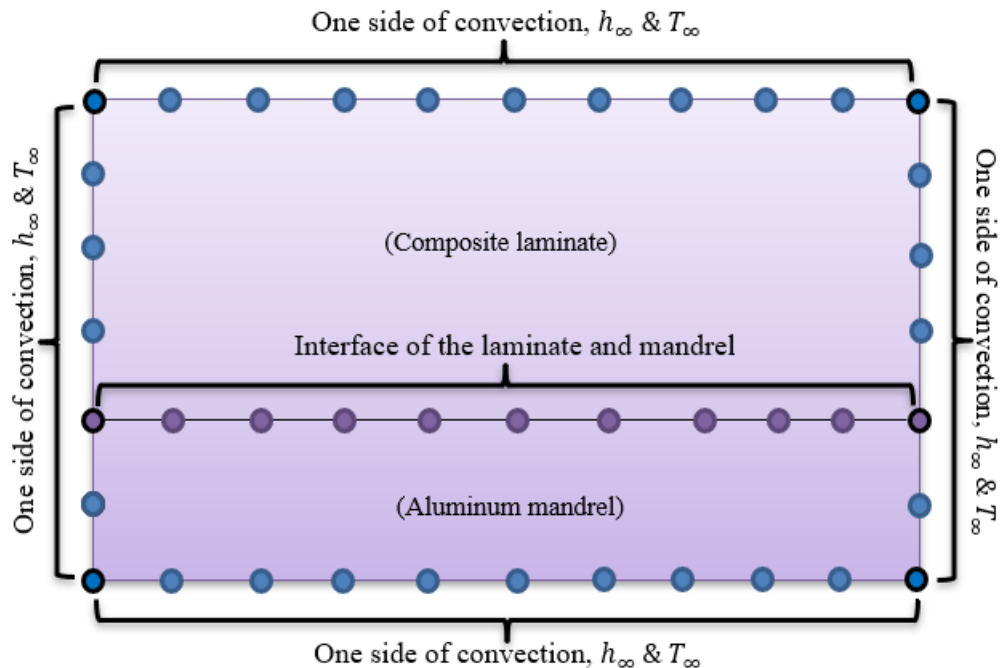
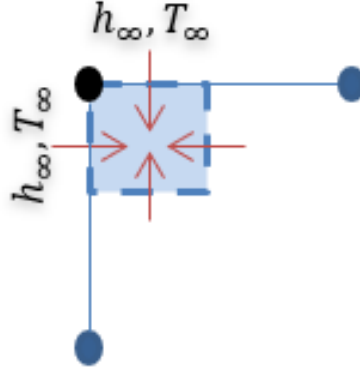


Figure 5.2: Schematic illustration of boundary nodes for the time between each pass

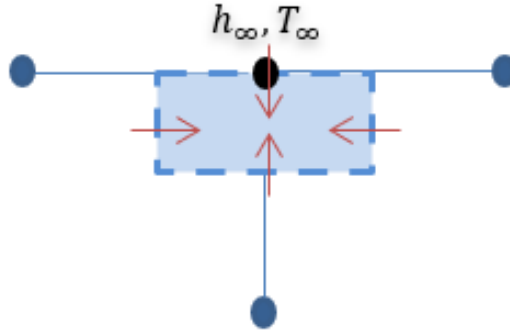
1. Two top corner nodes (two sides of convection)



$$T_{1,j}^{i+1} = \frac{2\Delta t}{\rho C_p} \left[h_{\infty} T_{\infty} \left(\frac{1}{\Delta x} + \frac{1}{\Delta y} \right) + \frac{K_x T_{2,j}^i}{(\Delta x)^2} + \frac{K'_y T_{1,j-1}^i}{(\Delta y)^2} \right] + \left[1 - \frac{2\Delta t}{\rho C_p} \left(h_{\infty} \left(\frac{1}{\Delta x} + \frac{1}{\Delta y} \right) + \frac{K_x}{(\Delta x)^2} + \frac{K'_y}{(\Delta y)^2} \right) \right] T_{1,j}^i \quad (36)$$

$j = N + N_m + 1$. The temperature of top right corner node is found similarly.

2. Top boundary nodes with only one side of convection



$$T_{m,j}^{i+1} = \frac{2\Delta t}{\rho C_p} \left[\frac{h_{\infty} T_{\infty}}{\Delta y} + \frac{K_x (T_{m-1,j}^i + T_{m+1,j}^i)}{2(\Delta x)^2} + \frac{K'_y T_{m,j-1}^i}{(\Delta y)^2} \right] + \left[1 - \frac{2\Delta t}{\rho C_p} \left(\frac{h_{\infty}}{\Delta y} + \frac{K_x}{(\Delta x)^2} + \frac{K'_y}{(\Delta y)^2} \right) \right] T_{m,j}^i \quad (37)$$

$j = N + N_m + 1$ and $2 \leq m \leq M$.

5.3. Procedure to determine the substrate temperature considering temperature history and effects of time between each pass

To consider the temperature history during material deposition in the heat transfer model, the temperatures of both previously deposited thermoplastic layers and tool were recorded at the end of each pass using the developed MATLAB code and Microsoft Excel. Then, it takes time for the

torch to get back to its initial position to deposit the next layer. For this specific amount of time, which is called the time between each pass in this study, the substrate and tool cool down (exposed to ambient air 25°C). To determine the effects of time between each pass on the temperature of the substrate, the transient heat transfer model presented in 5.2 was used. The procedure to include the temperature history and time between each pass is as follows:

1. The temperatures of both layer 1 and tool were determined during the deposition of layer 1 using the first heat transfer model, which has been presented in chapter 4. Then, the temperatures of layer 1 and the tool at the end of the first pass (course) were recorded and used as the initial temperatures of the second heat transfer model (presented in 5.2).
2. Using the second heat transfer model, the temperatures of both layer 1 and tool were determined during the time between each pass, which in this study is assumed to be equal to 8 seconds. Next, the temperatures of layer 1 and the tool at the end of the time between each pass were recorded and used as the initial temperatures of the first heat transfer model.
3. Using the first heat transfer model, the temperatures of the tool and layers 1 and 2 were calculated during the deposition of layer 2. The temperatures of the tool and layers 1 and 2 at the end of the second pass (course) were recorded and used as the initial temperatures of the second heat transfer model.
4. Using the second heat transfer model, the temperatures of the tool and layers 1 and 2 were calculated during the time between each pass. The temperatures of the tool and layers 1 and 2 at the end of the time between each pass were recorded and used as the initial temperatures of the first heat transfer model.
5. The mentioned processes repeat until the required number of layers are deposited.

By doing so, the temperature history and effects of time between each pass were included in the process of material deposition (layer by layer).

5.4. Effects of temperature history and time between each pass for aluminum mandrels

To investigate the effects of temperature history and the time between each pass, the laminate temperatures were calculated for two different cases with aluminum mandrel. In the first case, it was assumed that the time between each pass time is equal to zero. In the second case, it was assumed that time between each pass time is equal to eight seconds.

Table 5.1: Characteristics of the system and materials properties

Length of laminate	Velocity of torch	Temperature of torch	Material	Mandrel
508mm(20in)	25.4mm/s(1in/s)	875°C	Carbon fiber PEEK(AS4/APC-2) tapes	Aluminum with initial temperature of 25°C

Case 1: Dwell time = 0

In this case, it is assumed that the time between each pass is equal to zero. Figure 5.3 shows the substrate temperatures when layer 5 is being deposited, and figure 5.4 illustrates the substrate temperatures when layer 10 is being deposited.

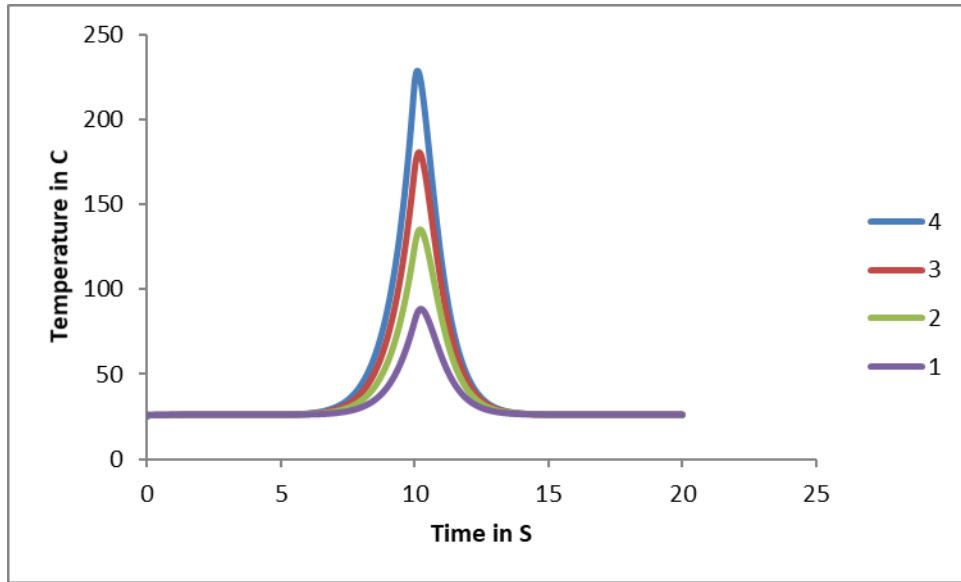


Figure 5.3: Temperature at the mid-section of the substrate while layer 5 is being deposited, the time between each pass is equal to zero

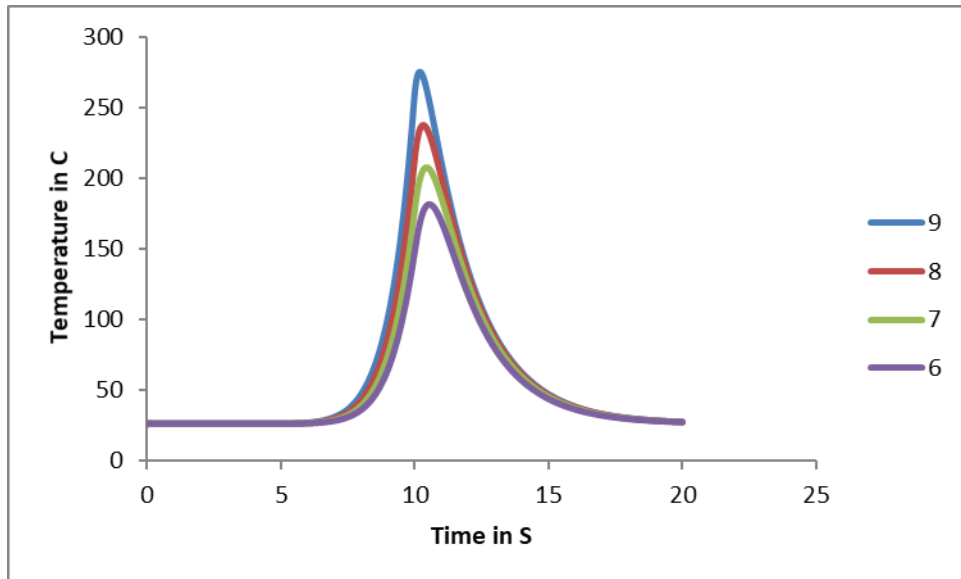


Figure 5.4: Temperature at the mid-section of the substrate while layer 10 is being deposited, the time between each pass is equal to zero

Case 2: Dwell time = 8 seconds

In this case, it is assumed that the time between each pass is equal to eight seconds. Figure 5.5 shows the substrate temperatures when layer 5 is being deposited, and figure 5.6 illustrates the substrate temperatures when layer 10 is being deposited.

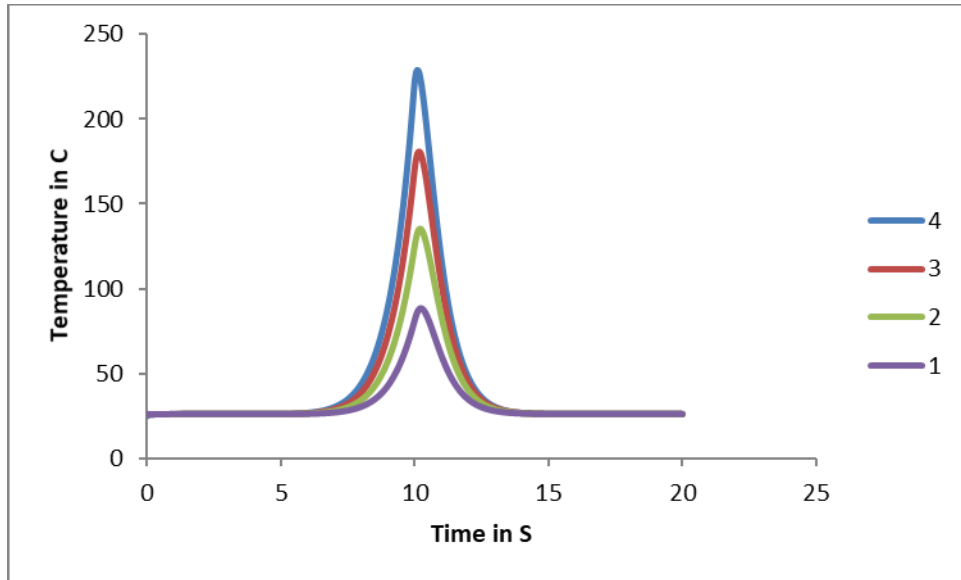


Figure 5.5: Temperature at the mid-section of the substrate while layer 5 is being deposited, the time between each pass is equal to eight seconds

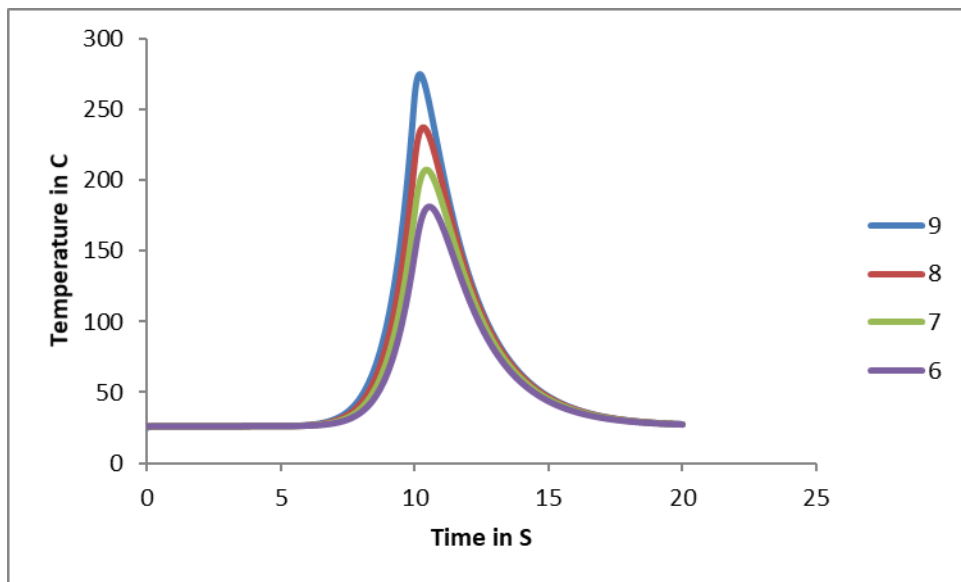


Figure 5.6: Temperature at the mid-section of the substrate while layer 10 is being deposited, the time between each pass is equal to eight seconds

Comparison of the results:

Note: Starting temperature is the temperature of the substrate where the torch is at initial position (torch is at $x = 0$).

The starting temperatures in figures 5.3 and 5.5 are about the same. This indicates that the difference in dwell times (0 seconds and 8 seconds) does not change the starting temperature very much, for the case where only 5 layers are considered. This occurs due to the length of the laminate. The length of the laminate in this study is 508mm (20in), and it takes 20 seconds for the torch to get back to its initial position (for the case where the time between each pass is equal to zero). This time is sufficient for the starting temperature of the laminate to cool down to room temperature. Adding an extra 8 seconds of dwell time does not make any difference. Figures 5.4 and 5.6 illustrate the substrate temperatures (layers 6 to 9) for the case where layer 10 is being deposited. According to these figures, starting temperature of layer 8 is equal to 26.6°C and 26.1°C for dwell time equal to zero and eight seconds, respectively. This shows that dwell time has effects on the starting temperature where more layers are involved.

5.5. Effects of mandrels and their initial temperature on the temperature distributions of the substrate

To investigate the effects of the mandrels, three different types of mandrels were considered. The first mandrel was an aluminum mandrel without extra heating (initial temperature of 25°C). The second mandrel was a ceramic mandrel without extra heating (initial temperature of 25°C), and the third one is an aluminum mandrel that is heated to maintain constant temperature at 100°C throughout the process. Table 5.2 shows the characteristics of the mandrels. In addition, two cases were considered. In case one, temperatures of layers 1 to 4 for different mandrels were found while layer 5 was being deposited. In case two, temperatures of layers 6 to 9 were determined while layer 10 was being deposited.

Table 5.2: Characteristics of the system and materials properties

Mandrel	Temperature of mandrel	Length of laminate	Velocity of torch	Time between each pass
Aluminum (Al)	Initial temperature of 25°C	508mm	25.4mm/s	8s
Ceramic (Cr)				
Hot aluminum (Hot Al)	Constant temperature of 100°C			

Note: Temperature history has been considered. The material is carbon fiber PEEK(AS4/APC-2) tapes, and torch temperature equal to 875°C.

Case 1:

Temperatures of layers 1 to 4 for different mandrels in the case where layer 5 was being deposited. Figure 5.7 to 5.10 show the results.

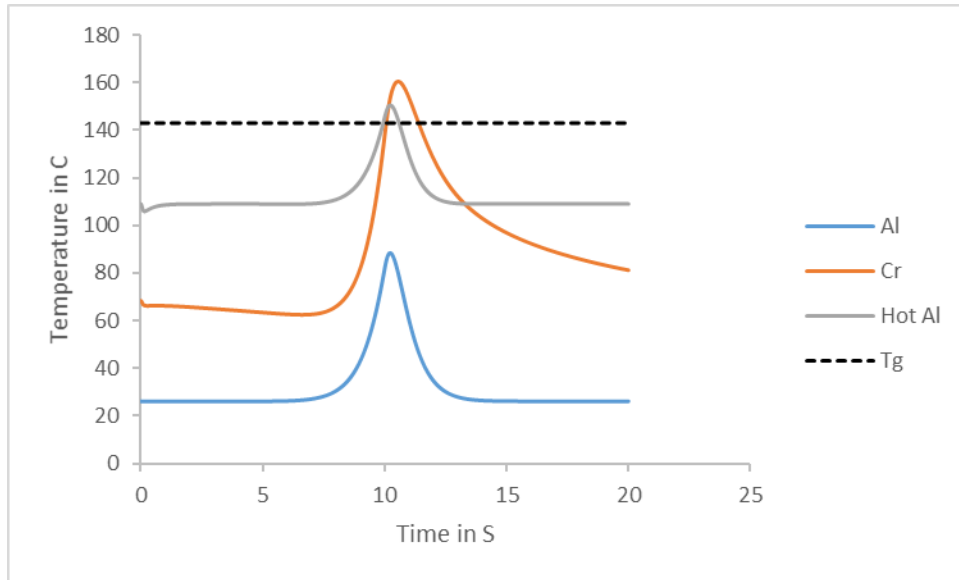


Figure 5.7: Temperature at the mid-section of layer 1 while layer 5 is being deposited for different mandrels

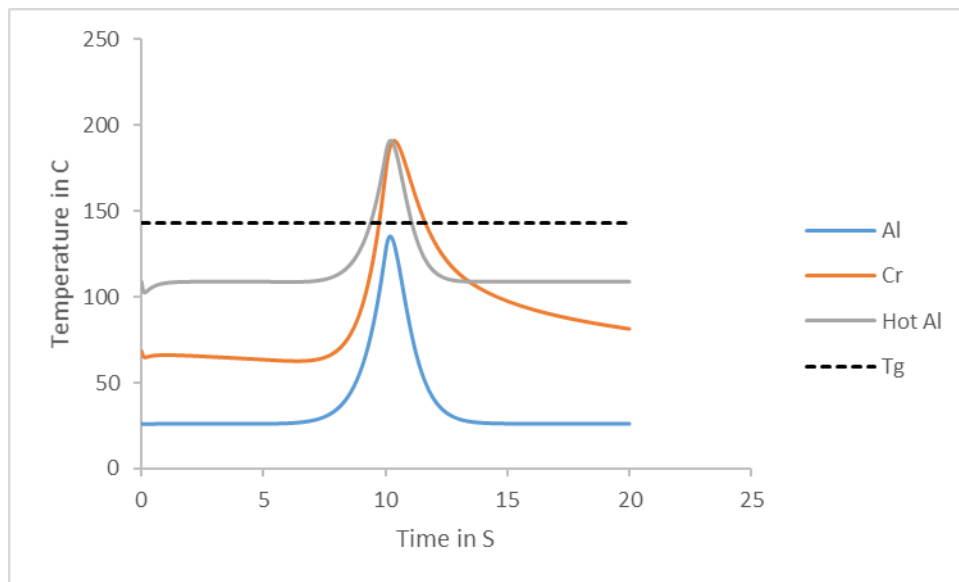


Figure 5.8: Temperature at the mid-section of layer 2 while layer 5 is being deposited for different mandrels

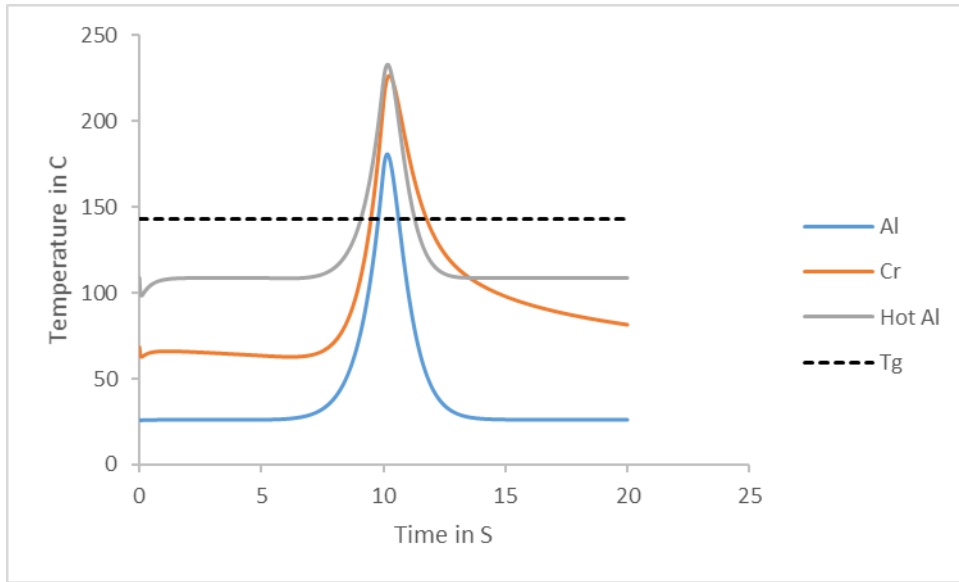


Figure 5.9: Temperature at the mid-section of layer 3 while layer 5 is being deposited for different mandrels

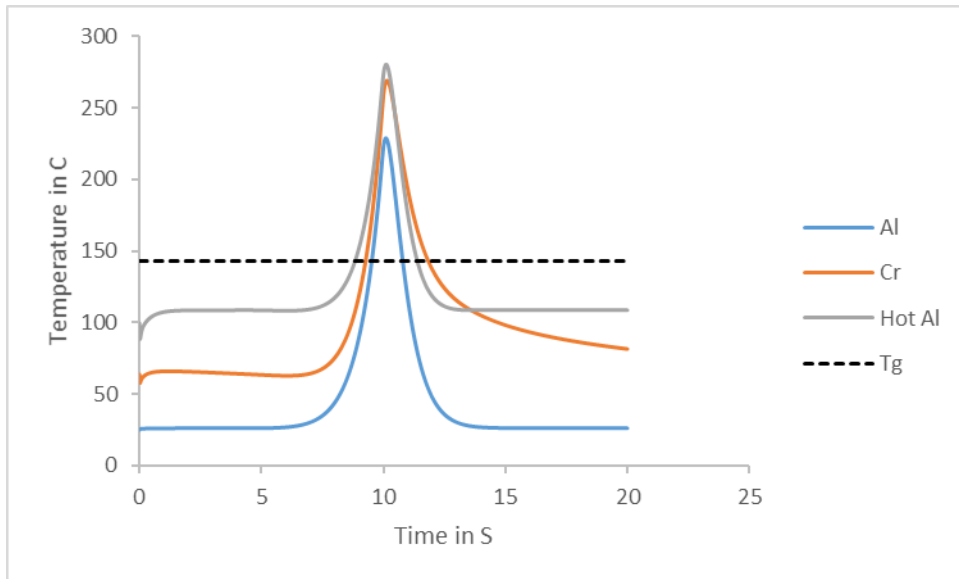


Figure 5.10: Temperature at the mid-section of layer 4 while layer 5 is being deposited for different mandrels

Comparison of the results:

1. The substrate with hot aluminum mandrel has the highest start and end temperatures in all layers, and the substrate with aluminum mandrel (initial temperature of 25°C) has the lowest start and end temperatures in all layers.

2. The substrate with aluminum mandrel shows the lowest temperature at all layers including peak temperatures.
3. The highest peak temperature for the first layer belongs to the substrate with the ceramic mandrel. Nevertheless, the peak temperature of the substrate with hot aluminum mandrel is the highest for layers 2 to 4. The reason is that ceramic is a thermal insulator, and the temperature of the first layer is mainly dependent upon heat exchange between the first layer and mandrel.
4. The temperature history is more significant for the substrates with ceramic and hot aluminum mandrel (higher start temperature).
5. The peak temperatures of the substrate with aluminum mandrel in layers 1 and 2 are below the glass transition temperature ($T_g = 143^\circ\text{C}$), but the peak temperature of layers 3 and 4 are above glass transition temperature.
6. The peak temperatures of the substrate with ceramic and hot aluminum mandrel are above the glass transition temperature for all layers.
7. The temperature graph for the substrate with ceramic mandrel is not as symmetric as the temperature graphs for the aluminum mandrels. This is due to the fact that ceramics are thermal insulators, and heat exchange between the bottom layers and the ceramic mandrel does not occur. Hence, the substrate cannot cool down and reach to the initial temperatures. The end temperature, for instance, is higher than the starting temperature, and this causes the temperature graph to be unsymmetrical.

Case 2:

Temperatures of layers 6 to 9 for different mandrels in the case where layer 10 was being deposited. Figures 5.11 to 5.14 indicate the results.

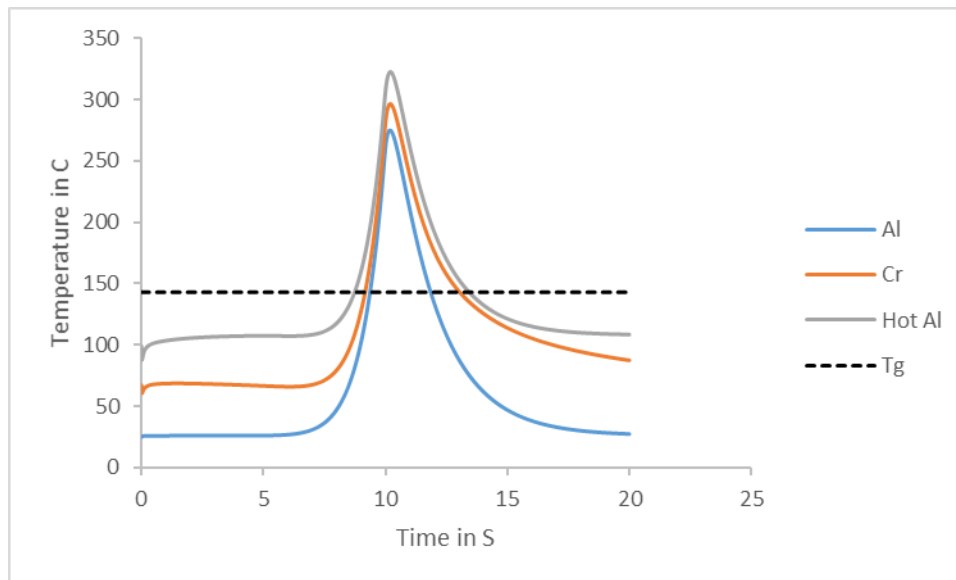


Figure 5.11: Temperature at the mid-section of layer 9 while layer 10 is being deposited for different mandrels

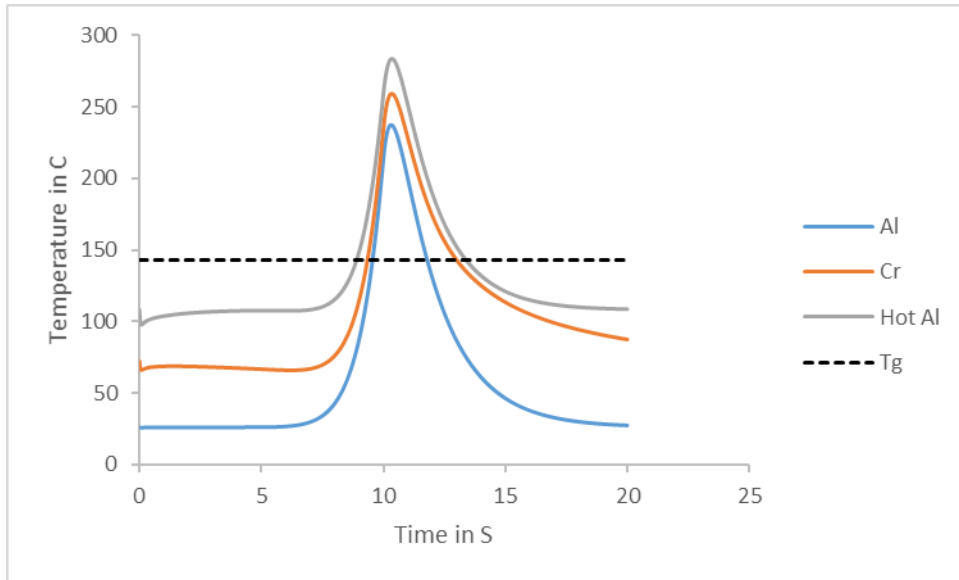


Figure 5.12: Temperature at the mid-section of layer 8 while layer 10 is being deposited for different mandrels

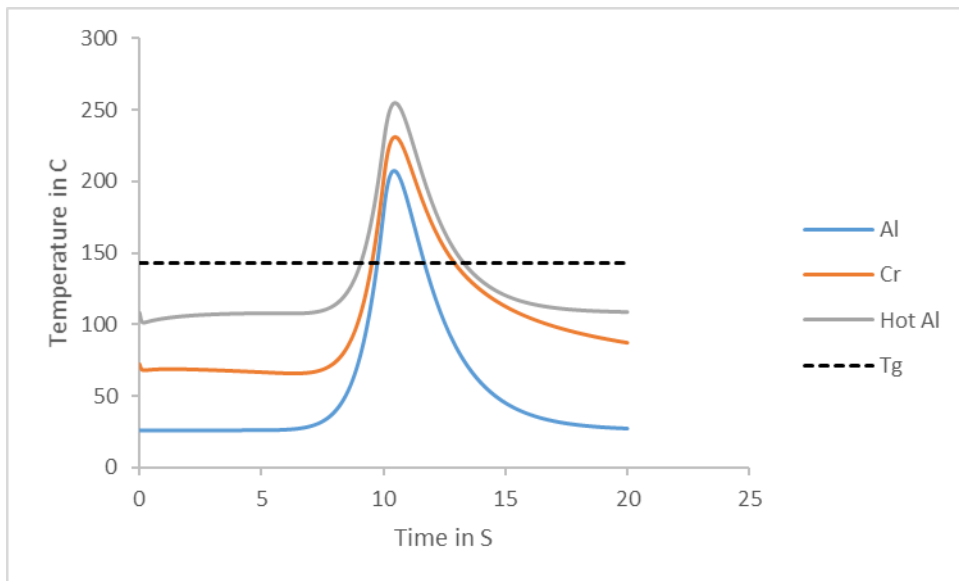


Figure 5.13: Temperature at the mid-section of layer 7 while layer 10 is being deposited for different mandrels

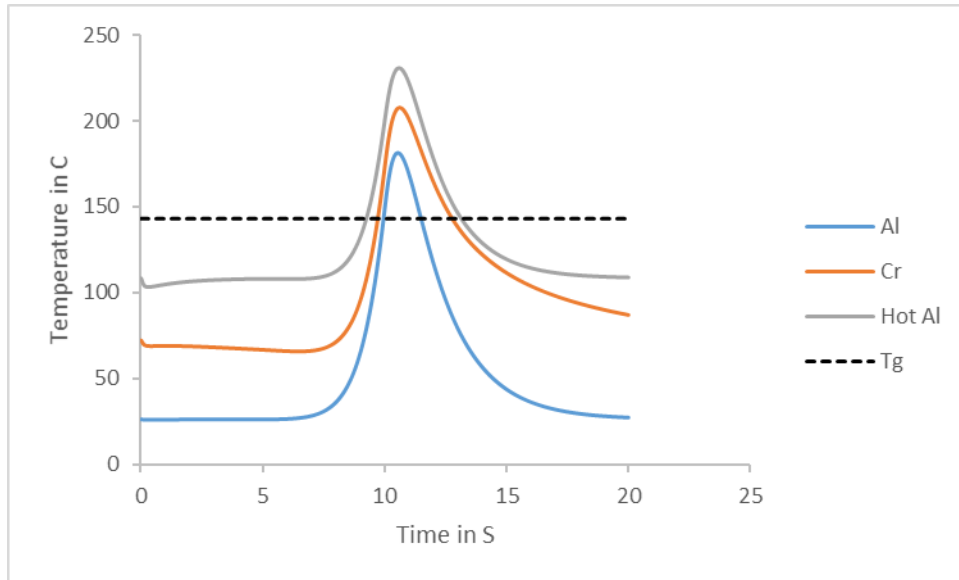


Figure 5.14: Temperature at the mid-section of layer 6 while layer 10 is being deposited for different mandrels

Comparison of the results:

1. The substrate with hot aluminum mandrel has the highest start, peak, and end temperatures in layers 6 to 9, and the substrate with aluminum mandrel (initial temperature of 25°C) has the lowest, start, peak, and end temperatures in layers 6 to 9.
2. The temperature history is more significant for the substrates with ceramic and hot aluminum mandrel (higher start temperature).
3. The peak temperatures of all substrates in layers 6 to 9 are above the glass transition temperature ($T_g = 143^\circ\text{C}$).
4. The effects of mandrels on the temperatures of substrates are more significant in the layers located at the bottom of the substrates (closer to mandrels). For instance, the temperatures of layer 9 are less different for various mandrels than temperatures of layer 6.

5.6. Temperatures of laminates at $t = 10s$ for different mandrels

In previous sections, the temperatures of the substrates versus time at a certain location were found. In this section, the temperatures of the substrates at a certain time were determined. The time between each pass is equal to 8 seconds, and temperature history has been considered.

5.6.1. Aluminum mandrel with an initial temperature of 25°C

Case 1:

The temperatures of layers 1 to 4 were determined while layer 5 was being deposited (figure 5.15).

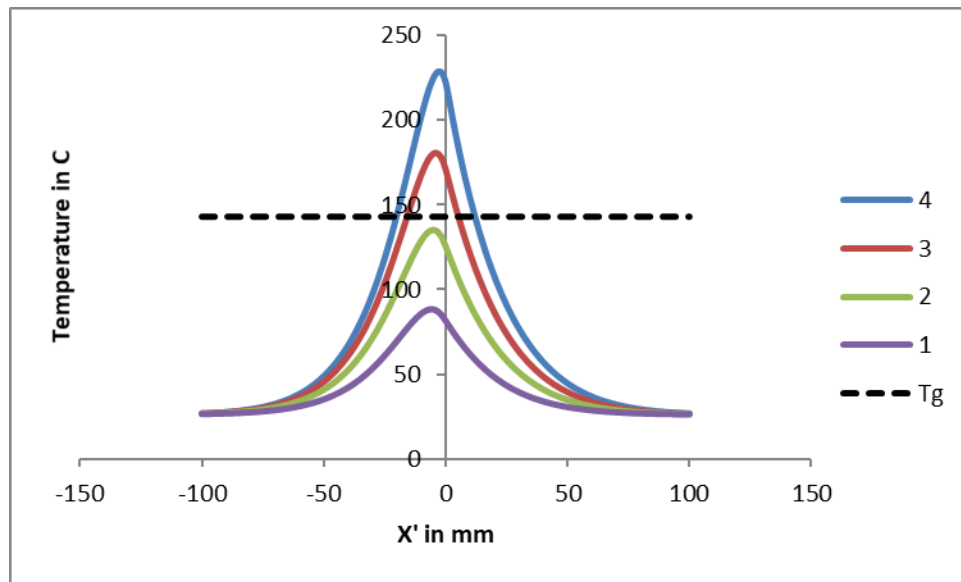


Figure 5.15: Temperatures of layers 1 to 4, layer 5 is being deposited

According to figure 5.15, temperatures decrease through the thickness of the substrate. Also, the peak temperatures of layers 1 and 2 are below the glass transition temperature.

Case 2:

The temperatures of layers 1 to 9 were determined while layer 10 was being deposited (figures 5.16 and 5.17).

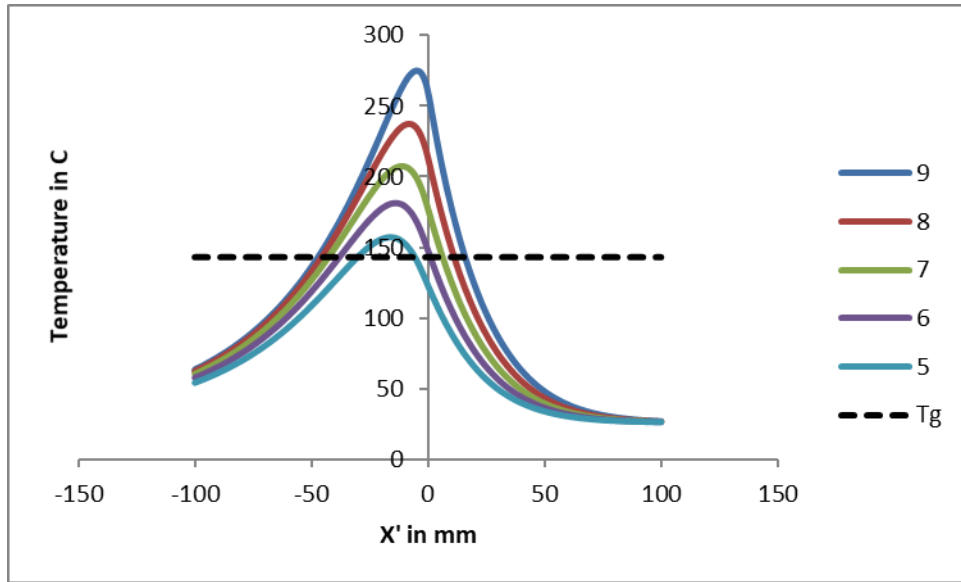


Figure 5.16: Temperatures of layers 5 to 9, layer 10 is being deposited

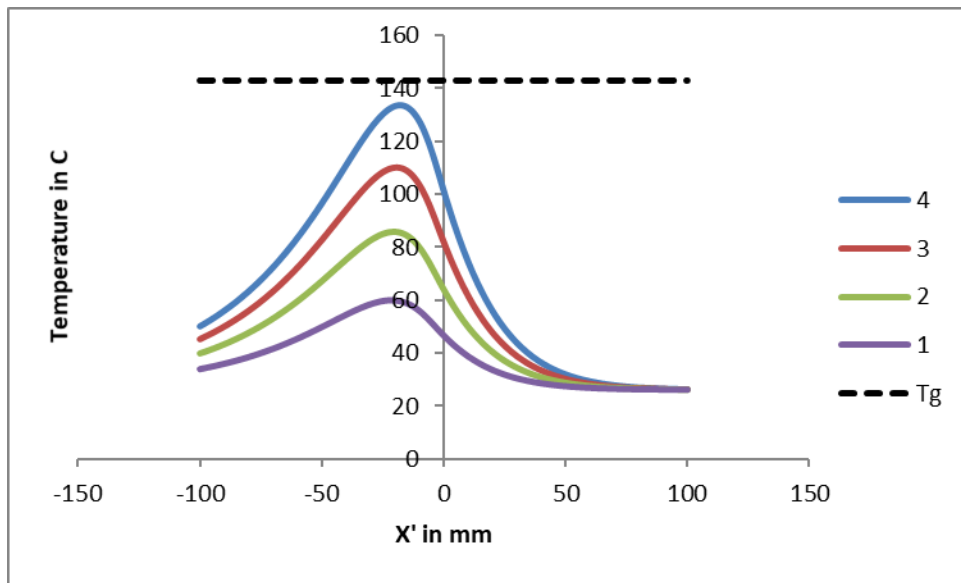


Figure 5.17: Temperatures of layers 1 to 4, layer 10 is being deposited

According to figures 5.16 and 5.17, temperatures decrease through the thickness of the substrate. The peak temperatures of layers 5 to 9 are above the glass transition temperature, and the peak temperatures of layers 1 to 4 are below the glass transition temperature.

5.6.2. Ceramic mandrel

Case 1:

The temperatures of layers 1 to 4 were determined while layer 5 was being deposited (figure 5.18).

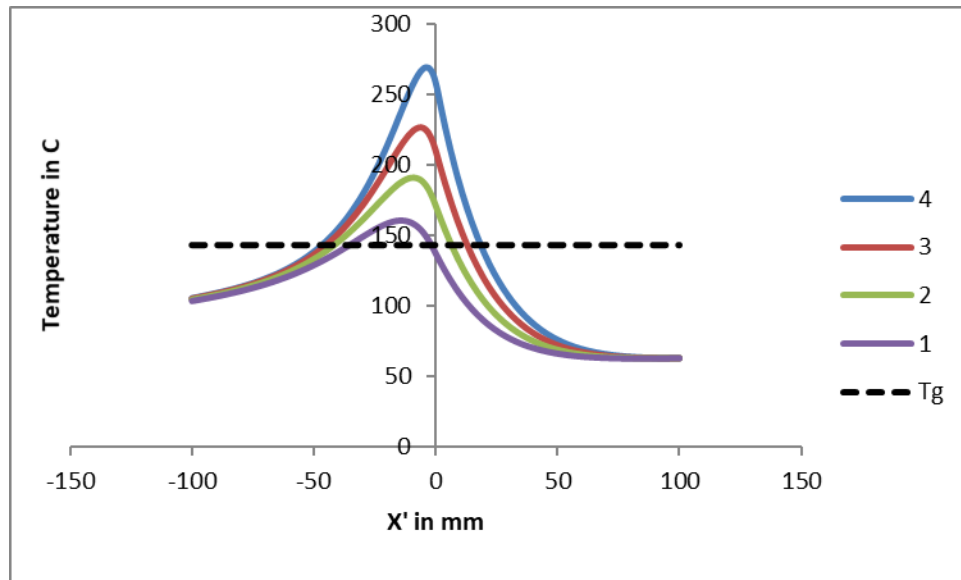


Figure 5.18: Temperatures of layers 1 to 4, layer 5 is being deposited

According to figure 5.18, temperatures decrease through the thickness of the substrate. Moreover, the peak temperatures of all layers (1 to 4) are above the glass transition temperature.

Case 2:

The temperatures of layers 1 to 9 were determined while layer 10 was being deposited (figures 5.19 and 5.20).

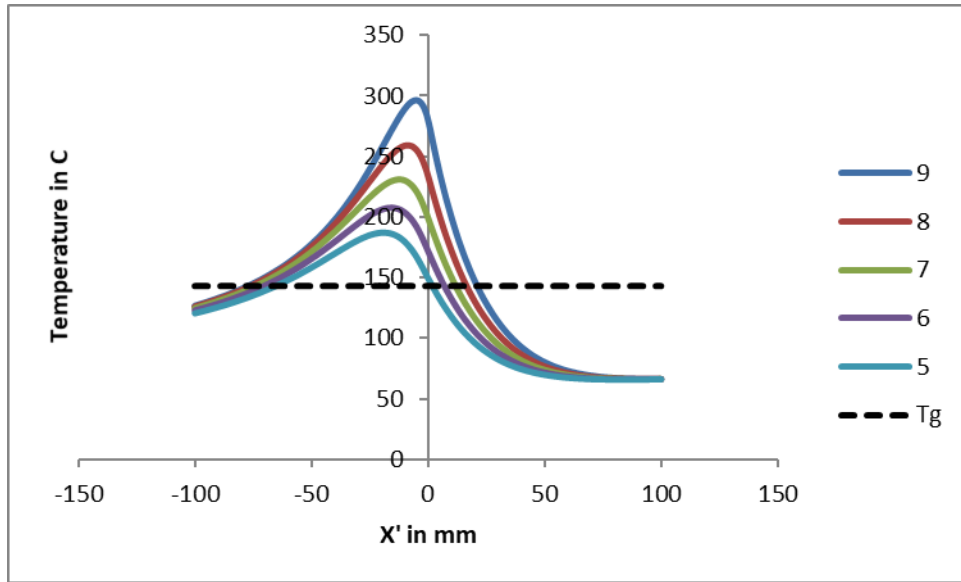


Figure 5.19: Temperatures of layers 5 to 9, layer 10 is being deposited

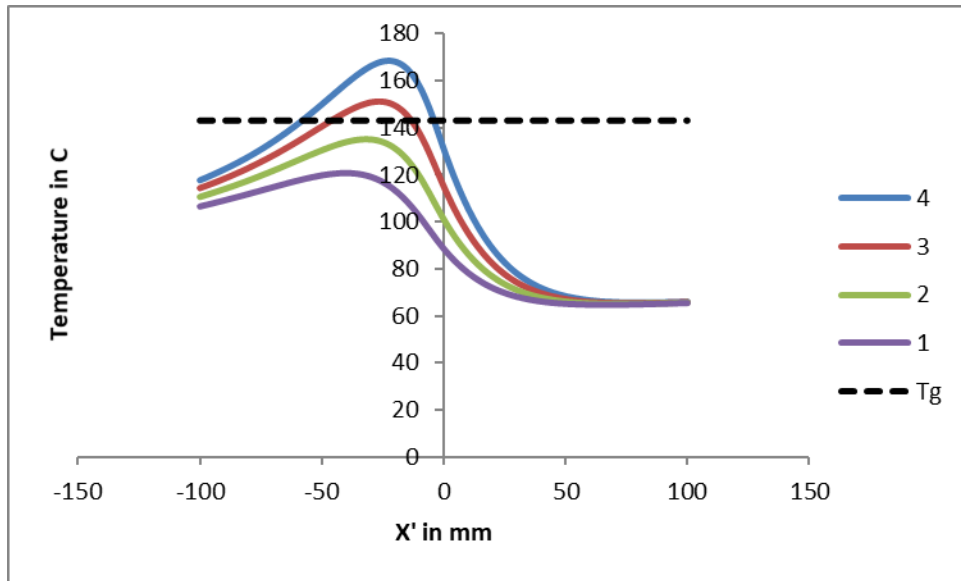


Figure 5.20: Temperatures of layers 1 to 4, layer 10 is being deposited

According to figures 5.19 and 5.20, temperatures decrease through the thickness of the substrate. The peak temperatures of layers 3 to 9 are above the glass transition temperature, and the peak temperatures of layers 1 to 2 are below the glass transition temperature.

5.6.3. Hot aluminum mandrel

Case 1:

The temperatures of layers 1 to 4 were determined while layer 5 was being deposited (figure 5.21).

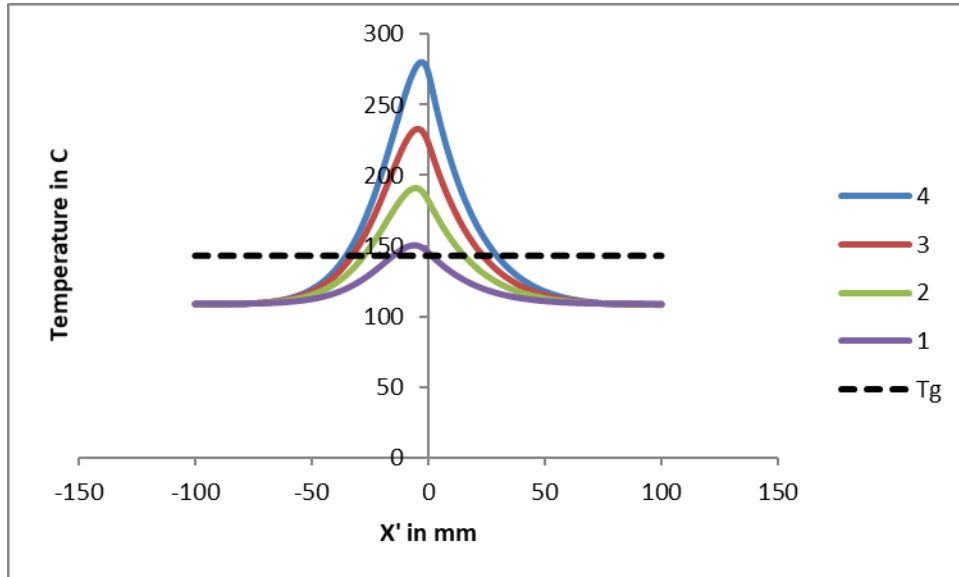


Figure 5.21: Temperatures of layers 1 to 4, layer 5 is being deposited

According to figure 5.21, temperatures decrease through the thickness of the substrate. The peak temperatures of all layers (1 to 4) are above the glass transition temperature.

Case 2:

The temperatures of layers 1 to 9 were determined while layer 10 was being deposited (figures 5.22, and 5.23).

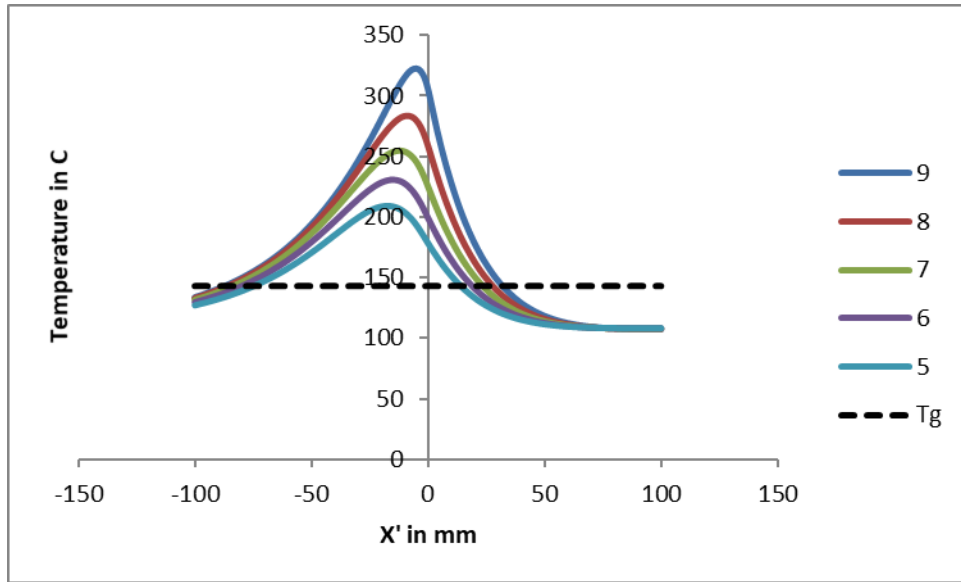


Figure 5.22: Temperatures of layers 5 to 9, layer 10 is being deposited

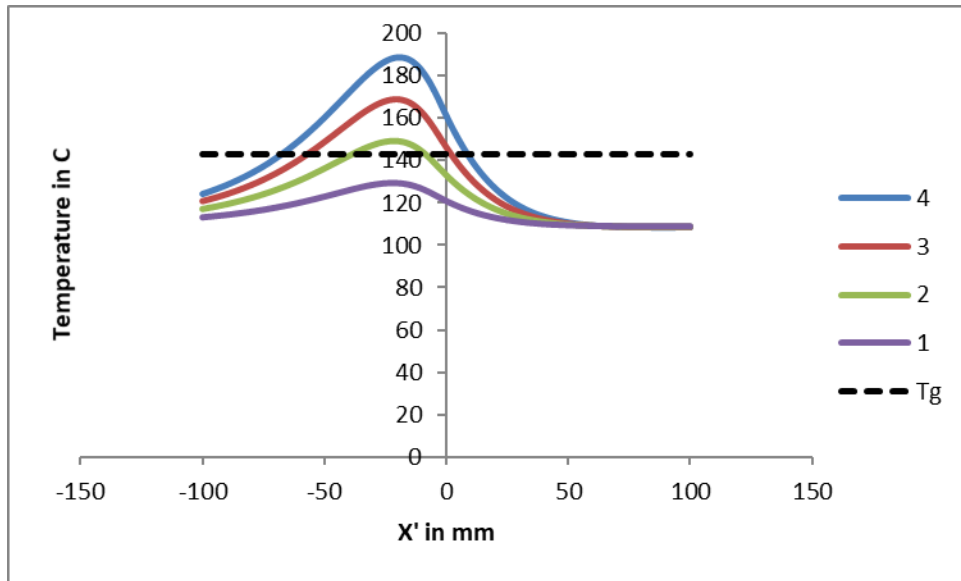


Figure 5.23: Temperatures of layers 1 to 4, layer 10 is being deposited

According to figures 5.22 and 5.23, temperatures decrease through the thickness of the substrate. The peak temperatures of layers 2 to 9 are above the glass transition temperature, and the peak temperatures of only layer 1 is below the glass transition temperature.

Comparison of the results:

Case 1 (layer 5 being deposited): The peak temperatures of all layers (1 to 4) are above the glass transition temperature for the substrates with ceramic and hot aluminum mandrels. However, the peak temperatures of layers 1 and 2 are below the glass transition temperature for aluminum mandrel. This leads to development of residual stresses and deformations in the substrate.

Case 2 (layer 10 being deposited): The peak temperatures of four layers (1 to 4) are below the glass transition temperature for aluminium mandrel. For the ceramic mandrel, the peak temperatures of two layers (1 and 2) are below the glass transition temperature. Only peak temperature of one layer (layer 1) is below the glass transition temperature for the hot aluminum mandrel. This indicates that using different mandrels such as ceramic or increasing the temperature of mandrel can resolve the issue of residual stress. Although the temperature of the hot aluminum mandrel was kept at a temperature lower than glass transition temperature (100°C), only the peak temperature of layer 1 fell below the glass transition temperature (while layer 10 being deposited).

5.7. Temperature gradients through the thickness for different mandrels

The length of the substrate is equal to 508mm (20in), and the velocity of the **torch** is equal to 25.4mm/s (1in/s). The time between each pass is equal to eight seconds, and temperature history has been considered in this section.

5.7.1. Aluminum mandrel

In This section, the temperatures and temperature gradients through the thickness and different cross sections have been determined for a substrate with aluminum mandrel (initial temperature of 25°C) while layer 10 is being deposited.

Case 1:

Temperature and temperature gradients through the thickness at $x = 6$ inches.

$G_{i,j}$: Temperature gradient through the thickness between layers i and j [$^{\circ}\text{C} / \text{mm}$].

Thickness of a layer = 0.125 mm

$G_{i,j} = (\text{temperature of top of layer } j - \text{temperature of top of layer } i) / 0.125.$

$G_{1,tool} = (\text{temperature of top of tool} - \text{temperature of top of layer } 1) / 0.125$

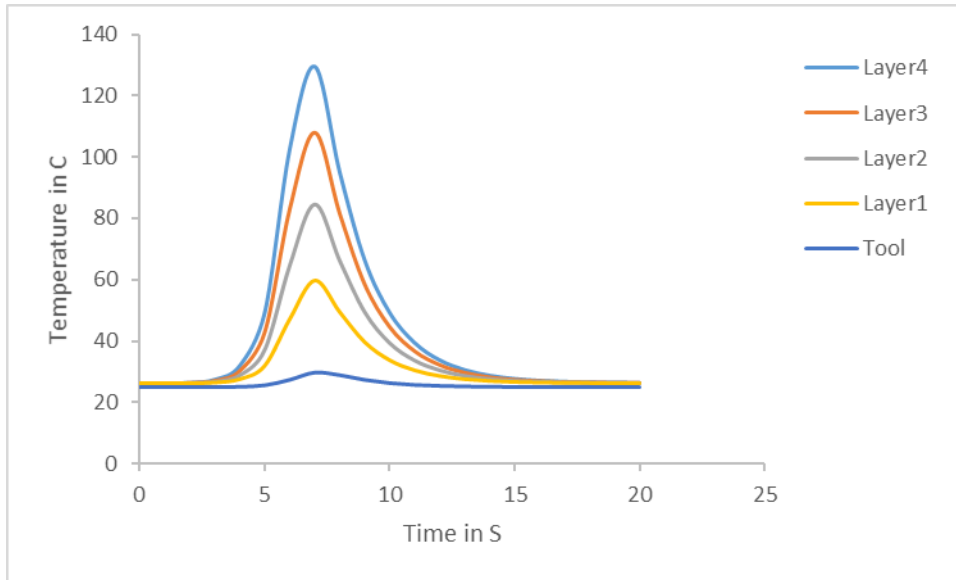


Figure 5.24: Temperatures through the thickness (tool to layer 4) at $x = 6\text{in}$

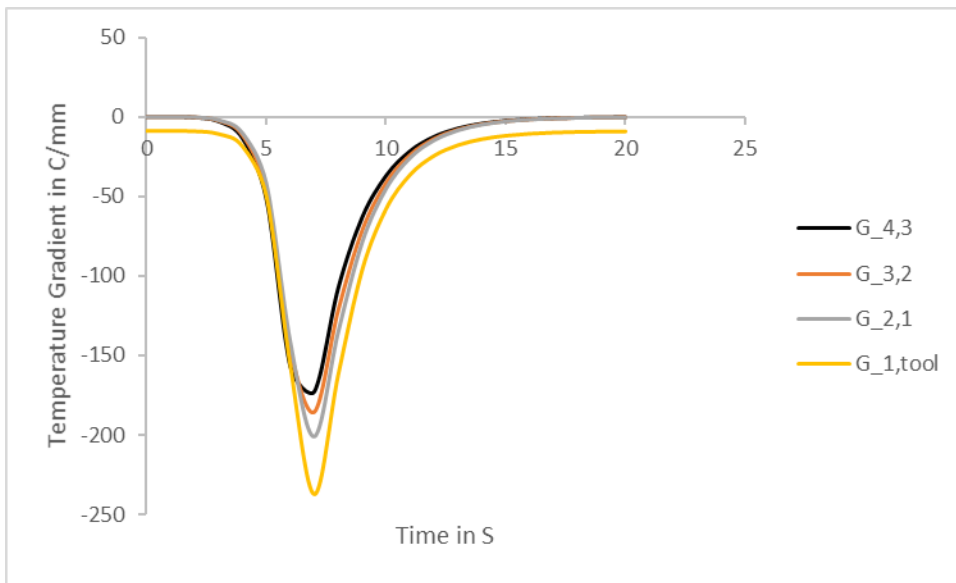


Figure 5.25: Temperature gradients through the thickness at $x = 6\text{in}$

According to figure 5.25, the highest absolute value of the temperature gradients is between layer 1 and aluminum tool ($G_{1, tool}$). Then, the absolute values of temperature gradients reduce gradually.

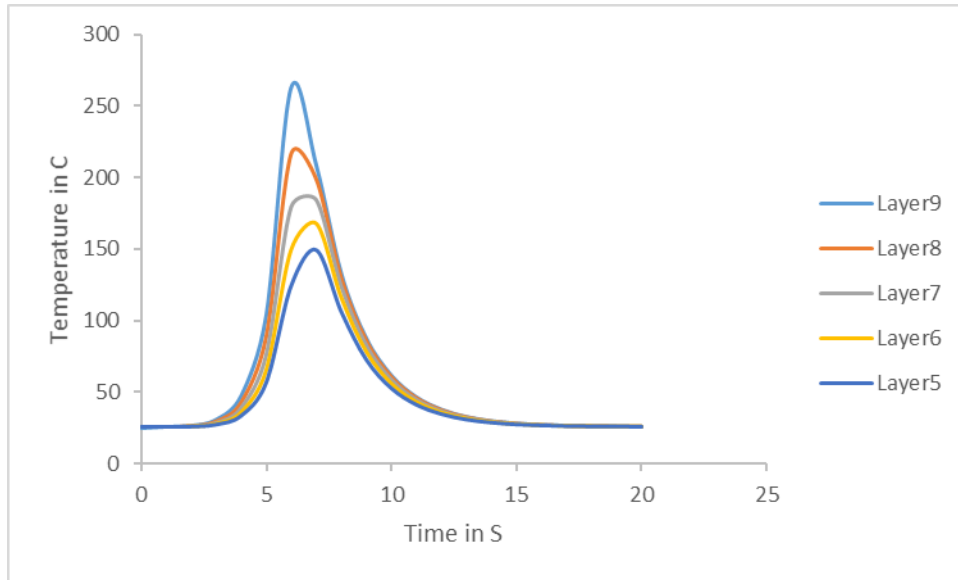


Figure 5.26: Temperatures through the thickness (layers 5 to 9) at $x = 6\text{in}$

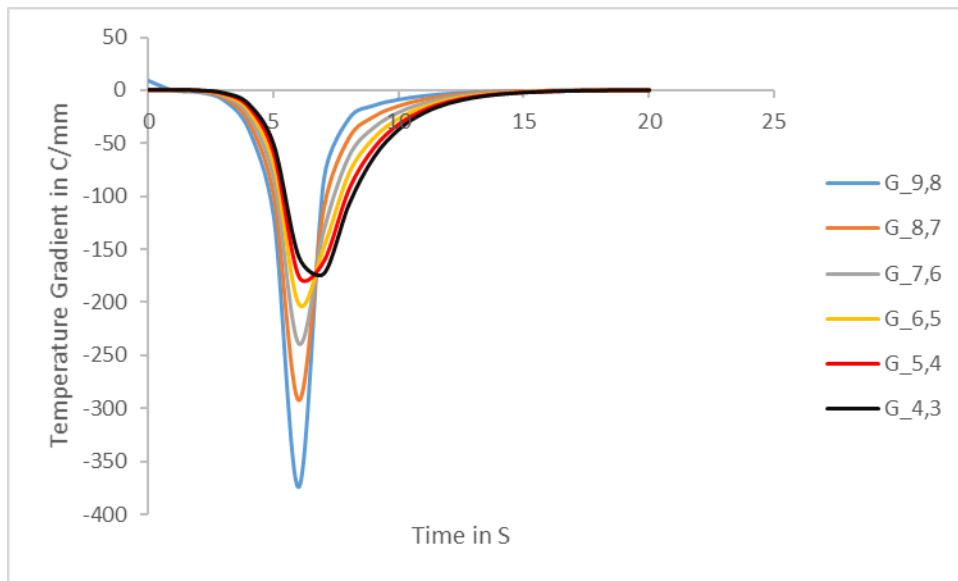


Figure 5.27: Temperature gradients through the thickness at $x = 6\text{in}$

According to figure 5.27, the highest absolute value of the temperature gradients is between layers 9 and 8 ($G_{9,8}$). Then, the absolute values of temperature gradients reduce gradually. Figure 5.25 shows that the absolute value of the temperature gradients decrease as one moves from the tool towards the top layers of substrate (until $G_{4,3}$). On the other hand, figure 5.27 shows that the absolute value of temperature gradients decreases by moving from the top layer of substrate towards the tool (until $G_{4,3}$). As such, there is a location within the laminate where the trend of the temperature gradients changes. In this case, which is a substrate of 10 layers with aluminum tool,

layer 3 is the trend change point. In addition, the highest absolute value of all temperature gradients is between layers 9 and 8 ($|G_{9,8}| > |G_{1,tool}|$, figures 5.25 and 5.27).

Case 2:

Temperature and temperature gradients through the thickness at $x = 8$ inches.

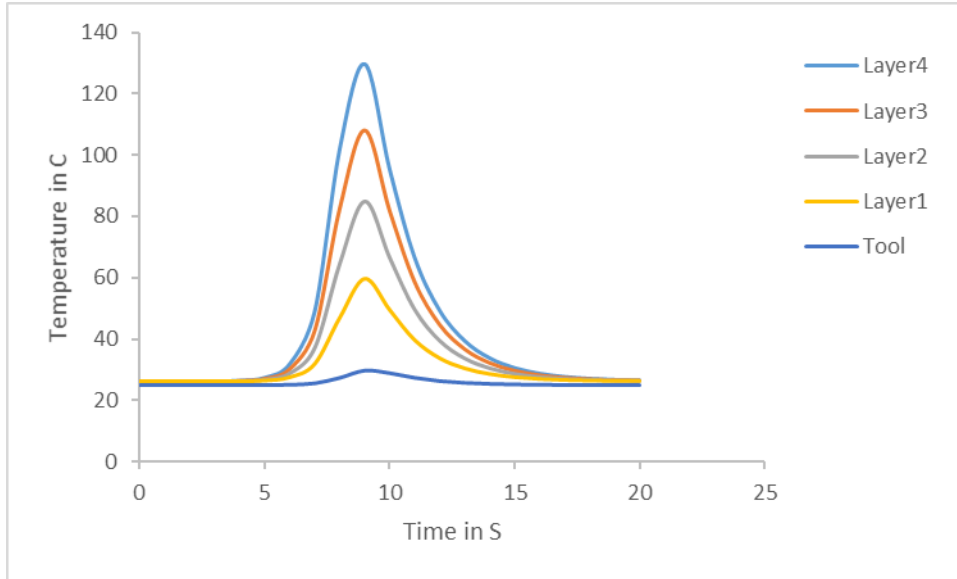


Figure 5.28: Temperatures through the thickness (tool to layer 4) at $x = 8$ in

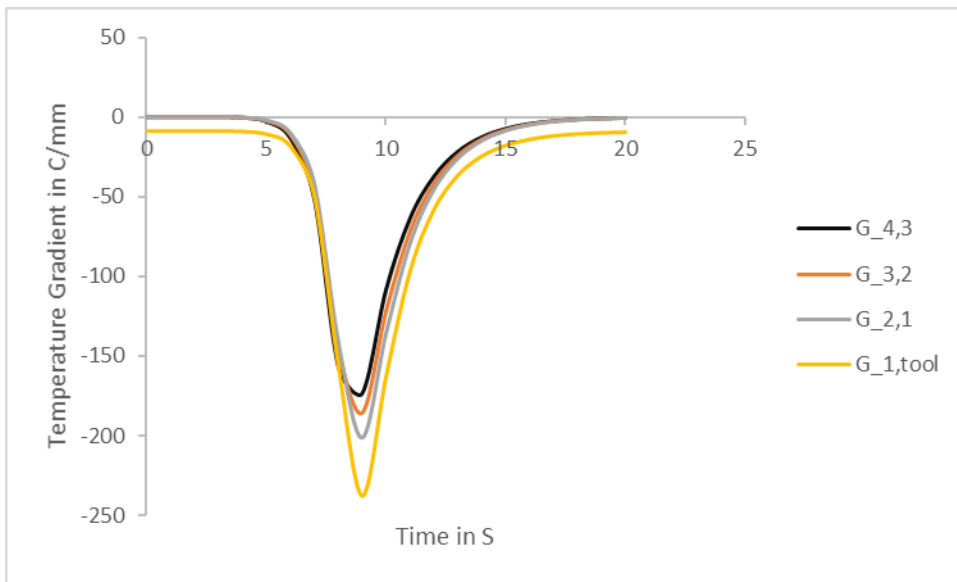


Figure 5.29: Temperature gradients through the thickness at $x = 8$ in

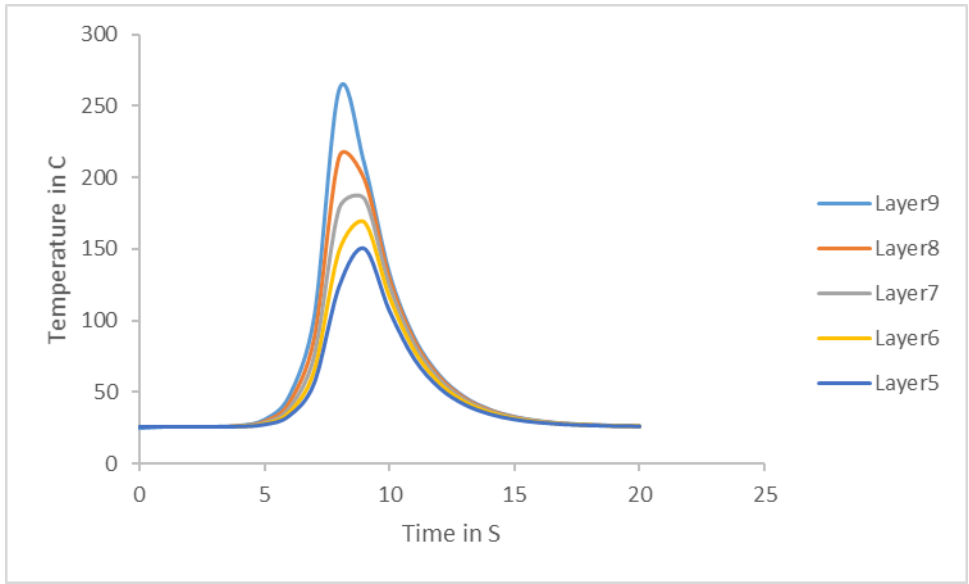


Figure 5.30: Temperatures through the thickness (layers 5 to 9) at $x = 8in$

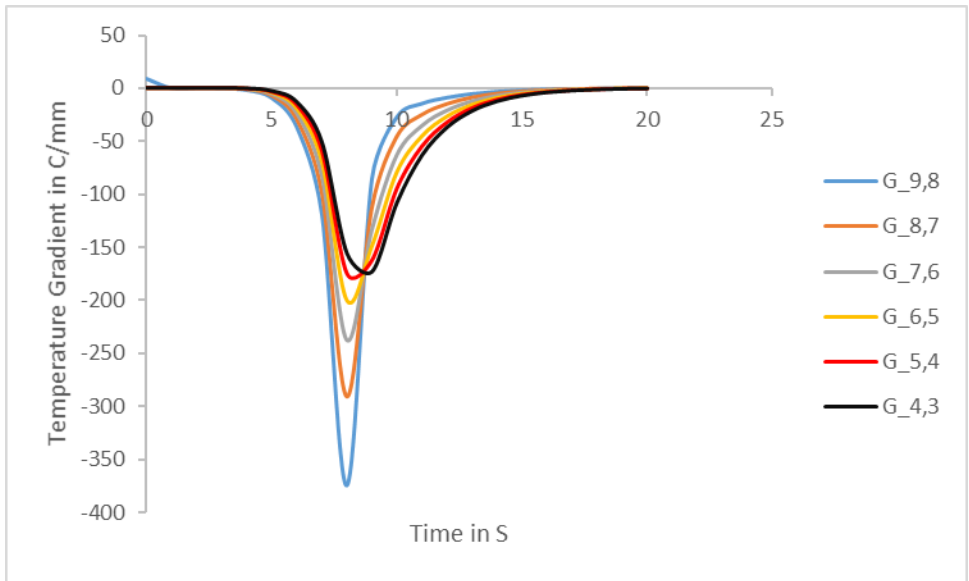


Figure 5.31: Temperature gradients through the thickness at $x = 8in$

Case 3:

Temperature and temperature gradients through the thickness at $x = 10$ inches.

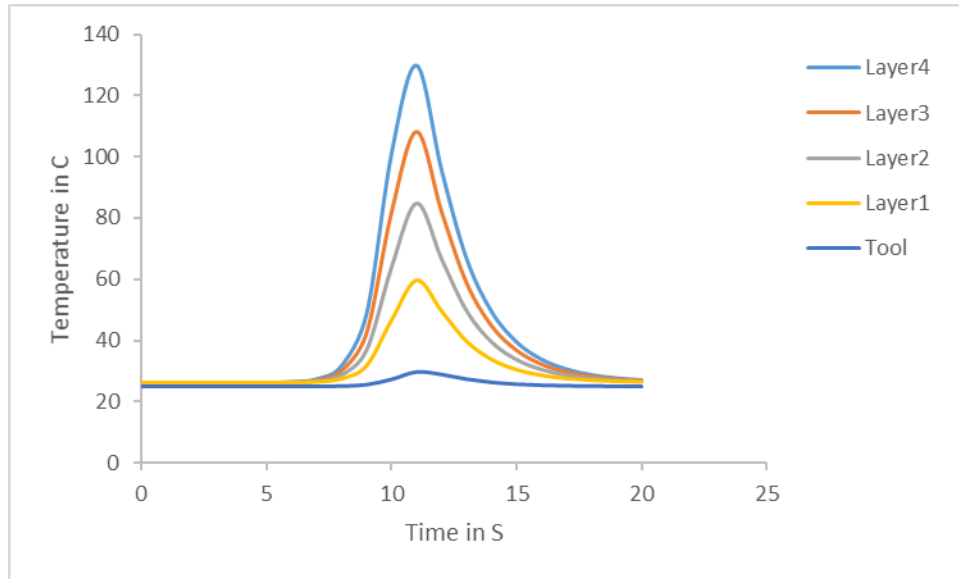


Figure 5.32: Temperatures through the thickness (tool to layer 4) at $x = 10in$

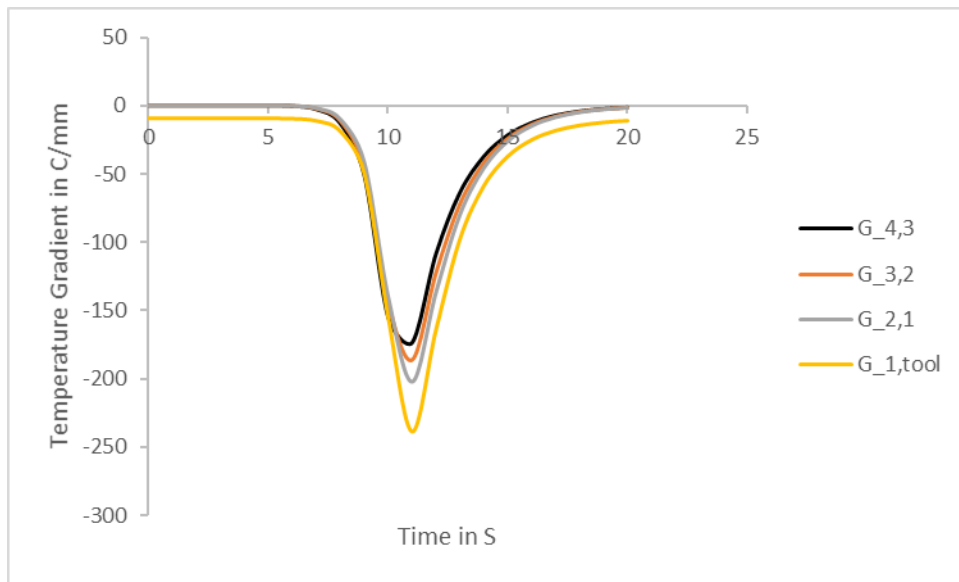


Figure 5.33: Temperature gradients through the thickness at $x = 10in$

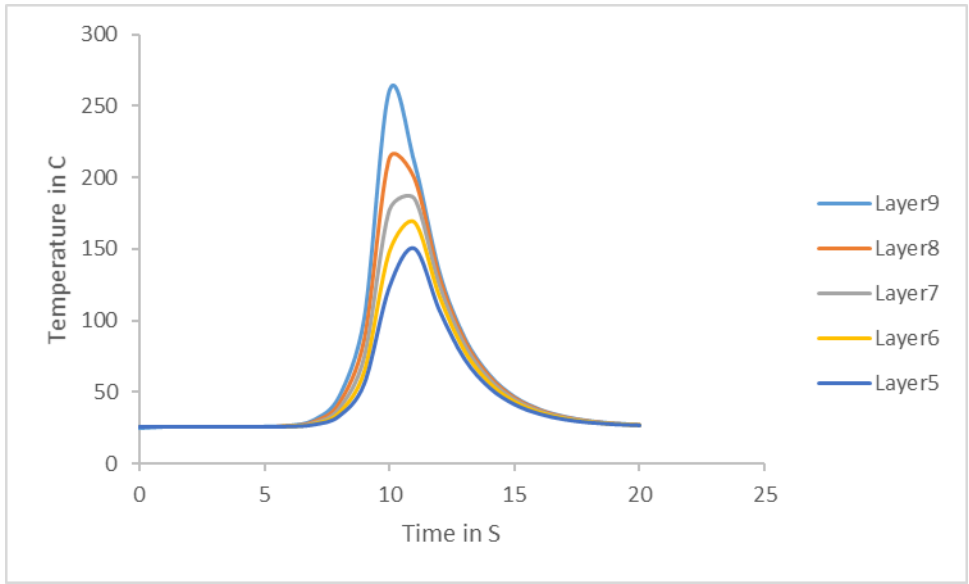


Figure 5.34: Temperatures through the thickness (layers 5 to 9) at $x = 10in$

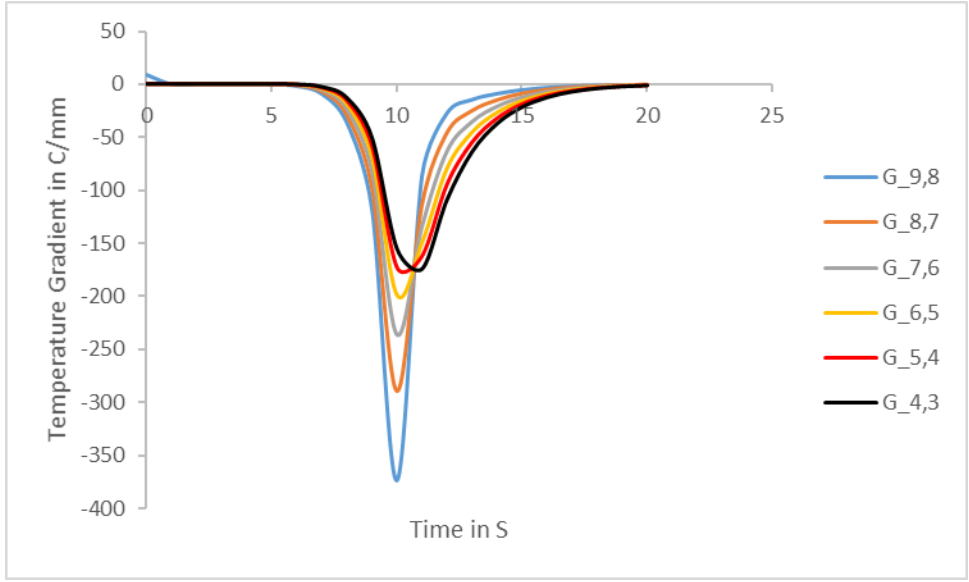


Figure 5.35: Temperature gradients through the thickness at $x = 10in$

Case 4:

Temperature and temperature gradients through the thickness at $x = 12$ inches.

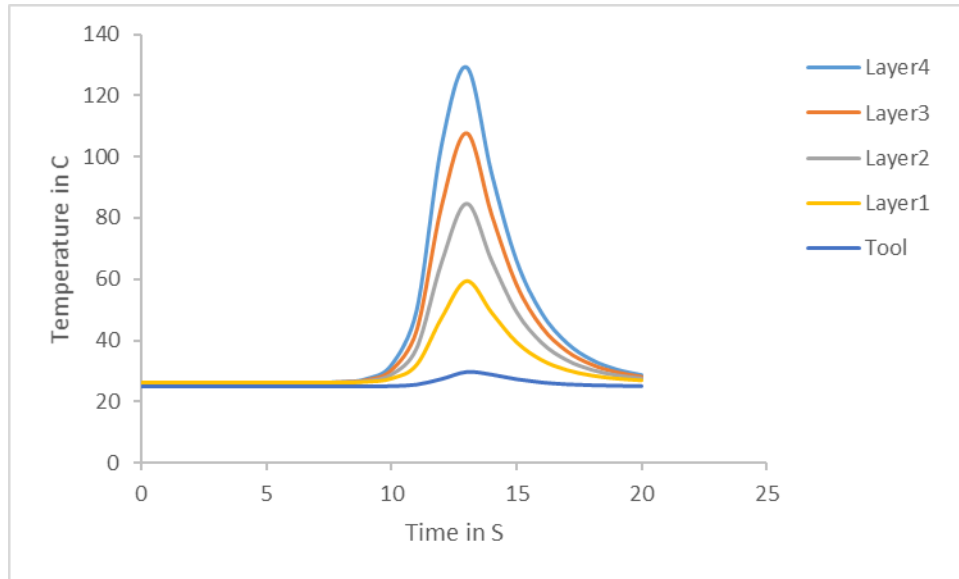


Figure 5.36: Temperatures through the thickness (tool to layer 4) at $x = 12in$

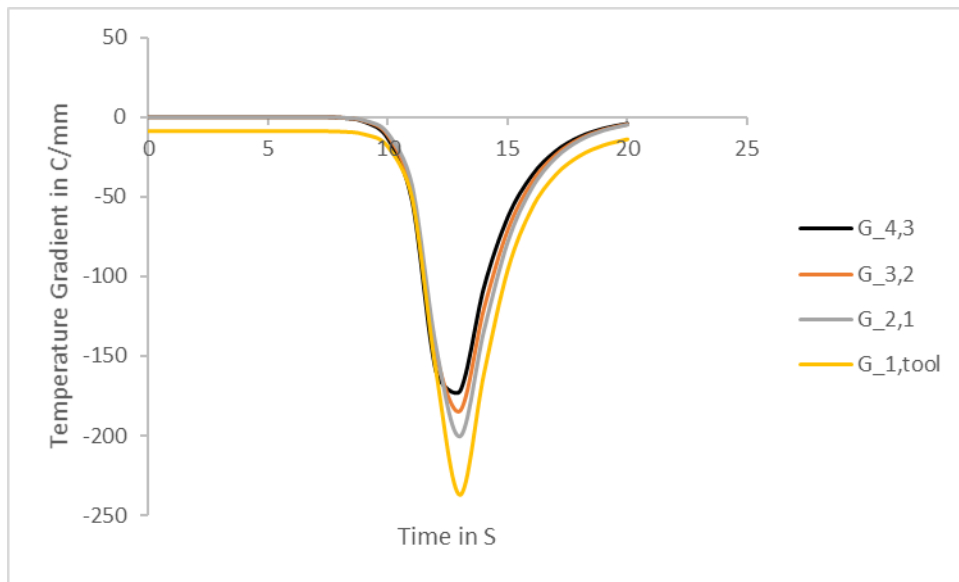


Figure 5.37: Temperature gradients through the thickness at $x = 12in$

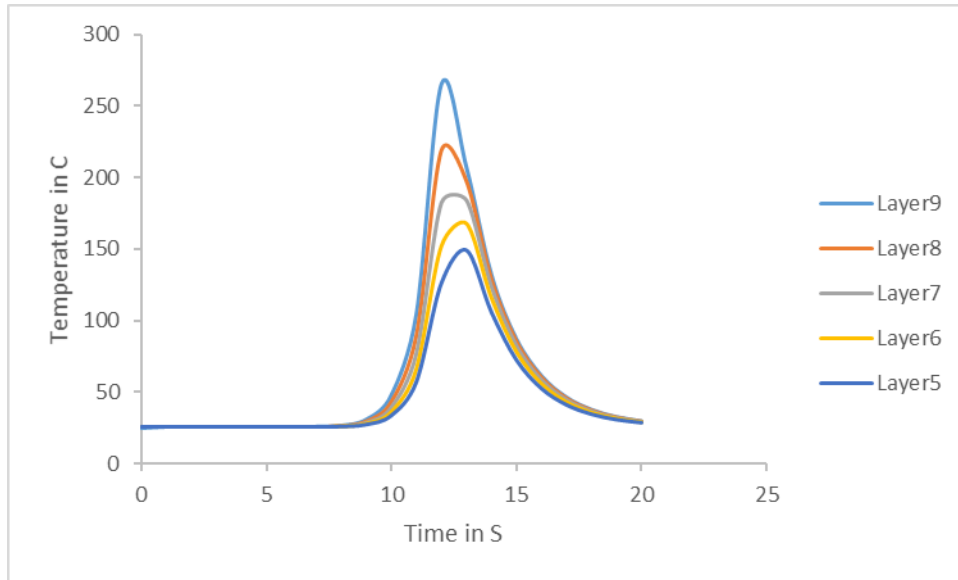


Figure 5.38: Temperatures through the thickness (layers 5 to 9) at $x = 12in$

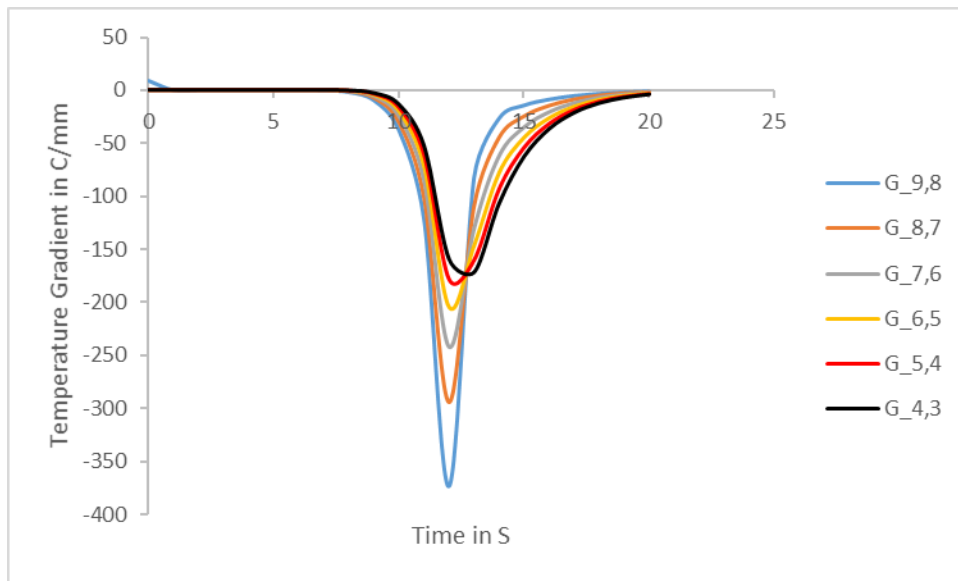


Figure 5.39: Temperature gradients through the thickness at $x = 12in$

Figures 5.24 to 5.39 illustrate that the temperatures and temperature gradients and their trends through the thickness are similar with a time shift based on the distance from the initial position of the torch.

5.7.2. Ceramic mandrel

Since the temperatures and temperature gradients through the thickness of the substrate are similar at different sections, they have been investigated only at $x = 6$ in for the ceramic mandrel. All the results are related to the case where layer 10 is being deposited, and the time between each pass is equal to eight seconds. The results are shown in figures 5.40 and 5.41.

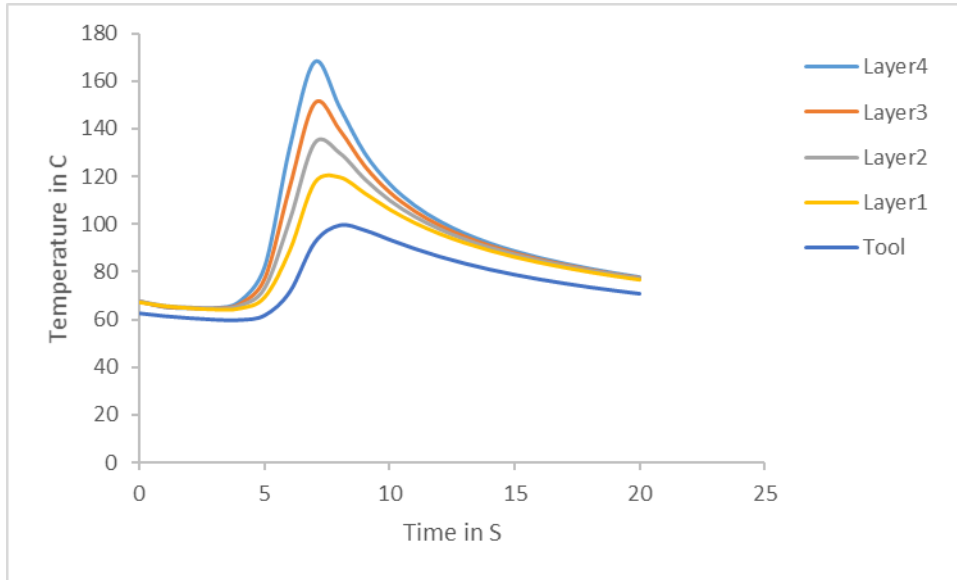


Figure 5.40: Temperatures through the thickness (tool to layer 4) at $x = 6$ in

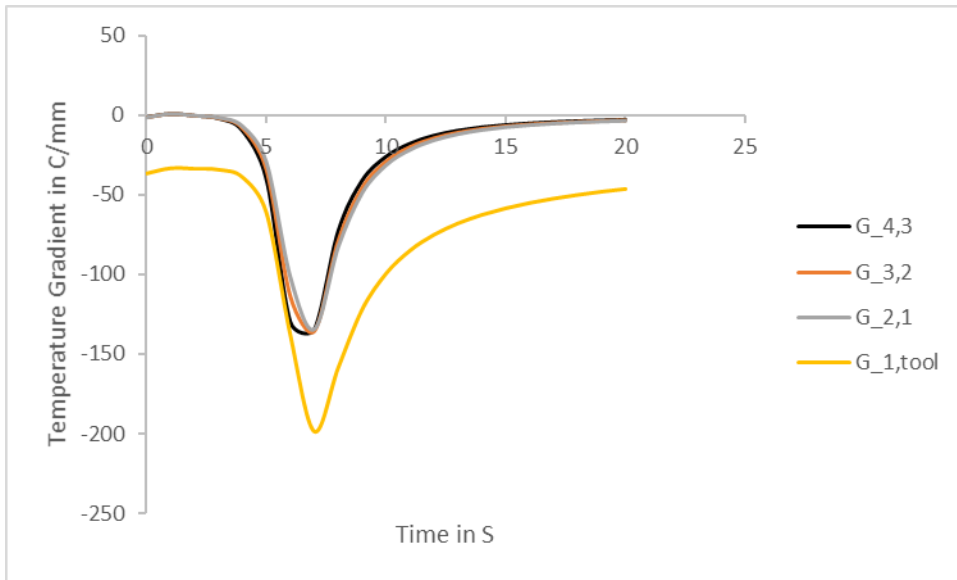


Figure 5.41: Temperature gradients through the thickness at $x = 6$ in

According to figure 5.41, the highest absolute value of the temperature gradients is between layer 1 and ceramic tool ($G_{1,tool}$). Then, the absolute value of the temperature gradient between layers 2 and 1 ($G_{1,2}$) reduces. The temperature gradients between layers 3 and 2 ($G_{3,2}$) and layers 4 and 3 ($G_{4,3}$) remains almost the same as $G_{2,1}$.

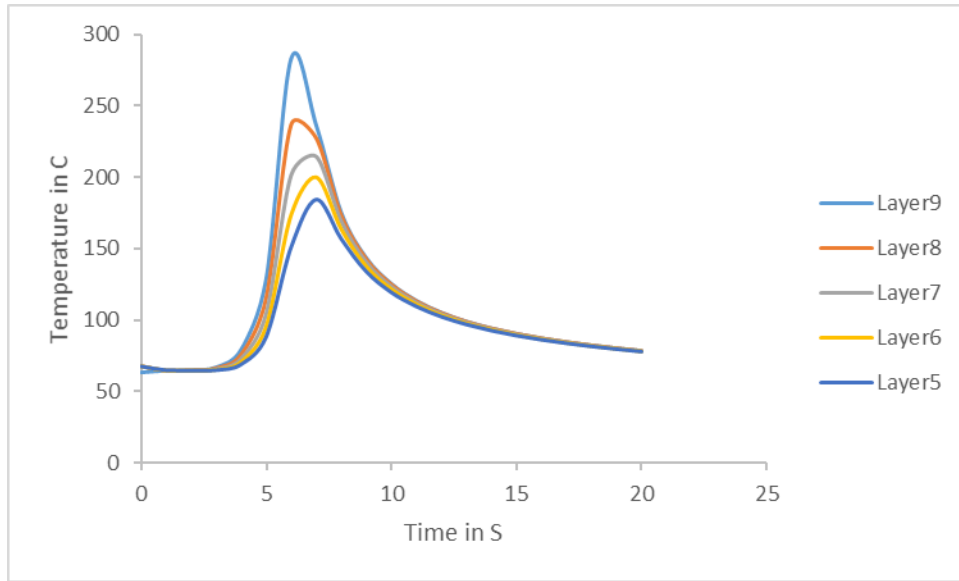


Figure 5.42: Temperatures through the thickness (layers 5 to 9) at $x = 6in$

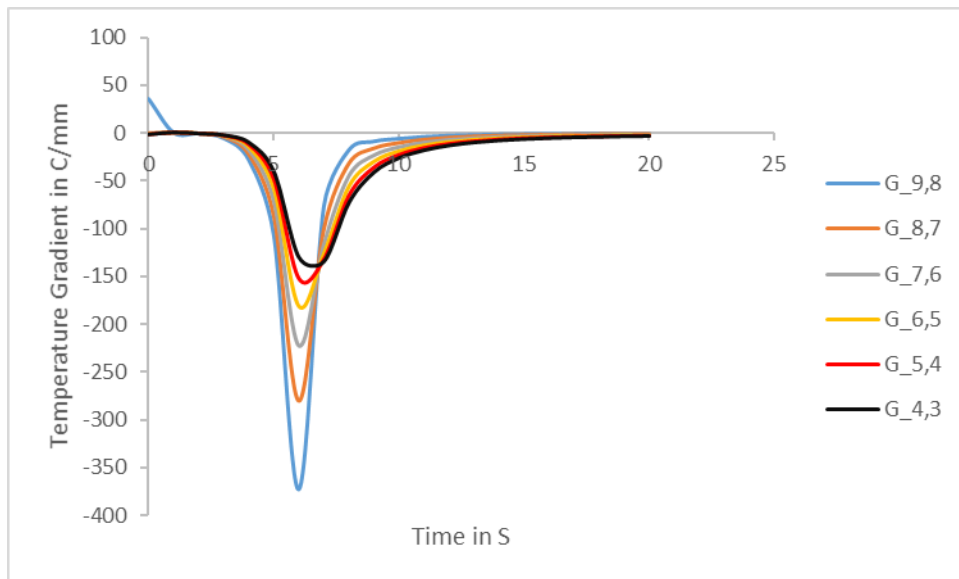


Figure 5.43: Temperature gradients through the thickness at $x = 6in$

According to figure 5.43, the highest absolute value of the temperature gradients is between layers 9 and 8 ($G_{9,8}$). Then, the absolute values of the temperature gradients reduce gradually. The results show that there is a layer at which the trend of temperature gradients changes. In this case, which is a substrate of 10 layers with ceramic tool, layer 3 is the trend change point. Moreover, the highest absolute value of all temperature gradients is between layers 9 and 8 ($|G_{9,8}| > |G_{1,tool}|$, figures 5.41 and 5.43).

5.7.3. Hot aluminum mandrel

In this section, temperatures and temperature gradients of the substrate have been investigated at $x = 6$ in for a hot aluminum mandrel. All results are for the case where layer 10 is being deposited, and the time between each pass is equal to eight seconds.

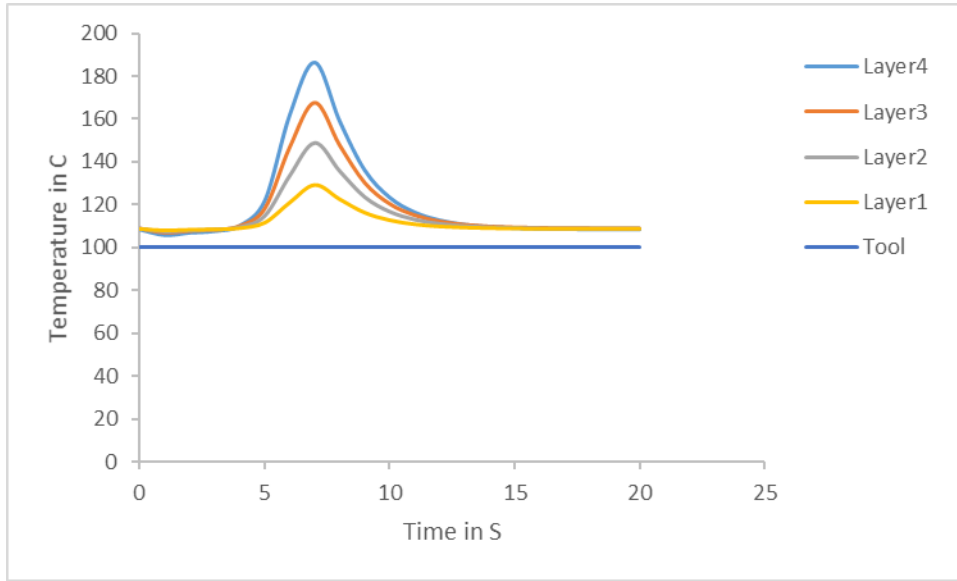


Figure 5.44: Temperatures through the thickness (tool to layer 4) at $x = 6$ in

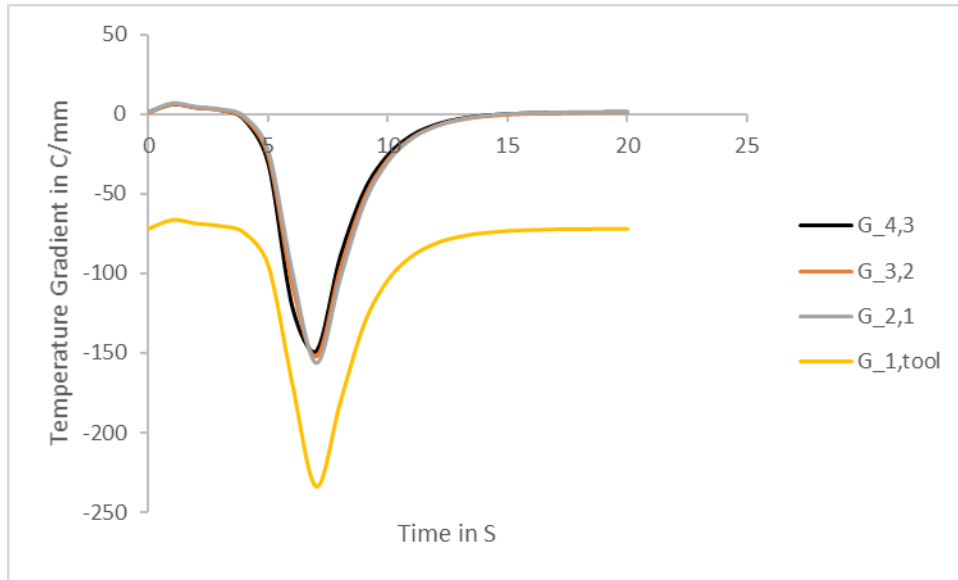


Figure 5.45: Temperature gradients through the thickness at $x = 6in$

According to figure 5.45, the highest absolute value of the temperature gradients is between layer 1 and the hot aluminum tool ($G_{1,tool}$). Then, the absolute value of the temperature gradient between layers 2 and 1 ($G_{2,1}$) reduces. The temperature gradients between layers 3 and 2 ($G_{3,2}$) and layers 4 and 3 ($G_{4,3}$) reduce slightly.

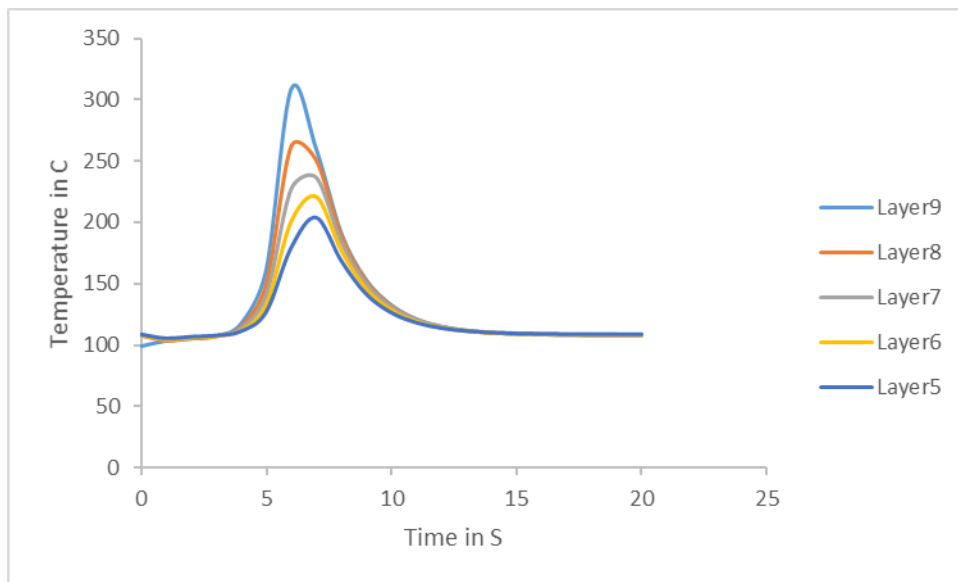


Figure 5.46: Temperatures through the thickness (tool to layer 4) at $x = 6in$

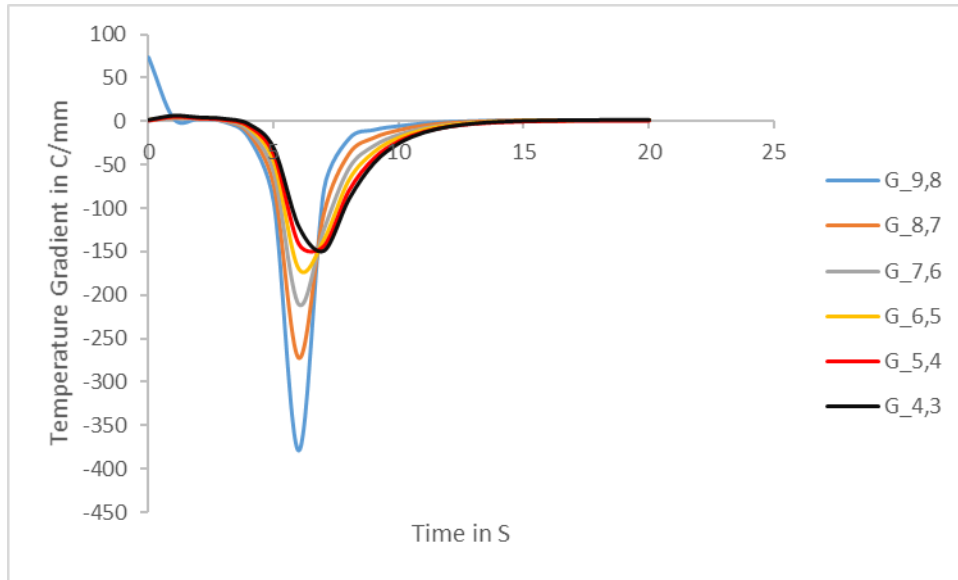


Figure 5.47: Temperature gradients through the thickness at $x = 6\text{in}$

According to figure 5.47, the highest absolute value of the temperature gradients is between layers 9 and 8 ($G_{9,8}$). Then, the absolute values of the temperature gradients reduce gradually until the temperature gradients between layers 5 and 4 ($G_{5,4}$). The temperature gradient between layers 4 and 3 ($G_{4,3}$) increases slightly. The results show that there is a layer at which the trend of temperature gradients changes. In this case, which is a substrate of 10 layers with hot aluminum tool, layer 4 is the trend change point. In addition, the highest absolute value of all temperature gradients is between layers 9 and 8 ($|G_{9,8}| > |G_{1,tool}|$, figures 5.45 and 5.47).

5.8. Comparison of temperature gradients through the thickness for different tools

In this section, temperature gradients for different tools have been compared in the case where layer 10 is being deposited at $x = 6$ in. The results include temperature history and eight seconds of time between each pass.

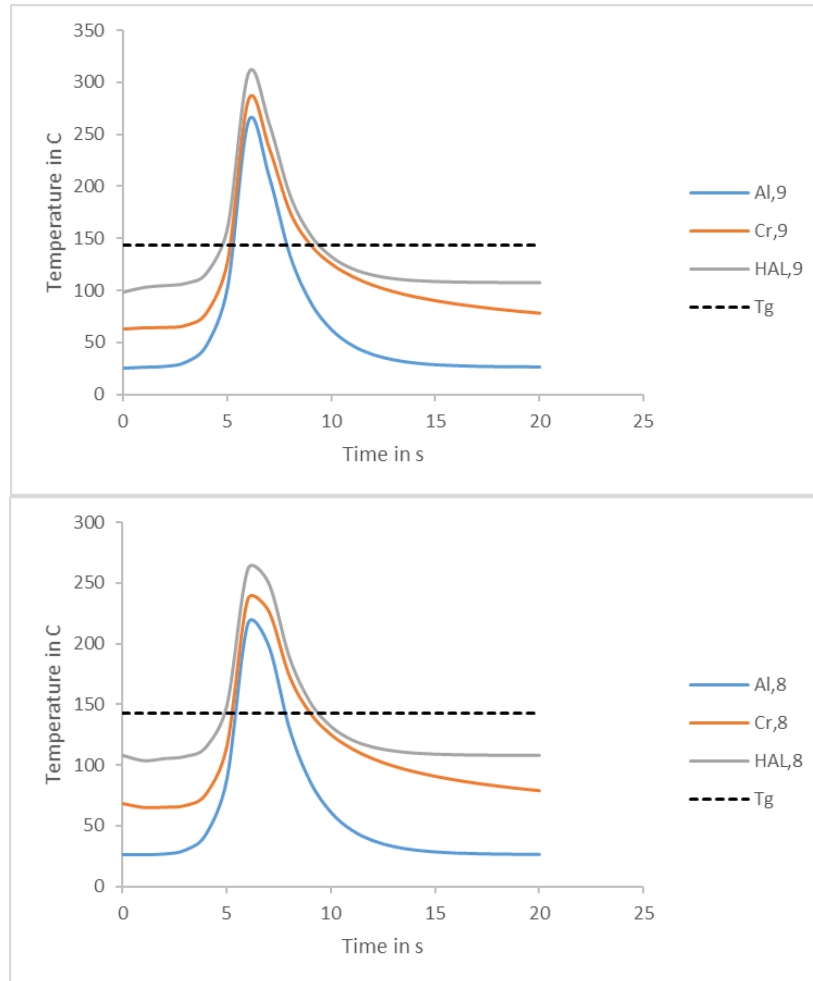


Figure 5.48: Temperature-time graph for different tools, layer 9 at top and layer 8 at bottom

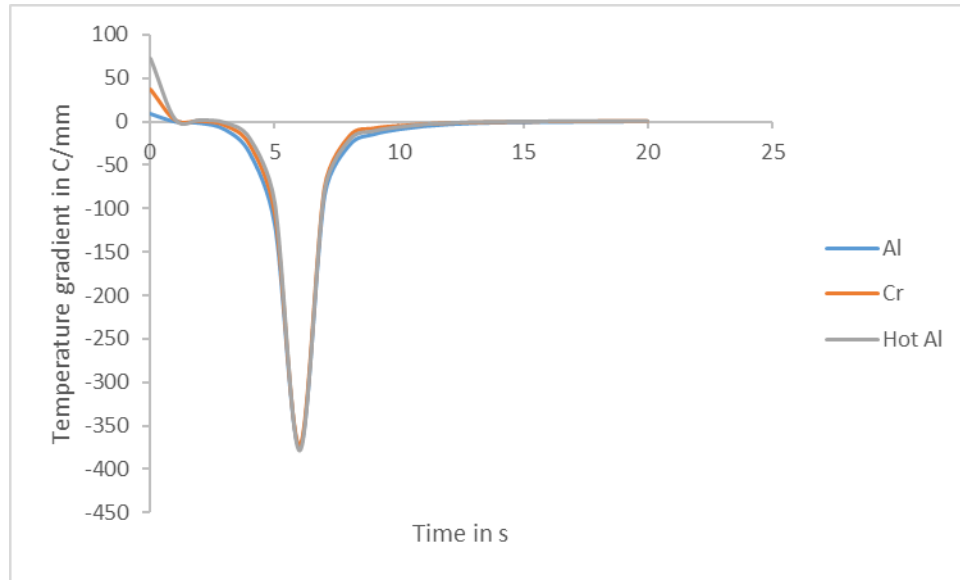


Figure 5.49: Temperature gradients between layers 9 and 8 ($G_{9,8}$) for different tools

According to figure 5.49, the temperature gradient between layers 9 and 8 ($G_{9,8}$) is positive at the beginning of the process for all tools. This occurs because the last layer, which has been deposited completely is layer 9. Layer 9 is exposed to the ambient air (25°C) during the time when the moving torch is far from the specified location ($x = 6 \text{ in}$) and for the time between each pass (eight seconds). This causes the temperature of layer 9 to reduce faster than layer 8. This creates a positive temperature gradient ($G_{9,8}$) at the beginning of the process (deposition of layer 10). As the torch moves along the substrate to deposit layer 10, the temperature of layer 9 increases faster than layer 8 because layer 9 is closer to the torch. Therefore, the temperature gradient between layers of 9 and 8 ($G_{9,8}$) becomes negative. According to figure 5.48, the substrate temperature in both layers 9 and 8 are different for different tools. However, the temperature gradients between these two layers ($G_{9,8}$) are almost the same. This indicates that as the number of layers increases, the temperature gradient at the top layers becomes independent from the tool.

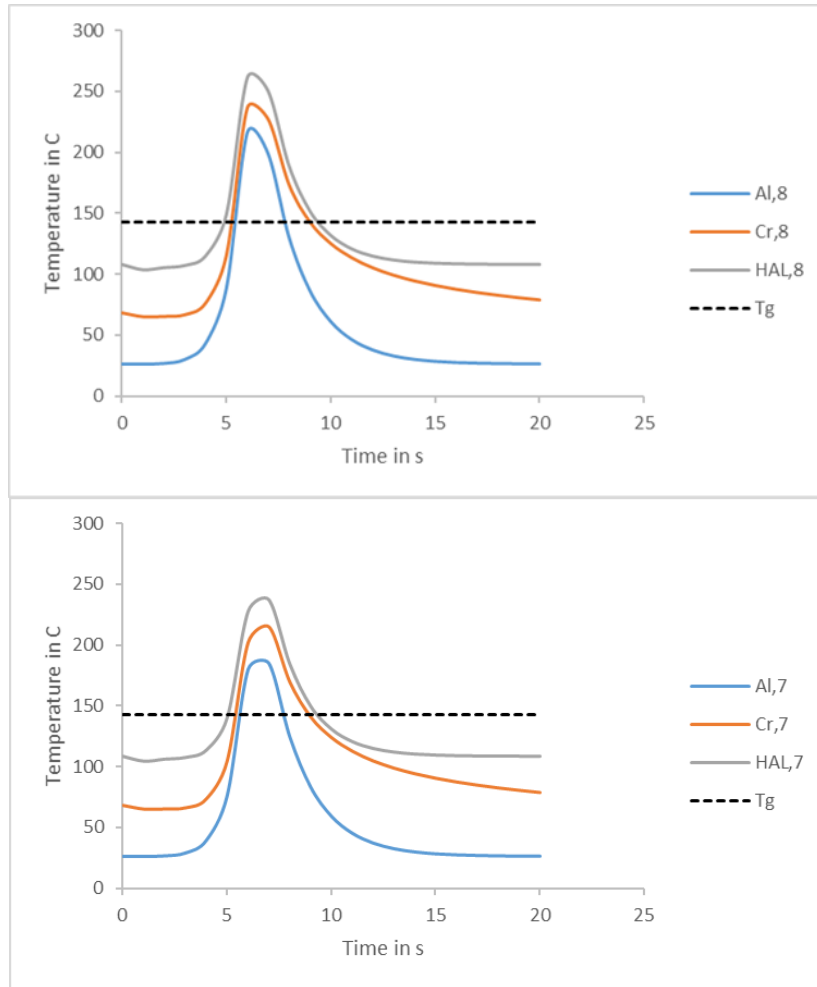


Figure 5.50: Temperature-time graph for different tools, layer 8 at top and layer 7 at bottom

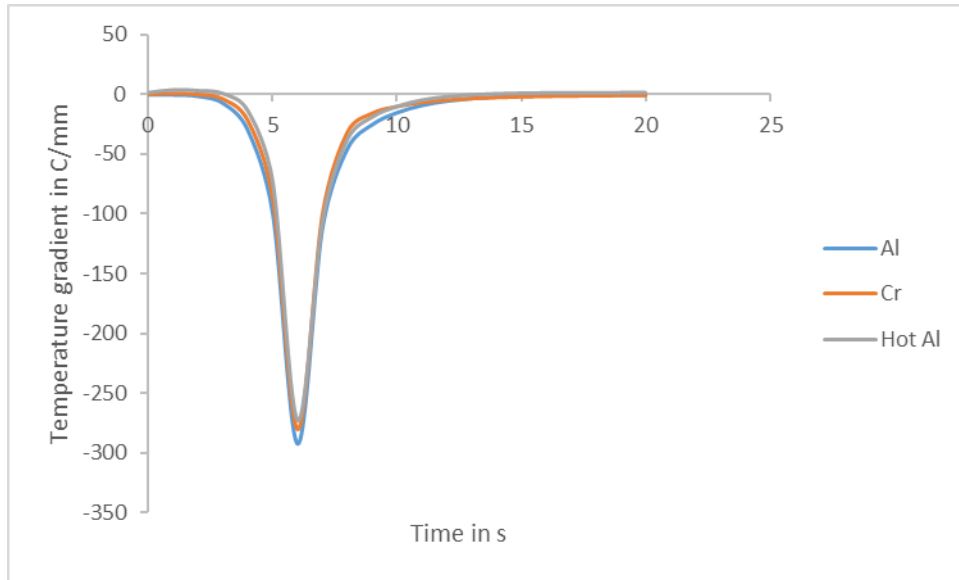


Figure 5.51: Temperature gradients between layers 8 and 7 ($G_{8,7}$) for different tools

According to figure 5.50, the substrate temperature in layers 8 and 7 are different for different tools, but the temperature gradients between layers 8 and 7 ($G_{8,7}$) are almost the same. Nevertheless, the maximum absolute values of temperature gradients are slightly different. Figure 5.51 illustrates that as the number of layers increases, the temperature gradient at the top layers becomes independent from the tool.

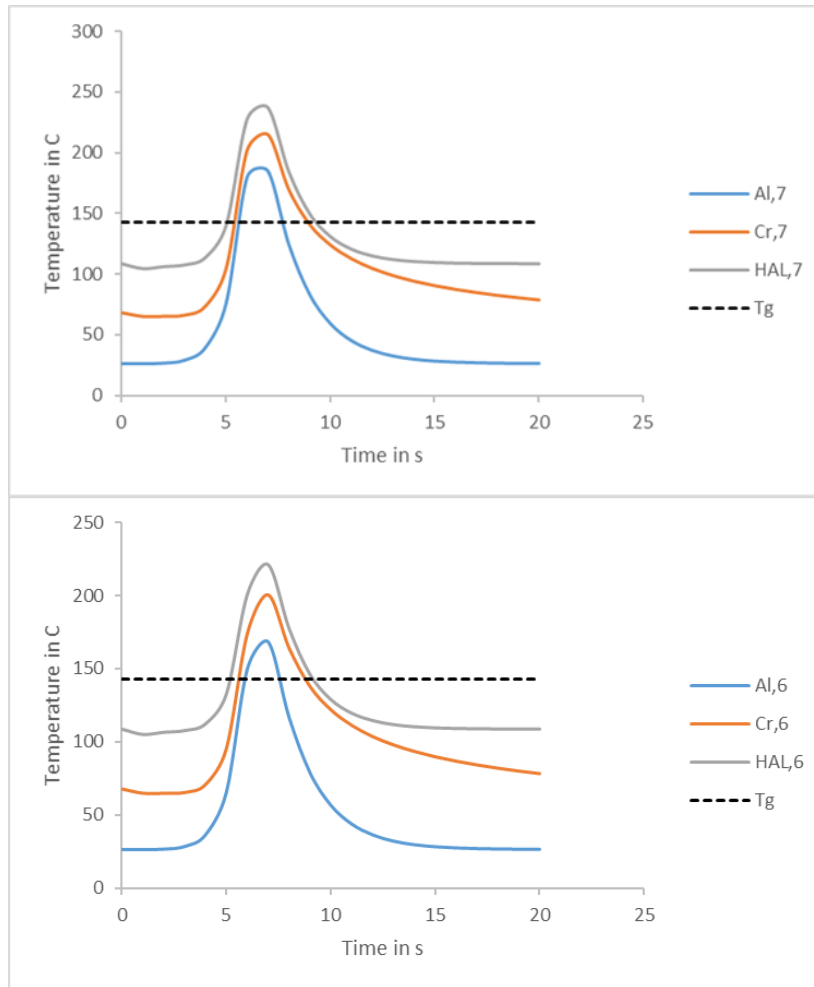


Figure 5.52: Temperature-time graph for different tools, layer 7 at top and layer 6 at bottom

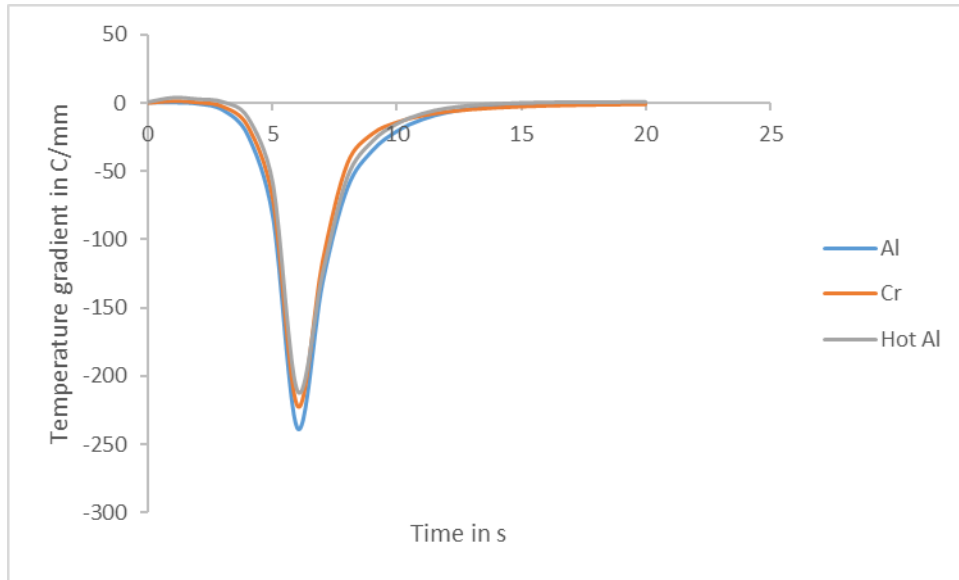


Figure 5.53: Temperature gradients between layers 7 and 6 ($G_{7,6}$) for different tools

According to figure 5.52, the substrate temperature in layers 7 and 6 are different in different tools, but the temperature gradients between layers 7 and 6 ($G_{7,6}$) are almost the same. Nonetheless, the maximum absolute values of temperature gradients are slightly different. The difference between the maximum absolute values of temperature gradients increases through the thickness of substrate. Despite the temperature gradients at the top layers are independent from the tool, the difference between the maximum absolute values of the temperature gradients rises by moving from the top layers towards the bottom layers. This has been shown in figures 5.49, 5.51, and 5.53.

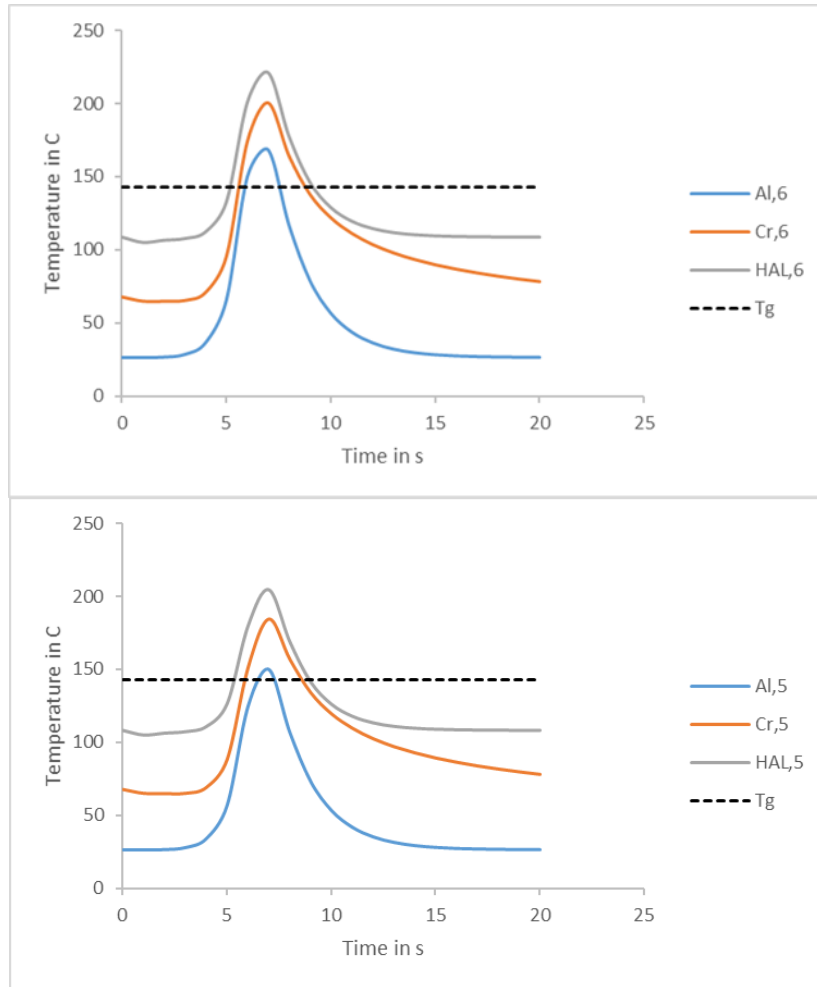


Figure 5.54: Temperature-time graph for different tools, layer 6 at top and layer 5 at bottom

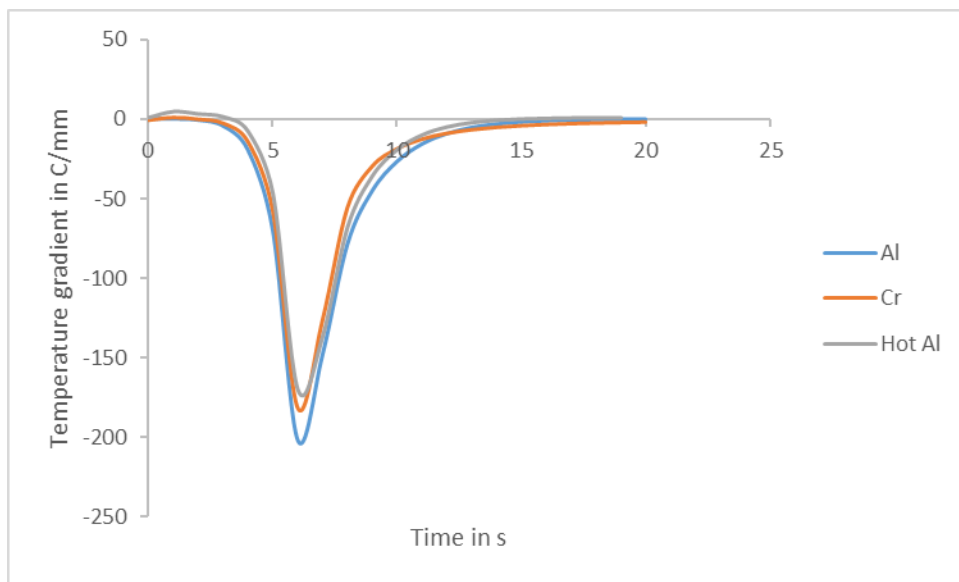


Figure 5.55: Temperature gradients between layers 6 and 5 ($G_{6,5}$) for different tools

Figure 5.55 indicates that moving towards the bottom of the substrate magnifies the difference between the temperature gradients for various tools. This means that tools and their temperatures become more effective in the development of temperature gradients in the bottom layers. According to figure 5.55, the highest absolute value of the temperature gradient belongs to the aluminum tool, and the lowest one belongs to the hot aluminum tool.

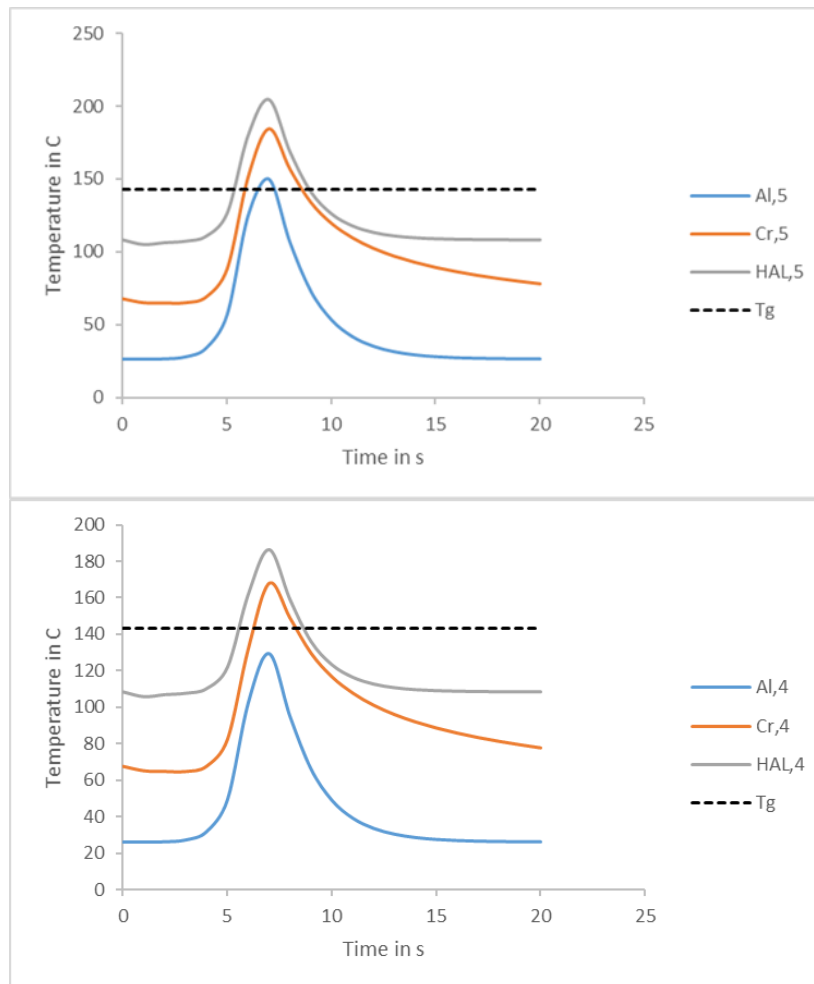


Figure 5.56: Temperature-time graph for different tools, layer 5 at top and layer 4 at bottom

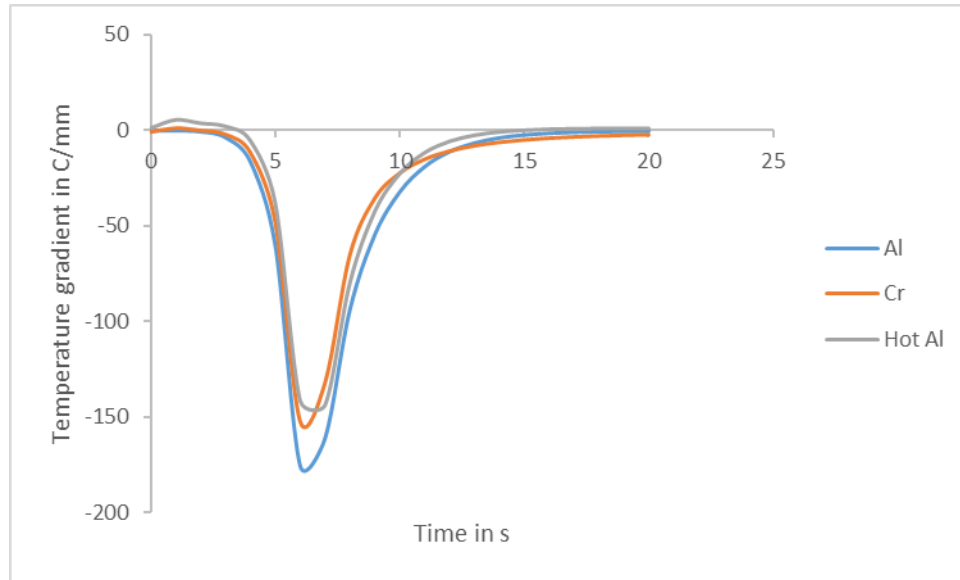


Figure 5.57: Temperature gradients between layers 5 and 4 ($G_{5,4}$) for different tools

According to figure 5.57, the highest absolute value of the temperature gradients develops in the substrate with aluminum tool, and the lowest one develops in the substrate with hot aluminum tool. The temperature gradients of the substrate with ceramic tool falls in between. This indicates that both the material and temperature of the tool affect the temperature gradients.

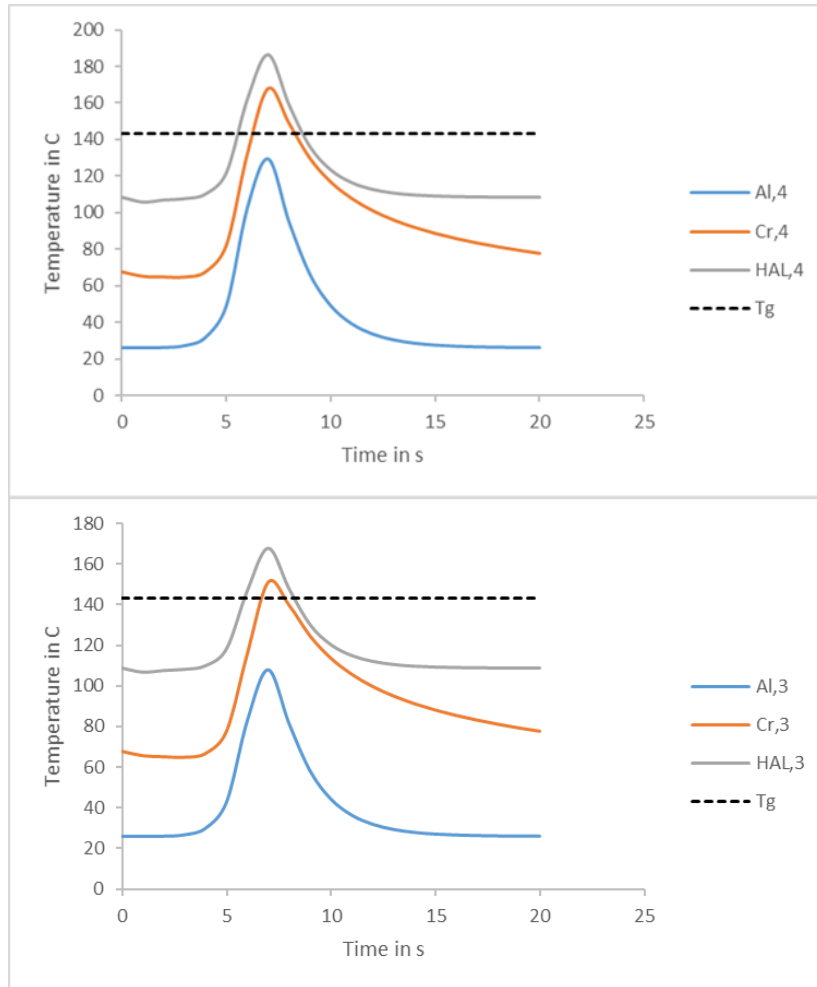


Figure 5.58: Temperature-time graph for different tools, layer 4 at top and layer 3 at bottom

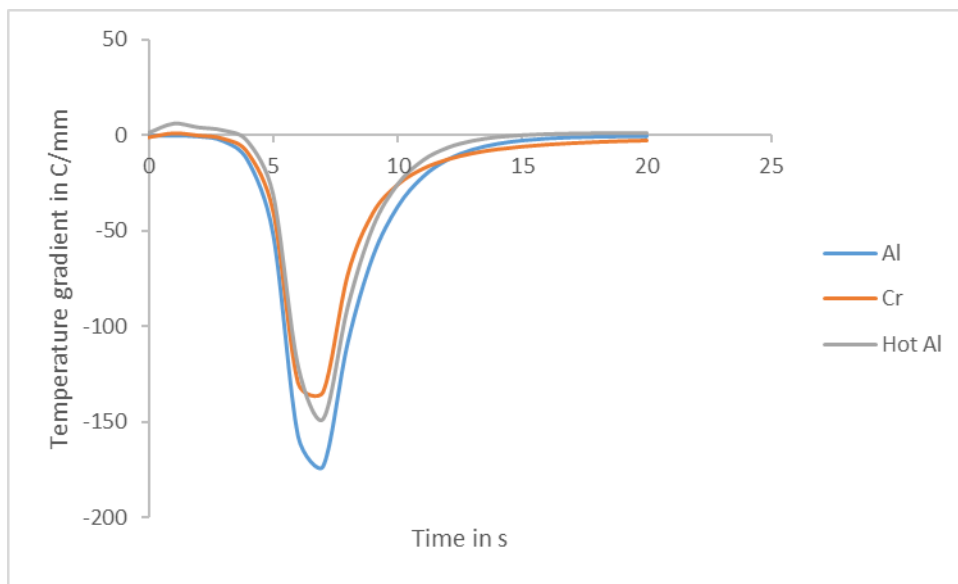


Figure 5.59: Temperature gradients between layers 4 and 3, $G_{4,3}$ for different mandrels

According to figure 5.59, the highest absolute value of the temperature gradients belongs to the substrate with aluminum tool, and the lowest one belongs to the substrate with ceramic tool. The temperature gradients of the substrate with hot aluminum tool falls in between. This means that the material of the tools could become more dominant (in comparison to the tool temperature) in the development of the temperature gradients for the layers which are close to the tool.

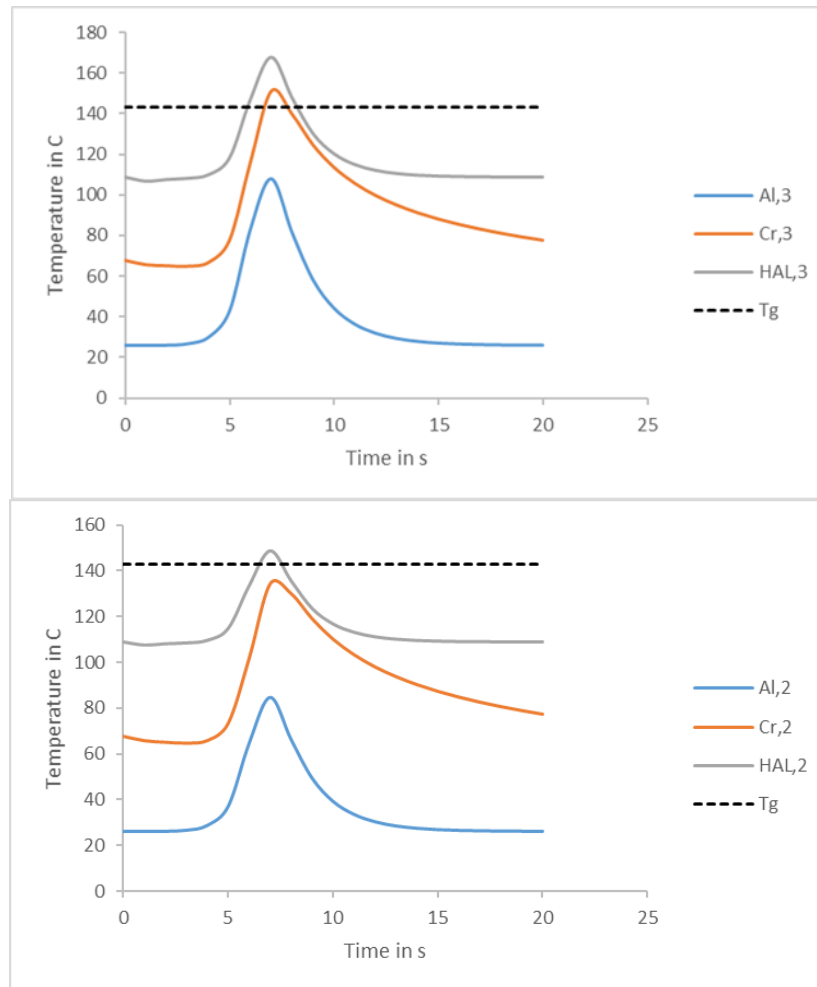


Figure 5.60: Temperature-time graph for different tools, layer 3 at top and layer 2 at bottom

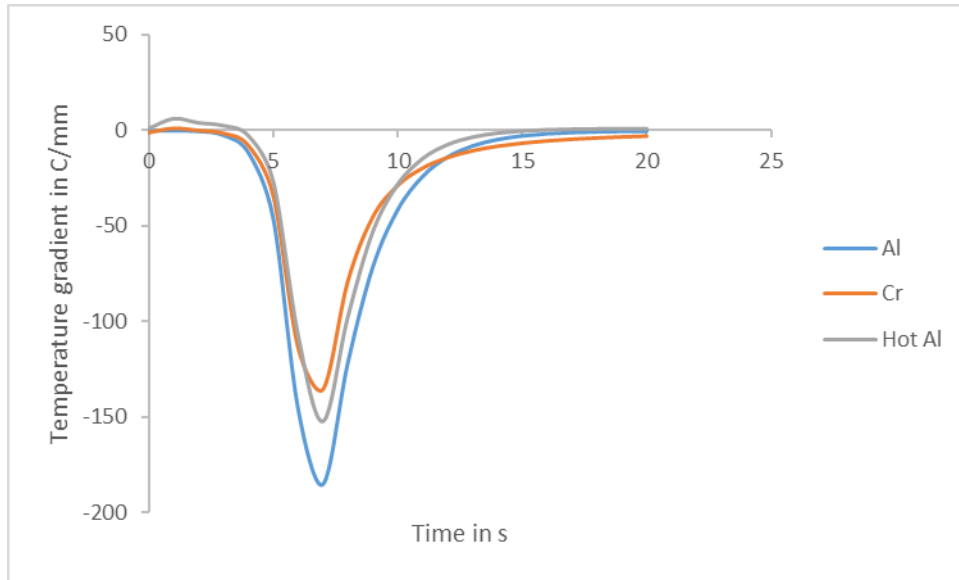


Figure 5.61: Temperature gradients between layers 3 and 2 ($G_{3,2}$) for different tools

According to figure 5.61, the highest absolute value of the temperature gradients develops in the substrate with aluminum tool, and the lowest one develops in the substrate with ceramic tool. The temperature gradients of the substrate with hot aluminum tool falls in between. This shows that the material of the tools becomes more dominant in the development of the temperature gradients in the substrates by getting closer to the tool.

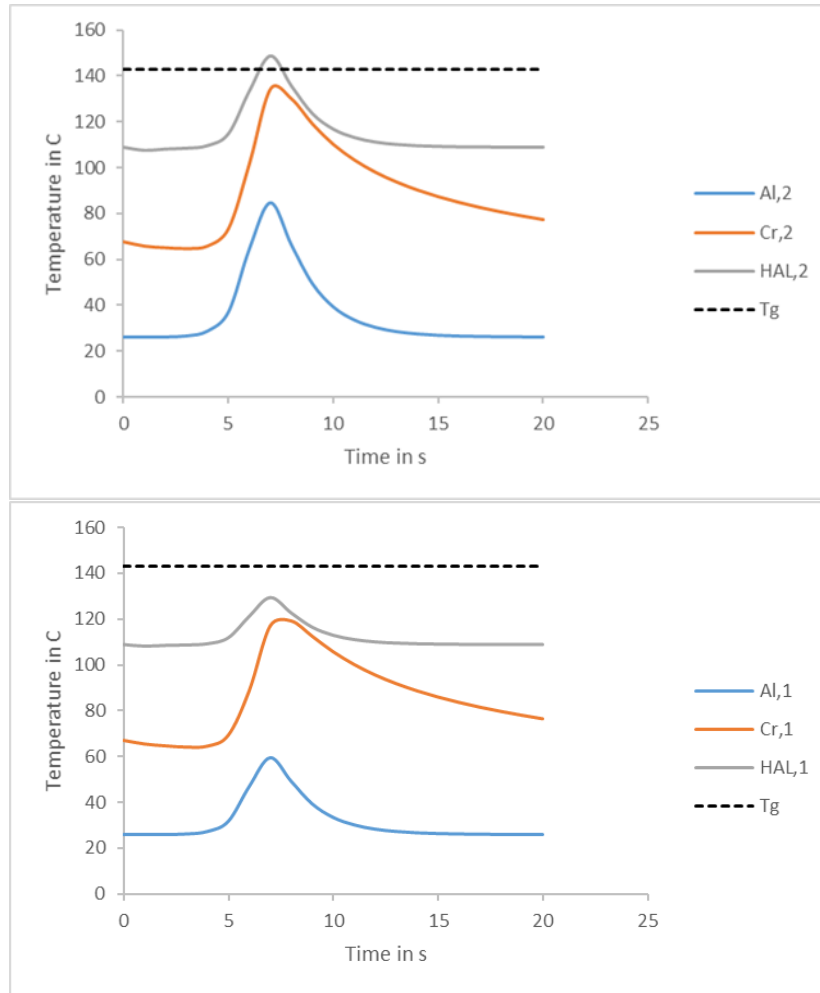


Figure 5.62: Temperature-time graph for different tools, layer 2 at top and layer 1 at bottom

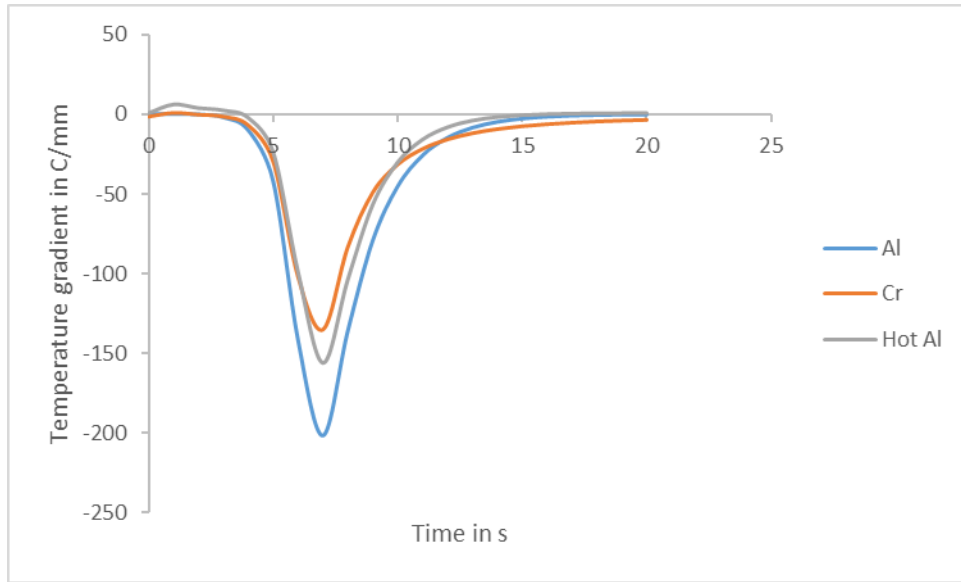


Figure 5.63: Temperature gradients between layers 2 and 1 ($G_{2,1}$) for different tools

According to figure 5.63, the highest absolute value of the temperature gradients develops in the substrate with aluminum tool, and the lowest one develops in the substrate with ceramic tool. The temperature gradients of the substrate with hot aluminum tool falls in between.

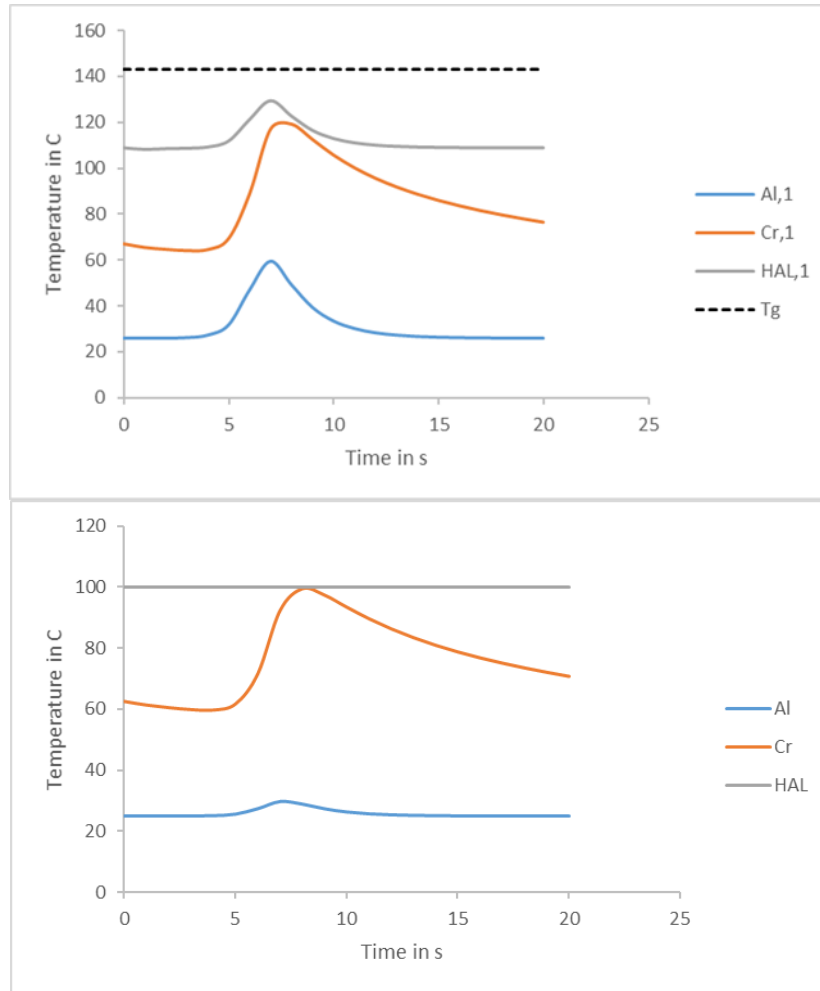


Figure 5.64: Temperature-time graph for different tools, layer 1 at top and tool at bottom

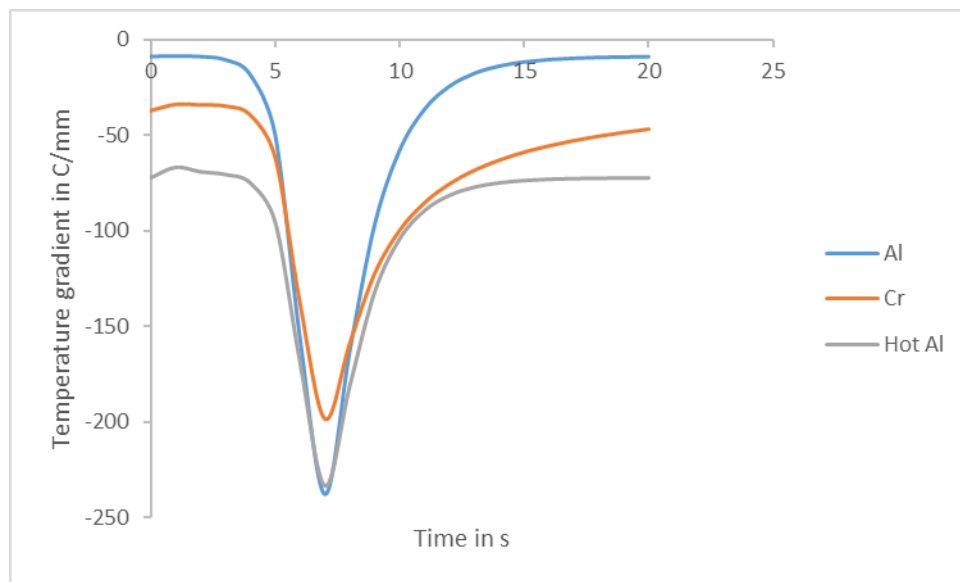


Figure 5.65: Temperature gradients between layer 1 and tool ($G_{1,tool}$) for different tools

According to figure 5.65, the highest absolute value of the temperature gradients exists in both substrate with aluminum and hot aluminum tool (both have almost the same value). This is despite the fact that the temperatures of layer 1 and tool are different for the substrates with aluminum and hot aluminum tool. This indicates that at the first layer the only factor that affects the development of temperature gradients is the material of the tool. The lowest absolute value of the temperature gradient has been developed in the substrate with ceramic tool. This is because ceramic is a thermal insulator and has a much lower thermal conductivity in comparison to aluminum. This confirms that by moving towards the bottom of substrate the temperature gradients become more dependent upon the tool's material rather than tool's temperature.

Chapter 6: Conclusions and Future Work

6.1. Conclusions

Both thermoplastic and thermoset composite structures can be manufactured using automated fiber placement method. Thermoplastic composites provide advantages over thermosets such as possibility of recycling and no shelf-life effects on manufacturing. However, manufacturing of thermoplastic structures with free edges using AFP process faces a major issue. Development of temperature gradients and residual stresses during the manufacturing process causes the thermoplastic structures with free edges to deform. The deformation occurs even during the manufacturing process of unidirectional laminates. To resolve this issue, development of accurate heat transfer models is essential. To date, most studies in heat transfer analysis of AFP processes are related to laser-assisted AFP machines. Thermal inputs in heat transfer models related to AFP process with hot gas torch are different from thermal inputs of laser-assisted AFP process. Hot gas/air temperature and convection coefficient distributions in the vicinity of substrate (thermal inputs) play the main role in the accuracy of heat transfer models for AFP process with hot gas torch.

In this study, a heat transfer model was developed for AFP process with hot gas torch using finite difference method (presented in chapter 4). The model includes the following aspects, which are essential for accurate heat transfer models of AFP process with hot gas torch:

- Transient nature of the process was considered.
- Temperature dependencies of the material properties were considered.
- Non-linear mathematical models for both hot gas/air temperature and convection coefficient distributions (thermal inputs) were developed. Furthermore, it was assumed that the thermal inputs were related linearly. This assumption was validated using experimental results. The non-linear thermal inputs led the accuracy of the theoretical results to improve such that they were in proper agreements with the experimental ones.
- Inter-layer thermal contact resistance was considered and investigated.
- The heat transfer model was validated using experimental results.

Although the accuracy of the theoretical results is highly dependent upon the thermal inputs, the inter-layer thermal contact resistance can affect the accuracy of the heat transfer model. The effects of inter-layer thermal contact resistance depend upon the quality of bonding between layers. The results indicated that the effects of inter-layer thermal contact resistance are not significant in this study. This is mainly due to the quality of the laminate manufactured by the AFP machine available at Concordia University.

To include the effects of time between each pass and temperature history during material deposition, a second heat transfer model was developed using finite difference method, MATLAB, and Microsoft Excel (presented in 5.2). The temperature gradients and effects of tools in their development were investigated using the validated heat transfer models. Based on the results, the followings can be concluded:

- For substrates with aluminum tools(25°C) and with low number of layers such as 5, the time between passes does not have significant effect due to the length of the substrates. As the number of layers increases (e.g., 10 layers), time between passes needs to be considered in the heat transfer model.

- The material of tools and their temperatures during the manufacturing process affect the temperatures of substrates at all layers including top layers. For instance, the temperatures of substrates with ceramic and hot aluminum tools are higher than aluminum tool (25°C). This can affect the number of layers which fall below the glass transition temperature (T_g) for substrates with different tools.
- The material of the tools and their temperatures can affect temperature histories in substrates. The temperature histories in substrates with ceramic and hot aluminum tool is more significant than aluminum tool (25°C).
- As the number of layers increases, the temperature gradients at the top layers of substrates become independent from the tool material or its temperature (dependent upon the torch).
- By moving through the thickness of substrates (from top layers to bottom), the material and temperatures of the tools affect the temperature gradients. However, the temperature gradient of the first layer (closest layer to tool) is dependent more upon the tool's material rather than tool's temperature.
- The highest absolute value of the temperature gradient is between layers 9 and 8 for the case where layer 10 is being deposited. Then, it decreases through the thickness of the substrates. At a certain layer, which is called the trend-changing-point in this study, this trend changes from increasing to decreasing or vice versa. The trend changing point for aluminum and ceramic tools is at layer 3, and it is at layer 4 for the hot aluminum tool.
- In all substrates and regardless of the tool, temperature gradients between layers 9 and 8 is higher than temperature gradients between layer 1 and the tool.

6.2. Future Work

Manufacturing of thermoplastic structures with free edges using automated fiber placement method and its challenges open many research opportunities in this field. The main challenge is the undesirable distortion of these structures which occurs even during the manufacturing process for unidirectional laminates due to existence of temperature gradients and residual stresses. To investigate the residual stresses, further research is essential and recommended:

- Although the two-dimensional heat transfer models in this study provide accurate and acceptable results (width of the substrate is too small with respect to the length), considering the width of substrate to the models can make them more general.
- The compaction roller (diameter and geometry) and incoming tape were neglected for material deposition. Considering them in heat transfer model would be beneficial.
- Bonding quality and crystallization can be investigated using the results obtained from this study.
- Development of the residual stresses can be investigated using the results obtained from this study.

References

1. S.V. Hoa, *Principles of the manufacturing of composite materials*, 2nd ed. Destech Publications, Inc., 2018.
2. S. V. Hoa, “Development of composite springs using 4D printing method,” *Composite Structures*, vol. 210, pp. 869–876, 2019.
3. S. V. Hoa, “Factors affecting the properties of composites made by 4D printing (moldless composites manufacturing),” *Advanced Manufacturing: Polymer & Composites Science*, vol. 3, no. 3, pp. 101–109, 2017.
4. Li Z., Yang T., Du Y. “Dynamic finite element simulation and transient temperature field analysis in thermoplastic composite tape lay-up process”, *Journal of Thermoplastic composites*, 2015, 28, pp. 558-573.
5. Jeyakodi GK. 2016. "Finite Element Simulation of the In - Situ AFP process for Thermoplastic Composites using Abaqus", Master thesis at Delft University of Technology.
6. Di Francesco, M., Giddings PF, Scott M., et al, 2016, “Influence of laser power density on the meso structure of thermoplastic composite preforms manufactured by automated fiber placement”, International SAMPE conference, Long Beach, California, USA.
7. Cogswell F.N., 2013, *Thermoplastic aromatic polymer composites: A study of the structure, processing, and properties of carbon fiber reinforced polyetheretherketone and related materials*, Elsevier publication, Amsterdam, Netherlands.
8. Khan M.A., 2010, “Experimental and simulative description of the thermoplastic tape placement process with on line consolidation”, Ph.D thesis, Technischen universitat Kaiserslautern, Germany.
9. Li Z., Yang T., Du Y. “Dynamic finite element simulation and transient temperature field analysis in thermoplastic composite tape lay-up process”, *Journal of Thermoplastic composites*, 2015, 28, pp. 558-573.
10. Suong Van Hoa, Minh Duc Hoang, and Jeff Simpson, “Procedure for making flat thermoplastic composite laminates using automated fiber placement and their mechanical properties”, *Journal of Thermoplastic composites*, Vol. 30, No. 12, 2017, pp. 1693-1712.
11. O. A. Tafreshi, S. V. Hoa, F. Shadmehri, D. M. Hoang, and D. Rosca, “Heat transfer analysis of automated fiber placement of thermoplastic composites using a hot gas torch,” *Advanced Manufacturing: Polymer & Composites Science*, vol. 5, no. 4, pp. 206–223, 2019.
12. T. Aized and B. Shirinzadeh, “Robotic fiber placement process analysis and optimization using response surface method,” *The International Journal of Advanced Manufacturing Technology*, vol. 55, no. 1-4, pp. 393–404, 2010.
13. “Automated Fiber Placement (AFP) Laboratory,” *Concordia University*. [Online]. Available: <https://www.concordia.ca/ginacody/mechanical-industrial-aerospace-eng/research/automated-fiber-placement-lab.html>. [Accessed: 04-Feb-2022].
14. Cai Xiao “Determination of process parameters for the manufacturing of thermoplastic composite cones using automated fiber placement”, Master’s Thesis, Department of Mechanical and Industrial Engineering, Concordia university, 2012.

15. M. Moghadamzad and S. V. Hoa, "Models for heat transfer in thermoplastic composites made by automated fiber placement using Hot Gas Torch," *Composites Part C: Open Access*, vol. 7, p. 100214, 2022.
16. M. Moghadamzad and S. V. Hoa, "Effect of thermal input on the temperature distribution of thermoplastic composites made by automated fiber placement (AFP)," Proceedings of the 36th annual conference of the *American Society for Composites 2021*, 2021.
17. A. Levy, D. Heider, J. Tierney, and J. W. Gillespie, "Inter-layer thermal contact resistance evolution with the degree of intimate contact in the processing of thermoplastic composite laminates," *Journal of Composite Materials*, vol. 48, no. 4, pp. 491–503, 2013.
18. A. Levy, J. Tierney, D. Heider, et al. "Modeling of inter-layer thermal contact resistance during thermoplastic tape placement, Baltimore, 21-24 May 2012, SAMPE 2012.
19. O. A. Tafreshi, "Heat Transfer Study of the in-situ automated fiber placement (AFP) for Thermoplastic Composites," Master's Thesis, Concordia university, Spectrum, 2019. [Online]. Available: <https://spectrum.library.concordia.ca/id/eprint/986269/>. [Accessed: 05-Feb-2022].
20. H. G. Karimiani, "Analysis of residual stresses in thermoplastic composites manufactured by automated fiber placement," Master's Thesis, Concordia University *Spectrum*, Sep-2015. [Online]. Available: <https://spectrum.library.concordia.ca/id/eprint/980539/>. [Accessed: 05-Feb-2022].
21. Hoa S.V., Duc Hoang M, Simpson J. 2017. "Manufacturing procedure to make flat thermoplastic composite laminates by automated fibre placement and their mechanical properties", *Journal of Thermoplastic Composite Materials*;30:1693–712.
22. Paul W, Binder K, Heermann DW, Kremer K. 1991. "Dynamics of polymer solutions and melts. Reptation predictions and scaling of relaxation times", *Journal of Chemical Physics*; 95:7726–40.
23. M. D. Hoang, "Procedure for making flat thermoplastic composite plates by automated fiber placement and their mechanical properties," Master's Thesis, Concordia university, *Spectrum*, Jul-2015. [Online]. Available: <https://spectrum.library.concordia.ca/id/eprint/979994/>. [Accessed: 04-Feb-2022].
24. Chapman TJ, Gillespie Jr JW, Pipes RB, Manson J.A, Seferis J.C. 1990. "Prediction of process-induced residual stresses in thermoplastic composites", *Journal of Composite Materials*; 24:616–43.
25. Sonmez FO, Hahn HT, Akbulut M. 2002. "Analysis of process-induced residual stresses in tape placement", *Journal of Thermoplastic Composite Materials*; 15:525–44.
26. Lamontia MA, Funck SB, Gruber MB, Cope RD, Waibel BJ, Gopez NM, 2003. "Manufacturing flat and cylindrical laminates and built-up structure using automated thermoplastic tape laying, fiber placement, and filament winding", *SAMPE Conference*; 39:30–43.
27. Lamontia MA, Gruber MB, Tierney JJ, Gillespie Jr JW, Jensen BJ, Cano RJ. 2009. "Modeling the accudyne thermoplastic in situ ATP process", 30th International SAMPE Europe Conference, Paris.
28. J. Tierney and J. W. Gillespie, "Modeling of heat transfer and void dynamics for the thermoplastic composite tow-placement process," *Journal of Composite Materials*, vol. 37, no. 19, pp. 1745–1768, 2003.
29. S.-C. Dai and L. Ye, "GF/PP tape winding with on-line consolidation," *Journal of Reinforced Plastics and Composites*, vol. 21, no. 1, pp. 71–90, 2002.

30. T. Weiler, M. Emonts, L. Wollenburg, and H. Janssen, "Transient thermal analysis of laser-assisted thermoplastic tape placement at high process speeds by use of Analytical Solutions," *Journal of Thermoplastic Composite Materials*, vol. 31, no. 3, pp. 311–338, 2017.
31. E. P. Beyeler and S. I. Güceri, "Thermal Analysis of Laser-Assisted Thermoplastic-Matrix Composite Tape Consolidation," *Journal of Heat Transfer*, vol. 110, no. 2, pp. 424–430, 1988.
32. M. G. Nejhad, R. Cope, and S. Güceri, "Thermal Analysis of in-situ Thermoplastic Composite Tape Laying," *Journal of Thermoplastic Composite Materials*, vol. 4, no. 1, pp. 20–45, 1991.
33. S. C. Mantell and G. S. Springer, "Manufacturing Process Models for Thermoplastic Composites," *Journal of Composite Materials*, vol. 26, no. 16, pp. 2348–2377, 1992.
34. F. O. Sonmez and H. T. Hahn, "Modeling of Heat Transfer and Crystallization in Thermoplastic Composite Tape Placement Process," *Journal of Thermoplastic Composite Materials*, vol. 10, no. 3, pp. 198–240, 1997.
35. Li Z., Yang T., Du Y. "Dynamic finite element simulation and transient temperature field analysis in thermoplastic composite tape lay-up process", *Journal of Thermoplastic composites*, 2015, 28, pp. 558-573.
36. Z. Han, Z. Cao, Z. Shao, and H. Fu, "Parametric study on heat transfer for tow placement process of thermoplastic composite," *Polymers and Polymer Composites*, vol. 22, no. 8, pp. 713–722, 2014.
37. Q. Zhao, S. V. Hoa, and Z. J. Gao, "Thermal stresses in rings of thermoplastic composites made by automated fiber placement process," *Science and Engineering of Composite Materials*, vol. 18, no. 1-2, pp. 35–49, 2011.
38. D. L. James and W. Z. Black, "Thermal analysis of continuous filament-wound composites," *Journal of Thermoplastic Composite Materials*, vol. 9, no. 1, pp. 54–75, 1996.
39. Y. M. Toso, P. Ermanni, and D. Poulidakos, "Thermal Phenomena in Fiber-reinforced Thermoplastic Tape Winding Process: Computational Simulations and Experimental Validations," *Journal of Composite Materials*, vol. 38, no. 2, pp. 107–135, 2004.
40. N. Hassan, J. E. Thompson, R. C. Batra, A. B. Hulcher, X. Song, and A. C. Loos, "A Heat Transfer Analysis of the Fiber Placement Composite Manufacturing Process," *Journal of Reinforced Plastics and Composites*, vol. 24, no. 8, pp. 869–888, 2005.
41. C. M. Stokes-Griffin and P. Compston, "A combined optical-thermal model for near-infrared laser heating of thermoplastic composites in an automated tape placement process," *Composites Part A: Applied Science and Manufacturing*, vol. 75, pp. 104–115, 2015.
42. A. Levy, D. Heider, J. Tierney, and J. W. Gillespie, "Inter-layer thermal contact resistance evolution with the degree of intimate contact in the processing of thermoplastic composite laminates," *Journal of Composite Materials*, vol. 48, no. 4, pp. 491–503, 2013.
43. A. Levy, J. Tierney, D. Heider, et al. "Modeling of inter-layer thermal contact resistance during thermoplastic tape placement, Baltimore, 21-24 May 2012, SAMPE 2012.
44. A. Kollmannsberger, R. Lichtinger, F. Hohenester, C. Ebel, and K. Drechsler, "Numerical analysis of the temperature profile during the laser-assisted automated fiber placement of

- CFRP tapes with thermoplastic matrix,” *Journal of Thermoplastic Composite Materials*, vol. 31, no. 12, pp. 1563–1586, 2017.
45. X. Wang, M. Weber, and J.-M. Charrier, “Heating of Thermoplastic-Based Unidirectional Composite Prepregs,” *Journal of Thermoplastic Composite Materials*, vol. 2, no. 2, pp. 105–121, 1989.
 46. H. J. Kim, S. K. Kim, and W. I. Lee, “A study on heat transfer during thermoplastic composite tape lay-up process,” *Experimental Thermal and Fluid Science*, vol. 13, no. 4, pp. 408–418, 1996.
 47. P.-J. Shih and A. C. Loos, “Heat Transfer Analysis of the Thermoplastic Filament Winding Process,” *Journal of Reinforced Plastics and Composites*, vol. 18, no. 12, pp. 1103–1112, 1999.
 48. L. Zacheri, F. Shadmehri, and K. Rother, “Determination of convective heat transfer coefficient for hot gas torch (HGT)-assisted automated fiber placement (AFP) for thermoplastic composites,” *Journal of Thermoplastic Composite Materials*, p. 089270572098236, 2021.
 49. Çengel Yunus A., A. J. Ghajar, and Kanoğlu Mehmet, *Heat and mass transfer: fundamentals & applications*. New Delhi: McGraw Hill Education (India), 2016.
 50. Tafreshi OA, Hoa S. V., Hoang DM, et al. 2019 Heat transfer by a moving heat source in automated fiber placement (AFP) thermoplastic composites manufacturing. *Proceedings of the 4th International Symposium on Automated Composites Manufacturing*, Montreal, April 2019, published by Destech Publications.